Indian J Pure & Appl Phys, Vol 21 No 11 pp 619-682
NOVEMBER 1983
CODEN : IJOPAU ISSN : 0019-5596
21(11) 619-682 (1983)

CSIR Regional Lab. Jorhat
Dy/Acc No 1308
Dat 12.3.84
Chh Road ASSAM

INDIAN JOURNAL OF PURE & APPLIED PHYSICS

Published by
PUBLICATIONS & INFORMATION DIRECTORATE, CSIR
NEW DELHI
in association with
THE INDIAN NATIONAL SCIENCE ACADEMY, NEW DELHI

CSIR SCIENTIFIC PERIODICALS

JOURNAL OF SCIENTIFIC & INDUSTRIAL RESEARCH (Monthly)

With a fine record of over 45 years' service to the scientific community, this journal has grown into India's leading general science periodical. Intended to fulfil the responsibility of helping the research workers to keep themselves abreast of current developments in various fields of science and technology, the journal carries editorial features highlighting important scientific events in India and abroad, articles on science policy and management of science review articles on topics of current research interest, technical reports on international and national conferences, reviews of scientific and technical publications, and notes on major advances in various fields.

Annual subscription	Rs 120.00	$ 40.00	£ 23.00
Single copy	12.00	4.00	2.30

INDIAN JOURNAL OF CHEMISTRY (Monthly)

Section A: Started in the year 1963, the journal is devoted to papers in Inorganic, Physical, Theoretical and Analytical Chemistry.

Annual subscription	Rs 160.00	$ 53.00	£ 30.00
Single copy	16.00	5.30	3.00

Section B: This journal is devoted to papers in Organic Chemistry, including Medicinal Chemistry.

Annual subscription	Rs 160.00	$ 53.00	£ 30.00
Single copy	16.00	5.30	3.00

INDIAN JOURNAL OF PURE & APPLIED PHYSICS (Monthly)

Started in the year 1963, this journal is devoted to original research communications (full papers and short communications) in all conventional branches of physics (except radio and space physics).

Annual subscription	Rs 180.00	$ 60.00	£ 34.00
Single copy	18.00	6.00	3.40

INDIAN JOURNAL OF RADIO & SPACE PHYSICS (Bimonthly)

The journal, which is being published beginning from March 1972, is intended to serve as a medium for the publication of the growing research output in various areas of radio and space physics, such as ionospheric propagation, magnetosphere, radio and radar astronomy, physics and chemistry of the ionosphere; neutral atmosphere; airglow, winds and motion in the upper atmosphere; stratosphere-mesosphere coupling, ionosphere-magnetosphere coupling; solar-terrestrial relationship, etc.

Annual subscription	Rs 100.00	$ 34.00	£ 19.00
Single copy	20.00	6.80	3.80

INDIAN JOURNAL OF TECHNOLOGY (INCLUDING ENGINEERING) (Monthly)

This journal publishes papers reporting results of original research of applied nature pertaining to unit operations, heat and mass transfer, products, processes, instruments and appliances, etc. The journal is of special interest to research workers in departments of applied sciences in universities, institutes of higher technology, commodity research laboratories, industrial cooperative research institutes, and industrial research laboratories.

Annual subscription	Rs 120.00	$ 40.00	£ 23.00
Single copy	12.00	4.00	2.30

INDIAN JOURNAL OF EXPERIMENTAL BIOLOGY (Monthly)

This journal, devoted to the publication of research communications in the fields of experimental botany, zoology, microbiology, pharmacology, endocrinology, nutrition, etc., is the only one in India with such a wide coverage and scope.

Annual subscription	Rs 180.00	$ 68.00	£ 34.00
Single copy	18.00	6.80	3.40

INDIAN JOURNAL OF BIOCHEMISTRY & BIOPHYSICS (Bimonthly)

This journal, published in association with the Society of Biological Chemists (India), Bangalore, is the only research journal in India devoted exclusively to original research communications in biochemistry and biophysics.

Annual subscription	Rs 65.00	$ 23.00	£ 12.00
Single copy	13.00	4.60	2.40

INDIAN JOURNAL OF MARINE SCIENCES (Quarterly)

Commencing publication from June 1972, this journal is devoted to research communications (full papers and short communications) pertaining to various facets of marine research, viz. biological, physical, geological and chemical oceanography.

Annual subscription	Rs 90.00	$ 30.00	£ 17.00
Single copy	26.00	8.70	5.00

RESEARCH AND INDUSTRY (Quarterly)

Intended to serve as a link between science and industry, this journal is addressed primarily to technologists, engineers, executives and others in industry and trade. It publishes informative original articles containing practical details of processes and products devoted in India, which show promise of ready utilization, and technical digests on new processes, products, instruments and testing methods which are of interest to industry. Developments in Indian industry are regularly reported.

Annual subscription	Rs 70.00	$ 23.00	£ 13.00
Single copy	22.00	7.00	4.00

INDIAN JOURNAL OF TEXTILE RESEARCH (Quarterly)

Commencing publication from March 1976, this journal is devoted to the publication of papers reporting results of fundamental and applied researches in the field of textiles.

Annual subscription	Rs 50.00	$ 17.00	£ 10.00
Single copy	15.00	5.00	3.00

MEDICINAL & AROMATIC PLANTS ABSTRACTS (Bimonthly)

Carries informative abstracts of scientific papers published in important Indian and foreign journals relating to different aspects of medicinal and aromatic plants. Each issue contains about 350 abstracts with a subject index.

Annual subscription	Rs 120.00	$ 40.00	£ 23.00
Single copy	24.00	8.00	4.60

INDUSTRIAL NEWS DIGEST (Monthly)

Provides technical and techno-economic information for industrialists, prospective entrepreneurs and experts in both government and private agencies dealing with the management and planning of industry. Each issue carries at least one profile on a particular industry.

Annual subscription	Rs 40.00	$ 13.00	£ 8.00
Single copy	4.00	1.30	0.80

CURRENT LITERATURE ON SCIENCE OF SCIENCE (Monthly)

Carries abstracts, digests, book reviews, news & notes and R&D statistics with emphasis on problems of S&T in developing countries, it also covers the areas of science policy, R&D planning and management, technology transfer, technology assessment and science and society.

Annual subscription	Rs 100.00	$ 30.00	£ 12.00

Please contact

Manager (Sales & Advertisement)
PUBLICATIONS & INFORMATION DIRECTORATE, CSIR
Hillside Road, New Delhi-110012

RENEWAL NOTICE

Your subscription which expires with the despatch of December 1983 issue of the journal, stands for renewal. We request you to be so good as to return the enclosed order form duly filled early, so as to ensure continuity in despatch.

Manager (Sales & Advertisement)

DATED:

The Manager (Sales & Advertisement)
PUBLICATIONS & INFORMATION DIRECTORATE
HILLSIDE ROAD, NEW DELHI-110012 (INDIA)

Dear Sir,

Please renew my subscription/enrol me as subscriber to:

			Rs.	$	£
1	Journal of Scientific & Industrial Research	(Monthly)	120.00	40.00	23.00
2	Indian Journal of Chemistry, Section A	(Monthly)	160.00	53.00	30.00
3	Indian Journal of Chemistry, Section B	(Monthly)	160.00	53.00	30.00
4	Indian Journal of Experimental Biology	(Monthly)	180.00	68.00	34.00
5	Indian Journal of Technology	(Monthly)	120.00	40.00	23.00
6	Indian Journal of Pure & Applied Physics	(Monthly)	180.00	60.00	34.00
7	Indian Journal of Biochemistry & Biophysics	(Bimonthly)	65.00	23.00	12.00
8	Indian Journal of Radio & Space Physics	(Bimonthly)	100.00	34.00	19.00
9	Indian Journal of Marine Sciences	(Quarterly)	90.00	30.00	17.00
10	Indian Journal of Textile Research	(Quarterly)	50.00	17.00	10.00
11	Research & Industry	(Quarterly)	70.00	23.00	13.00
12	Current Literature on Science of Science	(Monthly)	100.00	30.00	12.00
13	Medicinal & Aromatic Plants Abstracts	(Bimonthly)	120.00	40.00	23.00
14	Industrial News Digest	(Monthly)	40.00	13.00	8.00

(Please tick off the periodicals you would like to subscribe).

for one year from January 1984 for which I/we have remitted to you a sum of Rs .....£ ..... $ ..... by Cheque/Demand Draft No. ..... dated ..... in favour of PUBLICATIONS & INFORMATION DIRECTORATE, NEW DELHI.

COMPLETE MAILING ADDRESS

Name .....

Address .....

Country/State .....

(Signature)

Note:
1. Subscribers at annual rates for all the periodicals are enlisted for the full volumes, i.e. for the period from January to December only.
2. The Cheque/Demand Draft may plese be drawn in favour of "PUBLICATIONS & INFORMATION DIRECTORATE, NEW DELHI". Banking charges shall be borne by the subscriber. For inland outstation cheques please add Rs. 3.50. For foreign cheques please add $ 1.00 or £ 0.45.
3. The supply will commence on receipt of subscription in advance.

Indian Journal of Pure & Applied Physics

EDITORIAL BOARD

Prof. D Basu
Indian Association for the Cultivation of Science
Calcutta

Prof. Probir Roy
Tata Institute of Fundamental Research
Bombay

Prof. B Buti
Physical Research Laboratory
Ahmedabad

Prof. E S Raja Gopal
Indian Institute of Science
Bangalore

Prof. S C Dutta Roy
Indian Institute of Technology
New Delhi

Prof. G Rajasekaran
Madras University
Madras

Dr R Hradaynath
Instruments Research & Development Establishment Dehra Dun

Dr A P B Sinha
National Chemical Laboratory
Pune

Prof. D Premaswarup
Nagarjuna University
Nagarjuna Nagar

Prof. C V Vishveshwara
Raman Research Institute
Bangalore

Prof. A N Mitra
Indian National Science Academy
New Delhi/University of Delhi
Delhi

Prof. M S Sodha
Indian National Science Academy
New Delhi/Indian Institute of Technology New Delhi

Shri Y.R. Chadha, Editor-in-Chief, *Ex-officio* Secretary

EDITORIAL STAFF

Editors

D S Sastry, K S Rangarajan & R P Goel

Assistant Editors

G N Sarma, J B Dhawan & Tarun Banerjee

Scientific Assistant

(Mrs) Poonam Bhatt

Published by the Publications & Information Directorate, CSIR, Hillside Road, New Delhi 110012
Editor-in-Chief : Y R Chadha

The Indian Journal of Pure & Applied Physics is issued monthly. The Directorate assumes no responsibility for the statements and opinions advanced by contributors. The editorial staff in its work of examining papers received for publication is assisted, in an honorary capacity, by a large number of distinguished scientists, working in various parts of India.

Communications regarding contributions for publication in the journal should be addressed to the Editor, Indian Journal of Pure & Applied Physics, Publications & Information Directorate, Hillside Road, New Delhi 110012.

Correspondence regarding subscriptions and advertisements should be addressed to the Sales & Distribution Officer, Publications & Information Directorate, New Delhi 110012.

Annual Subscription
Rs. 120.00 £20.00 $45.00

Single Copy
Rs. 12.00 £2.00 $4.50

50% Discount is admissible to research workers and students and 25% discount to non-research individuals, on annual subscription. Payments in respect of subscriptions and advertisements may be sent by cheque, bank draft. money order or postal order marked payable *only* to **Publications & Information Directorate, New Delhi 110012.** Claims for missing numbers of the journal will be allowed only if received within 3 months of the date of issue of the journal plus the time normally required for postal delivery of the journal and the claim.

© 1983 The Council of Scientific & Industrial Research, New Delhi.

Errata

Paper entitled, "Spatial Correlation & Thermal Compressibility in Interacting Bosons at Low Temperatures" by A N Phukan & P N Bora, Vol 21 September 1983, p. 527, Table 2, column headings and first row of data

As given:

T, K	χ_T, cm^2/dyn	$F(=kT\chi_T)$
2.2	95.0×10^{-13}	-288.42×10^{-13}

To be read as:

T, K	χ_T, cm^2/dyn	$F(=kT\chi_T) \times 10^{16}$
2.2	-95.0×10^{-13}	-288.42×10^{-13}

Indian Journal of Pure & Applied Physics

VOLUME 21 NUMBER 11 NOVEMBER 1983

CONTENTS

Solid State Physics

Thermoluminescence of Quartz: Part XI—Natural & Radiation-Induced Colouration 619
M David

Specific Heat of Praseodymium & Neodymium 623
J V S S Narayana Murthy & R Ramji Rao*

Optical Absorption & Thermoluminescence of Gd- & Sm-doped CaF_2 Single Crystals Irradiated with X-rays 627
R K Chaudhary, A V Krishna Rao & K V Rao*

Resonance Phenomena

EPR of Mn^{2+} in $Cs_2Zn(SeO_4)_2.6H_2O$ and $(NH_4)_2Fe(SeO_4)_2.6H_2O$ Single Crystals ... 631
S K Yadav, V P Seth* & R K Malhotra

^1H NMR & EPR Studies on Copper Complexes: $Cu(Pyrazole)_2Br_2.H_2O$ & $Cu(Benzoxazole)_2Br_2.2H_2O$ 635
K V G Reddy, K V Chary, B A Sastry*, G Ponticelli & R Pinna

Mathematical & Theoretical Physics

Non-Abelian Gauge Theory of Fields Associated with Dyons for Non-zero Mass System 638
B S Rajput, Satyaraj Kumar & O P S Negi*

Meson Spectroscopy for the Superposition of Linear-cum-Logarithmic Potential with a Modified Coulomb Potential 644
Anuradha Bhargava & L K Sharma*

Superluminal Lorentz Transformations in Six-Dimensional Space-Time 651
H C Chandola* & B S Rajput

NOTES

Thermoluminescence of Quartz: Part X—Pre-dose Sensitization Used to Evaluate the Crystallization Temperature 659
M David* & C M Sunta

A Study of Indium Phosphide Single Drift and Double Drift Avalanche Diodes from Computer Analysis of Field and Current Profiles 661
J P Banerjee, S P Pati & S K Roy*

Growth of Sb_2S_3 Films by Solution-Gas Interface Technique 665
S H Pawar*, (Miss) Shobha Tamhankar, P N Bhosale & M D Uplane

Photoionization of Deep Energy Levels in $Ga_{1-x}Al_xAs$ Alloys 668
Ashok K Saxena* & A K Sinha

HOMO & LUMO Energy Values for Bases of Nucleic Acids 670
K B Lal, V K Agarwal, A K Srivastava* & B Krishna

Continued overleaf

CONTENTS

Effect of Environment in Hypersensitive Transitions of Nd^{3+} Ternary Complexes ... 672
Anup K Gupta & M P Bhutra*

Spectral Study of Ternary Complexes of Rare Earths with Different Amino Acids ... 674
M P Bhutra* & Anup K Gupta

Spectra & Species of Fluorescein & 6-Hydroxy-9-Phenyl Fluoron in Frozen Solutions 677
J Shah*, N B Joshi & D D Pant

Vibrational Analysis of Some Axially Symmetric XYZ_3-type Molecules 680
S Mohan* & T J Bhoopathy

---

*The author for correspondence is indicated by (*) mark in case of papers with more than one author

Indian Journal of Pure & Applied Physics
Vol. 21, November 1983, pp. 619-622

Thermoluminescence of Quartz: Part XI—Natural & Radiation-Induced Colouration

M DAVID
Health Physics Division, Bhabha Atomic Research Centre,
Bombay 400 085

Received 5 *August* 1982

The rate of radiation-induced darkening in quartz sample depends on the amount of Al impurity concentration in the crystal. Different natural samples were tested for their absorbance (darkening) due to radiation exposure. Maximum rate of darkening was observed in a sample that had the highest concentration of Al impurity. It is shown that darkening induced by ionizing radiation is due to the trapping of holes at Al^{3+} substitutional sites and the consequent rejection of the compensating ion. It is also shown that a different type of centre is responsible for the natural smoky colour, even though, both (natural and radiation-induced) smoky colours originated from the substitutional Al in the crystal lattice.

1 Introduction

Quartz is one of the purest minerals[1] found in nature with total impurity contents rarely exceeding 0.1%. Analysis[2] of the optical spectrum of divalent cobalt (Co^{2+}) in synthetic blue quartz showed that this ion occupies interstitial positions of distorted tetrahedral symmetry of the crystal while the divalent ion (Fe^{2+}) in quartz occupies[3] the distorted octahedral positions. Substitutional incorporation of an impurity ion has been well demonstrated[4] for Al^{3+}, Fe^{3+}, Ti^{4+} and Ge^{4+}. It is also known that the most common impurity[5-8] in natural quartz is Al^{3+} which is found substituted at Si sites. The smoky colour induced by ionizing radiations in quartz is mainly attributed to these types of centres. This paper deals with the role of impurity in the crystal on the TL sensitivity of natural mineral-quartz.

2 Experimental Procedure

Natural quartz samples were crushed to powder (100 'Tyler' mesh) and used for recording TL glow curves. Five mg of the sample was used in each reading and the heating rate used was 60°C per min. Oxygen-free nitrogen atmosphere was maintained during the TL measurements over the sample to avoid tribo-luminescence. Irradiation of these samples was done using a Co-60 gamma source and a standard tungsten lamp was used as a light source during the transparency tests of the crystals.

3 Results

A natural pink quartz (Q13) was used for the following experiments. Aliquots of 5 mg sample were taken and each of them was given different gamma exposures up to 10^7 rad. These irradiated samples were used for recording the glow curves. It is observed that for lower doses only, the first glow peak (87°C) was prominent, and therefore, the peak height of the 87°C peak is plotted against the corresponding exposure in Fig. 1.

It is observed that the 87°C peaks grow supra-linear in the initial stage and at a dose above 10^5 rad, the growth follows a sub-linear pattern. It is also observed that the structure of the glow curve and that of emission spectra depend on the amount of exposure. The glow curves and emission spectra of four representative samples of the lot are shown in Fig. 2.

In another experiment, four natural quartz crystals [milky quartz (Q3A), transparent quartz (Q4), smoky quartz (Q8B) and pink quartz (Q13)] were cut perpendicular to their *c*-axes and plates of 3 mm

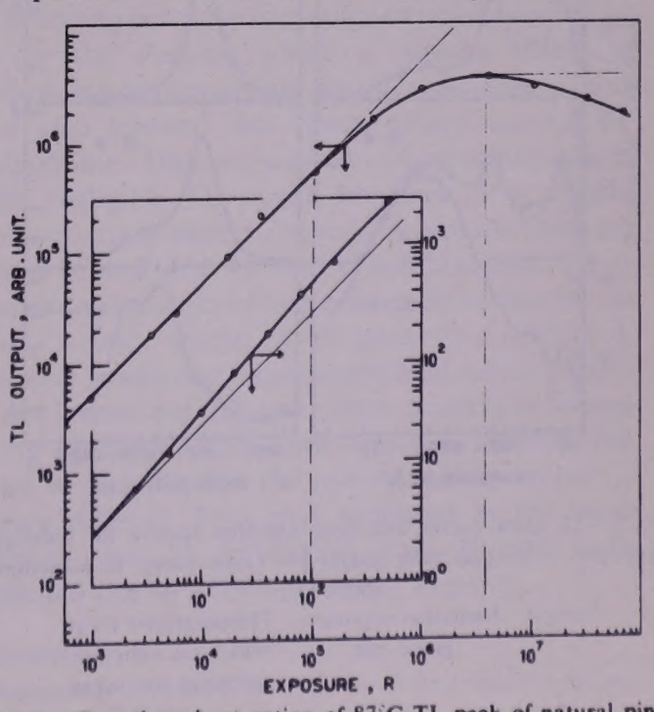

Fig. 1—Growth and saturation of 87°C TL peak of natural pink quartz [Note: (i) Supra-linear growth up to an exposure of 2×10^2 rad; (ii) linear growth between 2×10^2 rad and 10^5 rad and (iii) growth, saturation and reduction at exposures above 10^5 rad)

thickness were obtained. These were optically polished and used for the experiments. The polished plates were buried in a crucible of quartz powder (to avoid cracks due to thermal shock during heating) and heated up to 400°C in a muffle furnace to remove the natural colour. These plates were again irradiated to different doses up to 10^6 rad. It was observed that a smoky colour was induced during irradiation. Effect of this colouration on the transparency was tested using a tungsten lamp. A plot of the darkening (absorbance) against the radiation exposure is shown in Fig. 3 for the four natural samples. Analysis of these samples for Al-impurity was also done. The results are shown in Table 1 of the earlier paper (Part X) of this series (published in this issue of the journal).

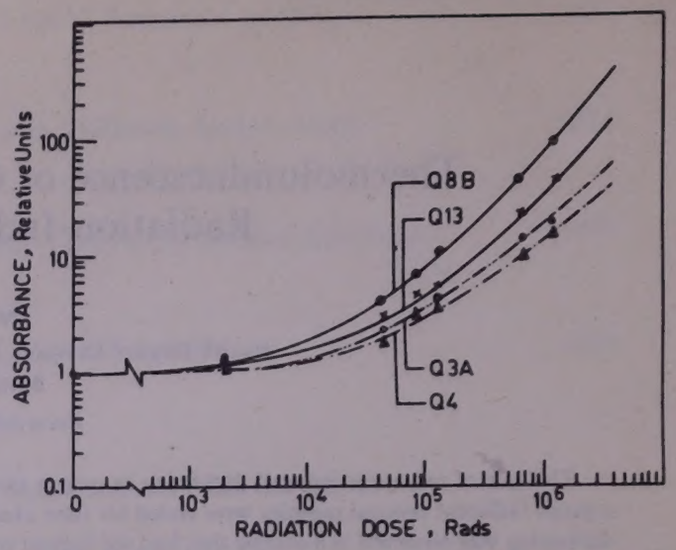

Fig. 3—Absorbance (total light) versus radiation dose in four different natural quartz samples [Q4, Transparent; Q3A, milky (massive); Q13, pink; Q8B, smoky]

4 Discussion

In an unirradiated quartz, Al^{3+} is found substituted at Si sites. The smoky colour[9] found in natural quartz and the colour produced during irradiation[10] are the effects of these Al centres. Because Al^{3+} is situated in a Si^{4+} site, there is a tendency for these defects to achieve the charge compensation by substituting a nearby +ve ion (H^+, Li^+, Na^+, etc.) from the open channel along the *c*-axis. The centres associated with Al-impurity vary in their characteristics depending upon the charge compensator.

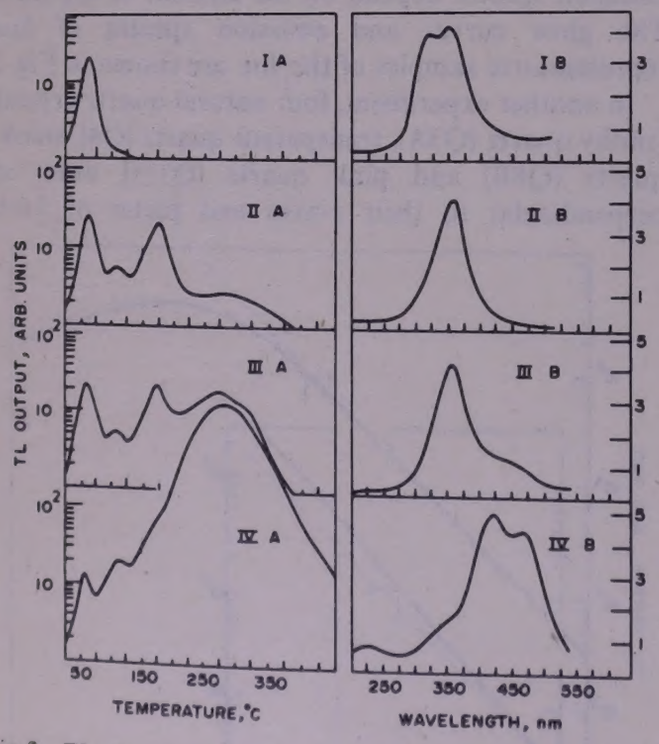

Fig. 2—TL glow curves and their emission spectra for different exposures in natural pink quartz [A, Glow curve; B, Emission-spectrum]

Sample	Radiation exposure given, rad	Temperature (°C) at which the emission spectrum was taken
I	1×10^2	50
II	2×10^4	150
III	2×10^6	150
IV	1.1×10^7	150

When the gamma ray impinges on the crystal, the primary interactions result in the formation of free electrons and an equal number of free holes. Most of these undergo recombination. These charge carriers can also be trapped at any defect site available in the lattice.

The trapped charge carriers can alter the stability of the existing defects. Trapping a hole at Al^{3+} substitutional site in quartz weakens the bond of the compensating ion at its site in the open channel along *c*-axis. This can help the formation of a new trapping centre.

It is known[11] that there can be a backward reaction too, during irradiation. The hole trapped at Al^{3+} can recombine with an ionization electron, thus leaving an uncompensated Al^{3+}. This state will again favour the return of the compensating positive ion (which formed the new trapping centre) back to the site. This will disturb the newly-formed trapping centre. These two reactions are continuously taking place in the crystal lattice during irradiation. Thus the resultant reaction will cause the colouration of the crystal.

In the initial stage of irradiation, the rate of formation of trapping centres is more by replacing the charge compensating +ve ion by a hole than by the annihilation of the newly-formed centres. The experimental observation also shows that in the initial stage, the TL peaks grow supra-linear with irradiation (corresponding to the creation of trapping centres) and after saturation rapidly reduce their intensity (corresponding to the annihilation of newly-formed trapping centre by backward reaction) (see Fig. 1). The saturation in the growth curve depends mainly on the trap and recombination centres. In quartz, the recombination centres are not affected by heavy

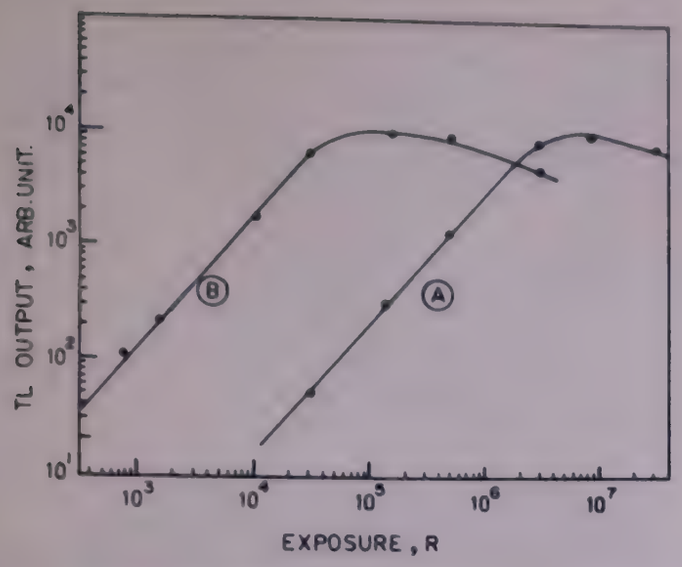

Fig. 4—Growth and saturation of TL (integrated) in natural pink quartz [(A). Virgin sample heated at 400°C for 90 min; (B), virgin sample + 10^7 rad + heated at 400°C for 90 min]

irradiation. The experimental evidence for this is shown in Fig. 4 where growth curves of both the natural and radiation-sensitized (after an exposure of 10^7 rad) samples are given. The TL saturation intensities are the same for both the samples while the relative intensity differs at the same dose. Because of the changed trap conditions (due to the disturbed state of the newly-formed trapping centres on heavy irradiation), the number of charge carriers in the traps are more at lower doses and hence yield more TL.

Development of a new peak at about 250°C and the structural variations in the emission spectra and glow curves on heavy irradiation[1,2] (see Fig. 2) could be attributed to the disturbance produced in the lattice due to heavy irradiation. In a sample which is irradiated to a small dose, concentration of these disturbed centres is less and thus we do not see clear variations in the structure of glow curve and emission spectra.

The induction of smoky colour in the natural quartz starts only after a heavy dose of 10^3-10^4 rad which corresponds to the annihilation of the newly-formed trapping centres (cf. Fig. 3). The rate of darkening in a crystal is observed to depend on the amount of Al impurity present in the crystal lattice. Maximum concentration of Al was observed in smoky quartz and the maximum darkening rate was also observed in the same sample.

The variations in the TL characteristics of a natural smoky quartz when heated are shown in Fig. 5. In smoky quartz, the natural TL peak appears at 250°C. When irradiated, the virgin sample shows prominent peaks at 115, 200 and 250°C. But when the sample is heated, the glow curve structure itself changes showing prominent peaks at 80 and 165°C. But the peaks at 115 and 250°C have almost disappeared. The glow peaks at

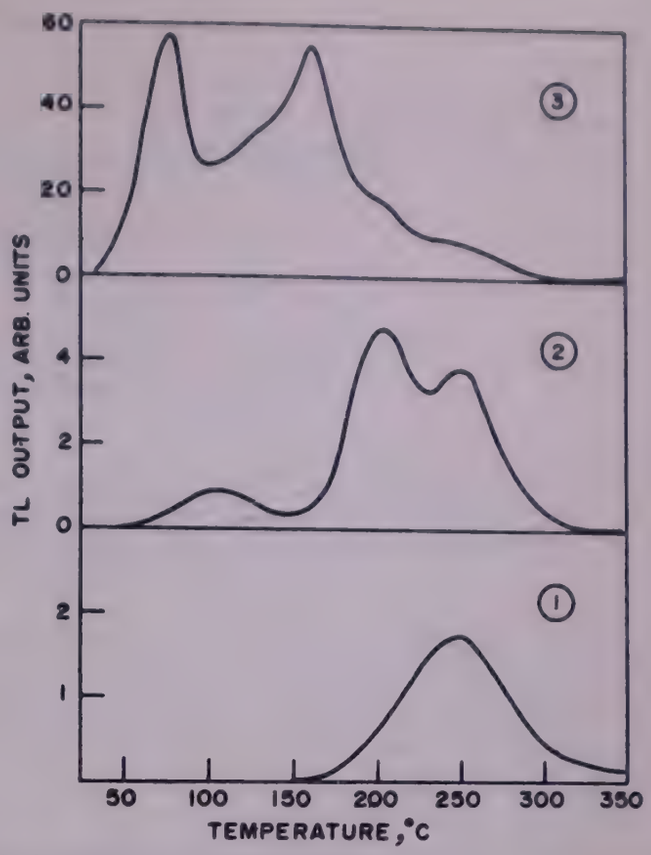

Fig. 5—Structural variations in TL glow curve of natural smoky quartz (Q8B) [(1) Virgin sample, (2) virgin sample + 4.2×10^4 rad, (3) virgin sample + 400°C for 90 min + 4.2×10^4 rad]

80 and 165°C are created or enhanced due to the effect of the heat-treatment on the colour centre patterns. The changes in the glow curve pattern due to heating are not observed for any other quartz sample except for smoky quartz.

The smoky colour in natural quartz is known[13] to be due to the electron which is missing from the nonbonding oxygen orbital near Al substitutional site. It is also known[8] that these colour centres are nonluminous. Thus, we see that natural smoky quartz yields negligible TL signal. Moreover, if a natural smoky quartz is heated, the missing electron from the oxygen orbital near to the Al substitutional site is compensated and the colour centre responsible for the natural smoky colour is permanently annihilated. Again, on irradiation, these annihilated colour centres are not formed but different colour centres are formed during irradiation (discussed earlier). Therefore, the centre responsible for the natural smoky colour is entirely different from that produced in the same specimen due to irradiation even though both originated due to Al substitutional impurity.

References

1 Bampaur H J, *Schweiz Mineral Petrogr Mitt (Switzerland)*, **41** (1961) 335.
2 Lehman G, *J Phys & Chem Solids (GB)*, **30** (1969) 395
3 Lehman G, *Z Naturforsch (Germany)*, **22a** (1967) 2080.
4 Lehman G, *Phys Kondens Mater (Germany)*, **13** (1971) 297

5 O'Brien M C M, *Proc R Soc London Ser A (GB)*, **231** (1955) 404.
6 Cohen A J, *Am Min (USA)*, **43** (1958) 48.
7 Kreft G B, *Radiat Eff (GB)*, **26** (1975) 249.
8 Yong Lee H, *J Appl Phys (USA)*, **39** (1968) 4850.
9 Taylor A L, *Can J Phys (Canada)*, **42** (1964) 595.
10 Ritter C J, *Am Min (USA)*, **51** (1966) 220.
11 Mattern P L, *Radiat Eff (USA)*, **26** (1975) 237.
12 David M & Sunta C M, *Indian J Pure & Appl Phys*, **16** (1978) 423.
13 Dennen W H & Blackburn W H, *Contrib Mineral Petrol (Germany)*, **27** (1970) 332.

Indian Journal of Pure & Applied Physics
Vol. 21, November 1983, pp. 623-626

Specific Heat of Praseodymium & Neodymium

J V S S NARAYANA MURTHY
Department of Physics, Sri Ramachandra Arts & Science College, Kothagudem 507 118
&
R RAMJI RAO
Department of Physics, Indian Institute of Technology, Madras 600 036

Received 6 *November* 1982

The elements of the dynamical matrix of an ideal dhcp lattice, with nearest neighbour central interactions, have been obtained in a homogeneously strained state. The dispersion relations along the [0001] direction, on this model, have been presented for Pr and Nd. The frequency distribution function $g(\omega)$ is obtained and the lattice specific heat is calculated for Pr and Nd and the temperature variation of the equivalent Debye temperature is presented.

1 Introduction

The lighter rare earth elements preaseodymium and neodymium crystallize in the double hexagonal close packed (dhcp) structure with axial ratios equal to 3.223 and 3.226 respectively, which are very near to the ideal value 3.266. The theoretical expressions for the second order elastic (SOE) constants and third order elastic (TOE) constants of the ideal dhcp structure have been derived by Ramji Rao and Narayana Murty[1] using central interactions extending upto fourth neighbours. The Cauchy relation $C_{13}=C_{44}$ is nearly valid experimentally at all temperatures as can be seen from the data of Griener *et al*[2,3] for Pr and Nd. The ratio of the linear compressibilities $\chi_\parallel/\chi_\perp$ calculated from the room temperature SOE constants, gives the values 1.014 and 1.045 for Pr and Nd respectively. The ratio $\chi_\parallel/\chi_\perp$ is exactly unity for the ideal dhcp lattice with nearest neighbour central interactions. These facts indicate that the forces in these metals are mostly central in character and farther neighbour interactions may be neglected.

2 Theory

The dhcp structure has an ABAC...' stacking sequence of close packed planes. The unit cell contains four atoms, and the position vectors of these in the unit cell are as follows:

$$\begin{aligned}\mathbf{R}_1 &= D(0,0,0)\\ \mathbf{R}_2 &= D[1/\sqrt{3},0,(2/3)^{1/2}]\\ \mathbf{R}_3 &= D[0,0,2(2/3)^{1/2}]\\ \mathbf{R}_4 &= D[1/2\sqrt{3},1/2,3(2/3)^{1/2}]\end{aligned} \quad \ldots (1)$$

The unit cell is spanned by the vectors

$$\begin{aligned}\mathbf{a}_1 &= D(\sqrt{3}/2,\ -1/2,\ 0)\\ \mathbf{a}_2 &= D(0,1,0)\\ \mathbf{a}_3 &= D[0,0,4(2/3)^{1/2}]\end{aligned} \quad \ldots (2)$$

where D is the lattice parameter in the basal plane. This structure can be viewed as three interpenetrating sublattices A, B and C. The atoms at $\mathbf{R}_1$ and $\mathbf{R}_3$ belong to the sublattice A. The atoms at $\mathbf{R}_2$ and $\mathbf{R}_4$ respectively belong to the B and C sublattices. More details about the various neighbours of each atom are given in Appendix A of Ref. 1.

The potential energy of the crystal is expanded in terms of the change in the square of the interatomic distance $\Delta R^2\begin{pmatrix}0 & M\\ \lambda & \mu\end{pmatrix}$:

$$\varphi=\frac{1}{2}\left[\sum_{\lambda M\mu}\frac{1}{2}O''\varphi(R)(\Delta R^2)^2+\frac{1}{6}O'''\varphi(R)(\Delta R^2)^3+\ldots\right] \quad \ldots (3)$$

where O'' and O''' are the second and third derivatives of the potential energy respectively, evaluated at $R=D$, i.e.

$$O''=[(O')^2]_{R=D} \quad O'''=[(O')^3]_{R=D}$$

and $$O'=\frac{\partial}{\partial R^2} \quad \ldots (4)$$

Further λ and μ take values from 1 to 4.
The lattice is homogeneously strained by:

$$\eta_{xx}=\eta_{yy}=\tfrac{1}{2}\varepsilon';$$
$$\eta_{zz}=\varepsilon'' \text{ and } \eta_{ij}(i\neq j)=0 \quad \ldots (5)$$

where ε' is a uniform areal strain in the basal plane and ε'' is a uniform longitudinal strain along the unique axis. These strains do not create any internal strains[1] and hence do not violate the definitions of the thermal expansion coefficients. The elements of the dynamical matrix are obtained in the usual manner up to first order in the strains and are listed below:

$$\begin{aligned}D_{xx}(\mu,\mu)=\alpha(16-12\,C1\,C3)+4\varepsilon'\\ [\alpha(8-C2-5\,C1\,C3)\\ +\tfrac{1}{3}\xi(10-9\,C1\,C3)]+16\varepsilon''(\alpha+\tfrac{1}{3}\xi)\end{aligned}$$

$$D_{yy}(\mu,\mu) = 4\alpha(4-2C2-C1C3) + 4\varepsilon'[\alpha(8-3C2-3C1C3) + \tfrac{1}{3}\xi(10-6C2-3C1C3)] + 16\varepsilon''(\alpha+\tfrac{1}{3}\xi)$$

$$D_{zz}(\mu,\mu) = 16\alpha + 4\varepsilon'[\alpha(4-C2-2C1C3)+\tfrac{4}{3}\xi] + 16\varepsilon''(3\alpha+\tfrac{4}{3}\xi)$$

$$D_{xy}(\mu,\mu) = \tfrac{4}{3}S1\,S3[(1+\varepsilon')\alpha+\varepsilon'\xi] \quad \ldots (6)$$

$$RD_{xx}(1,2) = -\tfrac{4}{3}\alpha(C4+\tfrac{1}{2}C1\,C5) - 2\varepsilon'[(\alpha+\tfrac{2}{9}\xi)C4+(\alpha+\tfrac{1}{9}\xi)C1C5] - \tfrac{8}{3}\varepsilon''[(\alpha+\tfrac{2}{3}\xi)C4+(2\alpha+\tfrac{1}{3}\xi)C1\,C5]$$

$$RD_{yy}(1,2) = -2\alpha C1\,C5 - \tfrac{2}{3}\varepsilon'[\alpha C4+(5\alpha+\xi)C1\,C5] - \tfrac{8}{3}\varepsilon''[\alpha C4+(2\alpha+\xi)C1\,C5]$$

$$RD_{zz}(1,2) = -\tfrac{2}{3}(C4+2C1\,C5)[4\alpha+\varepsilon'(\alpha+\tfrac{4}{3}\xi) + 4\varepsilon''(3\alpha+\tfrac{4}{3}\xi)]$$

$$RD_{xy}(1,2) = -\frac{2}{\sqrt{3}}[\alpha+\varepsilon'(\alpha+\tfrac{1}{3}\xi)+\tfrac{4}{3}\varepsilon''\xi]S1\,S5$$

$$RD_{xz}(1,2) = \frac{4\sqrt{2}}{3}[\alpha+\varepsilon'(\tfrac{1}{2}\alpha+\tfrac{1}{3}\xi) + \varepsilon''(\alpha+\tfrac{1}{3}\xi)](C1\,C5-C4)$$

$$RD_{yz}(1,2) = \frac{4\sqrt{2}}{\sqrt{3}}[\alpha+\varepsilon'(\tfrac{1}{2}\alpha+\tfrac{1}{3}\xi) + \varepsilon''(\alpha+\tfrac{1}{3}\xi)]S1\,S5$$

$$RD_{xx}(2,3) = -\tfrac{4}{3}\alpha(C7+\tfrac{1}{2}C1\,C6) - 2\varepsilon'[(\alpha+\tfrac{2}{9}\xi)C7+(\alpha+\tfrac{1}{9}\xi)C1C6] - \tfrac{8}{3}\varepsilon''[(\alpha+\tfrac{2}{3}\xi)C7+(2\alpha+\tfrac{1}{3}\xi)C1\,C6]$$

$$RD_{yy}(2,3) = -2\alpha C1\,C6 - \tfrac{2}{3}\varepsilon'[\alpha C7+(5\alpha+\xi)C1\,C6] - \tfrac{8}{3}\varepsilon''[\alpha C7+(2\alpha+\xi)C1\,C6]$$

$$RD_{zz}(2,3) = -\tfrac{2}{3}(C7+2C1\,C6)[4\alpha+\varepsilon'(\alpha+\tfrac{4}{3}\xi) + 4\varepsilon''(3\alpha+\tfrac{4}{3}\xi)]$$

$$RD_{xy}(2,3) = 2S1\,S6[\alpha+\varepsilon'(\alpha+\tfrac{1}{3}\xi)+\tfrac{4}{3}\varepsilon''\xi]/\sqrt{3}$$

$$RD_{xz}(2,3) = \frac{4\sqrt{2}}{3}[\alpha+\varepsilon'(\tfrac{1}{2}\alpha+\tfrac{1}{3}\xi) + \varepsilon''(\alpha+\tfrac{4}{3}\xi)](C7-C1\,C6)$$

$$RD_{yz}(2,3) = \frac{4\sqrt{2}}{\sqrt{3}}[\alpha+\varepsilon'(\tfrac{1}{2}\alpha+\tfrac{1}{3}\xi) + \varepsilon''(\alpha+\tfrac{4}{3}\xi)]S1\,S6 \quad \ldots (7)$$

Here $RD_{ij}(\lambda\mu)$ is the real part of the $D_{ij}(\lambda\mu)$. The imaginary part of $D_{ij}(\lambda\mu)$ can be obtained from $RD_{ij}(\lambda\mu)$, by replacing C4, C5, C6 and C7 by S4, S5, S6 and S7 respectively, and S5 and S6 by $-$C5 and $-$C6 respectively in the above expressions. Also

$D_{ij}(1,3) = 0$;

$D_{ij}(1,4) =$ complex conjugate of $D_{ij}(1,2) = D_{ij}^{*}(1,2)$

$D_{ij}(2,4) = 0$;

$D_{ij}(3,4) = D_{ij}(2,3)$ ... (8)

Here

$C1 = \cos\pi q_2$;

$C2 = \cos 2\pi q_2$;

$C3 = \cos\pi(2q_1+q_2)$;

$$C4 = \cos\frac{2\pi}{3}(2q_1+q_2+\tfrac{3}{4}q_3);$$

$$C5 = \cos\frac{\pi}{3}(\tfrac{3}{2}q_3-\overline{2q_1+q_2});$$

$$C6 = \cos\frac{\pi}{3}(2q_1+q_2+\tfrac{3}{2}q_3);$$

$$C7 = \cos\frac{2\pi}{3}(\tfrac{3}{4}q_3-\overline{2q_1+q_2}) \quad \ldots (9)$$

and S1 → S7 are the corresponding sine functions.

$$\alpha = \frac{D^4}{V_a}[O^{\parallel}\varphi(R)]_{R=D}$$

$$\xi = \frac{D^6}{V_a}[O^{\parallel\parallel}\varphi(R)]_{R=D} \quad \ldots (10)$$

3 Dispersion Relations Along [0001] Direction

The harmonic parameter α is obtained from the average of the values of C_{11} and C_{33}. The value of α for Pr is 0.26×10^{11} dyne/cm^2 and for Nd it is 0.282×10^{11} dyne/cm^2. V is the unit cell volume. The theoretical SOE constants calculated using the expressions given in Ref. 1 are presented in Table 1 for Pr and Nd. The experimental values of Griener *et al.*[2,3] are also given for comparison. Except for C_{12}, the agreement between the theory and experiment is good in both Pr and Nd. C_{12} goes off by about 20% in both cases.

Along [0001] direction, the 12×12 determinant factorises into three 4×4 determinants. Out of the three, two determinants yield doubly degenerate transverse modes. The dispersion relations (along the [0001] direction) are calculated for Pr and Nd on the present model and are presented in Fig. 1. The maximum frequency in both the cases is less than 2×10^{13} Hz.

4 Frequency Distribution Function and Specific Heat

The secular determinant is solved at 84 points of the irreducible volume of the Brillöuin zone, to obtain the normal mode frequencies. Taking multiplicity factors into account, this amounts to 12,000 frequencies. Using these, the frequency distribution function $g(\omega)$ is obtained by the root sampling technique. The width of

Table 1—Second Order Elastic Constants of Pr and Nd in 10^{11} dyne/cm^2

	Pr		Nd	
C_{ij}	Theory	Exp	Theory	Exp
C_{11}	5.113	4.935	5.546	5.482
C_{12}	1.82	2.295	1.974	2.462
C_{13}	1.387	1.43	1.504	1.660
C_{33}	5.547	5.74	6.016	6.086
C_{44}	1.387	1.36	1.504	1.504

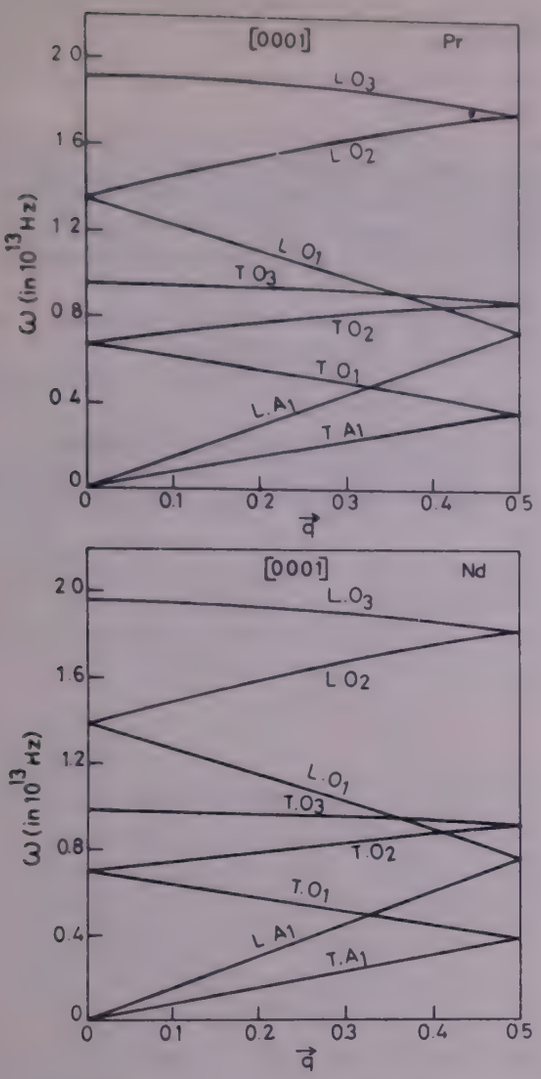

Fig. 1—Lattice dynamics of Pr and Nd along [0001] direction on the present model

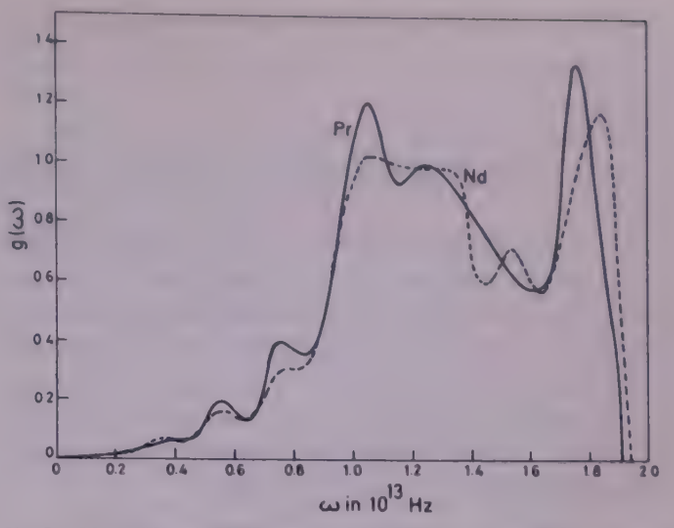

Fig. 2—Normalized frequency distribution function of praseodymium and neodymium

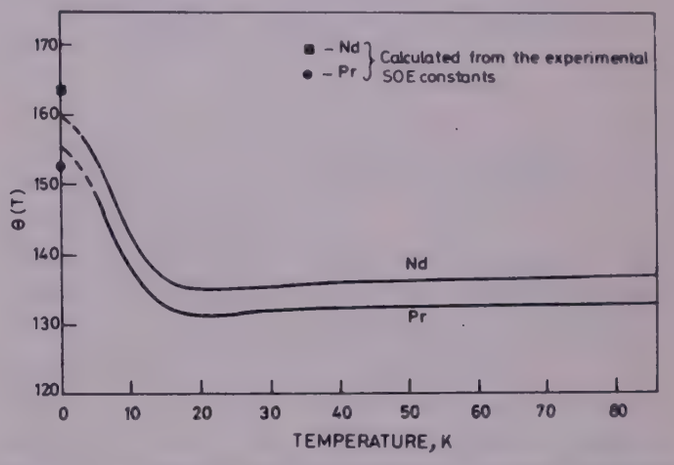

Fig. 3—Temperature variation of Debye θ for Pr and Nd on the present model

Table 2—Even Moments of the Frequency Distribution Function, μ and θ_∞ for Pr and Nd

	μ_2 $\times 10^{-26} s^2$	μ_4 $\times 10^{-52} s^4$	μ_6 $\times 10^{-78} s^6$	θ_∞	
				Theory	Ref. 6
Pr	1.823	4.154	10.791	133	138
Nd	1.927	4.641	12.744	137	148±8

the interval used in the sampling procedure is 0.1 $\times 10^{13}$ Hz. The normalized frequency distribution function is shown in Fig. 2 for Pr and Nd. The even moments of the frequency distribution function μ_2, μ_4, μ_6 are evaluated. The high temperature limit of the Debye θ is calculated using μ_2. The results are shown in Table 2 for Pr and Nd.

The lattice specific heat is calculated using the frequency distribution function, $g(\omega)$, as

$$C_v^l = 3R \int_0^{\omega_{max}} \sigma(\omega, T) g(\omega) d\omega$$

where R is the gas constant and $\sigma(\omega, T)$ is the Einstein's specific heat function. The theoretical lattice specific heat is converted into its equivalent Debye θ and is presented in Fig. 3 for Pr and Nd as a function of temperature. Both Pr and Nd exhibit magnetic ordering at low temperatures. The magnetic contribution to the total specific heat is to be separated out to obtain the lattice specific heat from the experimental data. Hence, it is not possible to compare the present results with experimental values.

5 Discussion

The longitudinal-A_1 and longitudinal-O_1, transverse-A_1 and transverse-O_1 branches in these dhcp metals look similar to those in the hcp metals. Both Pr and Nd exhibit nearly identical dispersion relations in the [0001] direction since the lattice is treated as ideal with nearest-neighbour central interactions.

It will be of interest of compare the ideal nearest-neighbour (n-n) dhcp lattice with the ideal n-n hcp lattice. In the ideal hcp lattice, $C_{144} = C_{155}$ though this is not a Cauchy relation and the low-temperature limits $\bar{\gamma}_{\|}(-3)$ and $\bar{\gamma}\ (-3)$ are equal[4,5]. Both these are not true in the case of an ideal dhcp lattice. The difference in the stacking sequence gives rise to

different internal strains and these are responsible for the different results. The moment one goes to farther neighbours, the differences will become apparent, because the number of neighbours and neighbour-distances are different in the two lattices (hcp and dhcp).

The high-temperature limit of the Debye θ agrees well with the value quoted by Gschneidner[6] for Pr and Nd, as seen from Table 2. The generalized Grüneisen parameters and hence the temperature deperature dependence of the effective lattice Grüneisen functions are calculated for Pr and Nd and the results have been presented at the Eighth International Thermal Expansion Symposium, NBS; USA[7].

References

1 Ramji Rao R & Narayana Murthy J V S S, *Physica (Netherlands)*, **B96** (1979) 194.

2 Griener J D, Schiltz R J (Jr), Tonnies J J, Spedding F H & Smith F, *J Appl Phys (USA)*, **44** (1973) 3862.

3 Griener J D, Schlader D M, Mc Masters O D, Gschneidner K A & Smith J F, *J Appl Phys (USA)*, **47** (1976) 3427.

4 Ramji Rao R & Srinivasan R, *Phys Status Solidi (Germany)*, **29** (1968) 865.

5 Srinivasan R & Ramji Rao R, *Inelastic scattering of neutrons*, Vol. 1, (IAEA, Vienna) 1965, 325.

6 Gschneidner K A (Jr), *Solid state physics*, (Academic Press, New York), Vol. 16, 1964, 414.

7 Narayana Murthy J V S S, Ramji Rao R & Ramanand A, *Proc. of the Eighth international thermal expansion symposium*, (Plenum Press, New York; NBS Maryland, USA) 1981.

Indian Journal of Pure & Applied Physics
Vol. 21, November 1983, pp. 627-630

Optical Absorption & Thermoluminescence of Gd- and Sm-doped CaF_2 Single Crystals Irradiated with X-rays

R K CHAUDHARY, A V KRISHNA RAO & K V RAO
Department of Physics, Indian Institute of Technology, Kharagpur 721 302

Received 3 *January* 1983; *revised received* 7 *June* 1983

Optical absorption measurements carried out on CaF_2 : Gd (0.2 mol%) show that it exhibits an absorption band at 272 nm. X-ray irradiation seems to remove this band but produces two absorption bands at 370 and 540 nm, the absorption in these bands increasing with X-ray dosage. CaF_2 : Sm (0.2 mol%) shows absorption bands at 240, 300, 412 and 630 nm. X-ray irradiation increases the absorption in these bands except in 412 nm which decreases with X-ray dosage. Partial thermal bleaching experiments bring out interesting changes in the absorption bands; when the X-ray-irradiated CaF_2 : Gd and CaF_2 : Sm are heated to 300°C, these crystals seem to attain their original absorption characteristics. Thermoluminescence light output of these samples irradiated with X-rays shows peaks at 107, 177 and 277°C for CaF_2 : Gd and at 100, 152 and 244°C for CaF_2 : Sm. An attempt is made to explain these results.

1 Introduction

As rare earth (RE)-doped CaF_2 is useful as a laser material, some work is being carried out in recent years on the optical absorption and thermoluminescence (TL) on various RE-doped CaF_2 crystals (irradiated with X-rays) yielding valuable information[1-3]. Merz and Pershan[4], studying the optical absorption and TL spectral characteristics of RE-doped CaF_2 irradiated below room temperature (RT) by X-rays and γ-rays, suggested that the RE ions in CaF_2 can be reduced from the trivalent to the divalent state; again conversion of divalent to trivalent ions was found to take place by warming these samples. Becker *et al.*[5] investigated the thermoluminescence of CaF_2 : Sm, irradiating the solid at low temperature with X-rays or UV radiation. They concluded that the mechanisms for TL emission with these two types of irradiation are different. It is found that the TL pattern of RE-doped CaF_2 is practically independent of the doped ion. Mostly, the reported work is in the low temperature region (liquid nitrogen temperature to about 100°C)the irradiation of doped CaF_2 being also done at low temperatures (LT). Interesting information seems to be obtained when RE-doped CaF_2 is irradiated with X-rays at RT and its optical absorption studied at RT and after partial thermal bleaching of the samples at high temperatures. So the aim of this paper is to present such data of our work on the optical absorption and TL of Gd- or Sm-doped (0.2 mol % in each case) CaF_2 single crystals irradiated with X-rays at RT ($\approx$30°C).

2 Experimental Details

The Gd- or Sm-doped CaF_2 (each doping is 0.2 mol %) crystals along with the specification of doping were obtained from Harshaw Chemical Company, USA. Samples were cut from the boules and optically polished, their final dimensions being 1 cm in diameter and 0.1 cm in thickness.

The samples were exposed to X-rays for the mentioned time (half the time on each side) keeping them at a distance of 2 cm from the window of a Machlett tube run at 35 kV and 10 mA.

Optical absorption measurements were taken on a Beckman model 26 spectrophotometer in the wavelength region 200-800 nm. TL glow peaks were recorded with an Esterline Angus recorder using a conventional set-up[6]. The heating rate was 0.5°C/sec.

3 Results

The optical absorption of Gd- and Sm-doped CaF_2 (0.2 mol % in each case) crystals before and after X-ray irradiation is shown in Figs 1 and 2 respectively. In both the samples, the absorption in the low wavelength region is moderately large (the absorption coefficient α is about 6 cm^{-1} at 200 nm). CaF_2 : Gd (0.2 mol %) exhibits an absorption band at 272 nm. X-ray irradiation seems to remove this band but produces two absorption bands at 370 nm and 540 nm; the absorption in these two bands increases with time of X-ray irradiation (i.e. X-ray dosage) tending to saturation at larger dosages.

CaF_2 : Sm (0.2 mol %) before X-ray irradiation shows a number of absorption bands with peaks at 240, 300, 412 and 630 nm. X-ray irradiation increases the absorption in these bands except in 412 nm which seems to gradually decrease and disappear at an X-ray irradiation time of 3 hr.

Figs 3 and 4 present the thermal bleaching characteristics of the absorption bands of CaF_2 : Gd (0.2 mol %) and CaF_2 : Sm (0.2 mol %) crystals X-ray

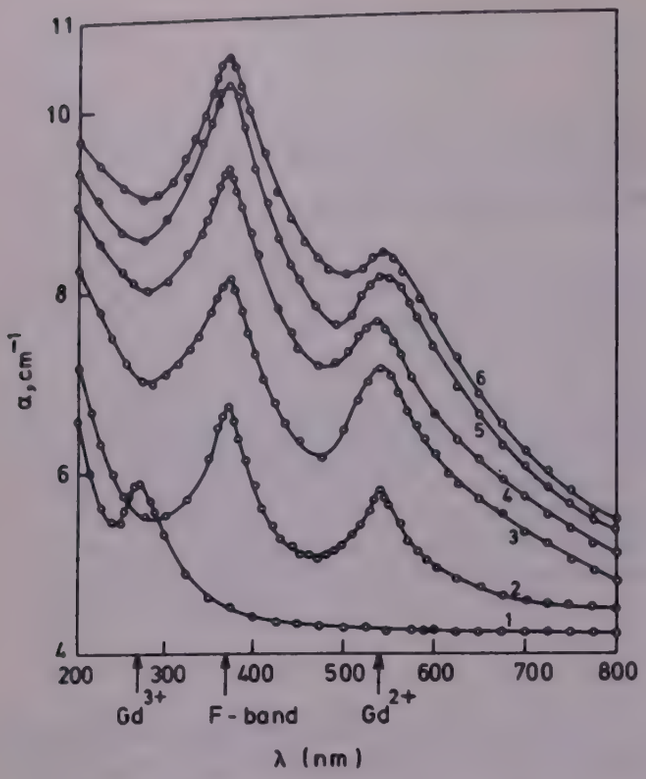

Fig. 1—Optical absorption as a function of wavelength at RT for CaF_2 : Gd crystals irradiated with X-rays for different times [Curves: 1, unirradiated; Irradiated for a period of: 2, ½ hr; 3, 1 hr; 4, 2 hr; 5, 3 hr; and 6, 4 hr]

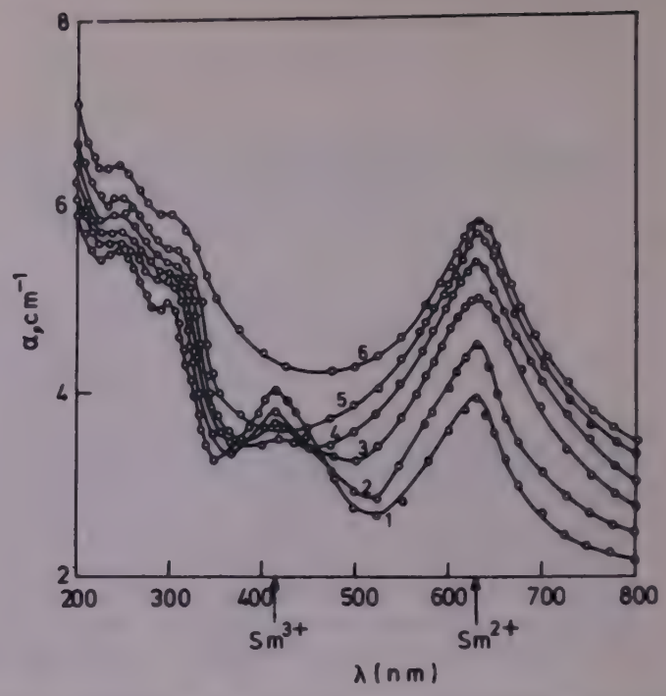

Fig. 2—Optical absorption as a function of wavelength at RT for CaF_2 : Sm crystals irradiated with X-rays for different times [Curves: 1, unirradiated; Irradiated for a period of: 2, ½ hr; 3, 1 hr; 4, 2 hr; 5, 3 hr; and 6, 4 hr]

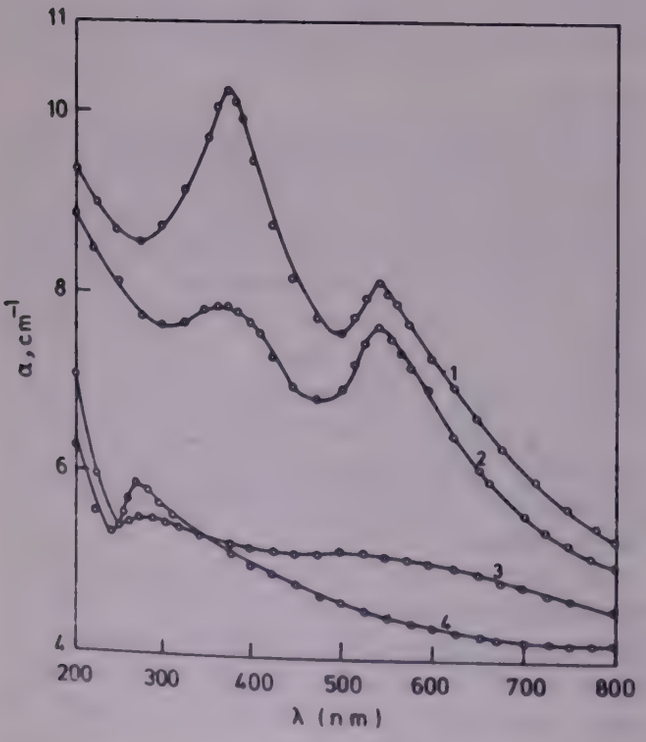

Fig. 3—Thermal bleaching characteristics of absorption bands of CaF_2 : Gd crystals X-ray irradiated at RT for 3 hr [Curves: 1, irradiated for 3 hr; bleached: 2, at 100 C; 3, at 180 C; and 4, at 280 C]

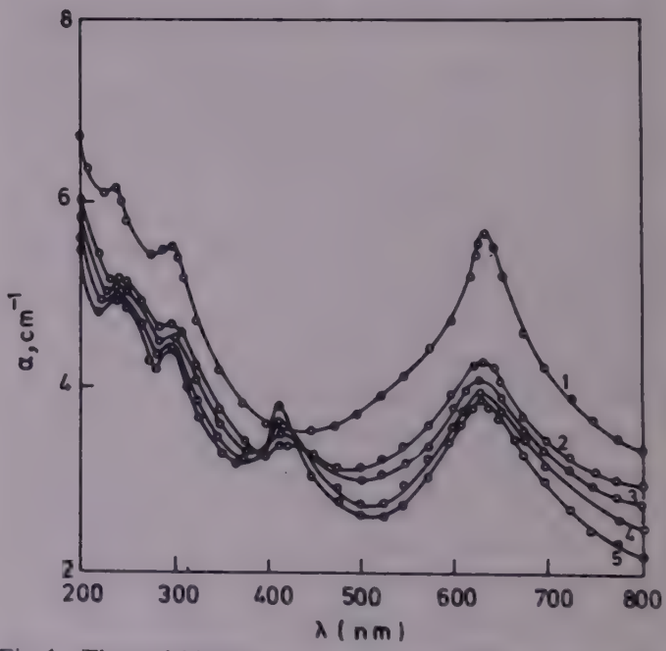

Fig. 4—Thermal bleaching characteristics of absorption bands of CaF_2 : Sm crystals X-ray irradiated at RT for 3 hr [Curves: 1, irradiated for 3 hr; bleached: 2, at 100°C; 3, at 150°C, 4, at 250°C; and 5, at 300°C.]

irradiated for 3 hr. The samples were heated initially to a particular temperature (in these crystals, these temperatures approximately corresponded to their TL peak positions); then the samples were slowly cooled to RT where the absorption measurements were always taken. When heated to 100°C, the absorption in the 370 and 540 nm bands of CaF_2 : Gd is decreased and these two bands are removed when the sample is bleached at 180°C; however, the absorption band at 272 nm

reappears and the sample seems to come back to its original condition when heated to 280°C. The increased absorption in the bands at 240, 300 and 630 nm, observed in X-ray-irradiated CaF_2:Sm gradually decreases with heating and the band at 412 nm reappears; finally when the X-ray-irradiated CaF_2:Sm is heated to 300°C, it also seems to attain its original condition.

The TL light output of CaF_2:Gd (0.2 mol %) and CaF_2:Sm (0.2 mol %) crystals X-ray irradiated respectively for 3 hr and 5 min exhibits three glow peaks each; the glow peak temperatures are 107, 177 and 277°C for CaF_2:Gd and 100, 152 and 244°C for CaF_2:Sm. It may be mentioned here that X-ray irradiation of CaF_2:Sm for 5 min. produced considerable TL light output-comparable to that given out by CaF_2:Gd irradiated for 3 hr. Also, CaF_2:Sm irradiated for 3 hr gave out too much TL light output but the TL pattern for this sample remains unchanged whether the irradiation is done for 3 hr or 5 min.

4 Discussion

When CaF_2 is doped with a trivalent impurity like Gd, it is known that it replaces Ca ions and also exists in the trivalent state. For charge balance fluorine ion interstitials are produced[7,8]. The Gd^{3+} ion with the interstitial fluorine ion forms dipoles; the relaxation effects due to such dipoles were observed[9-12]. As the ionic radius of Gd^{3+} (0.93 Å) is considerably smaller than that of Ca^{2+} ion (1.06 Å) lattice distortion will also occur. Due to this lattice distortion, the Gd^{3+} ion attached to the Frenkel pair (interstitial fluorine ion and the vacancy it created) at some regions in the lattice may be comparatively free. This means that in addition to the large concentration of Gd^{3+} ions existing in the lattice in the bound condition with the Frenkel pair, there are also present a small concentration of free Gd^{3+} ions. The observed absorption band at 272 nm may be due to the free Gd^{3+} ions. X-ray irradiation produces free electrons and holes. Some of these electrons can be caught up at Gd^{3+} ions making them Gd^{2+} which give an absorption band at 540 nm. Our measurements also show the presence of a band at 370 nm (which is similar to the F-band in alkali halides) that is not present in CaF_2 crystals X-ray irradiated at RT. The appearance of this band in X-ray-irradiated CaF_2:Gd indicates the presence of negative ion vacancies in CaF_2:Gd before irradiation and this can happen only if considerable lattice distortion is existing in these crystals. This is in support of our above conclusion.

Our measurements indicate that the absorption in F-band and the band at 540 nm increase with X-ray dosage. It is likely that X-ray irradiation breaks up the complex—Gd^{3+} ion attached to the Frenkel pair—and also converts Gd^{3+} ions into Gd^{2+} ions and the negative ion vacancies into F-centres. It is expected that such processes will saturate at larger dosages of X-rays as observed in the present measurements. Our measurements indicate that the hole-trapped centres do not give any absorption band in this wavelength region.

Looking into the details of the absorption data of CaF_2:Sm crystals, we may ascribe the absorption bands at 412 and 640 nm respectively to Sm^{3+} and Sm^{2+} (Ref. 4). The bands at 240 and 300 nm seem to be unconnected with the hole-trapped centres—some earlier workers tried to attribute these bands in CaF_2:Sm crystals with hole-trapped centres—as they are present in unirradiated samples. It is possible that these two absorption bands may be due to some unknown impurities in these samples. X-ray irradiation reduces the Sm^{3+} band and increases the Sm^{2+} band indicating the conversion of trivalent state of Sm into divalent state. Interestingly we do not notice any development of the F-band in these crystals. This seems reasonable as the lattice distortion in CaF_2:Sm is comparatively small due to the fact that the ionic radii of Ca and Sm^{3+} or Sm^{2+} (0.98 Å) do not differ very much—unlike in the case of Gd^{3+}.

The partial thermal bleaching experiments indicate that with heating, the divalent ions can be reconverted into the trivalent state. Also, we find that the X-ray-irradiated CaF_2:Gd and CaF_2:Sm crystals attain their original conditions when heated to 300°C; this means that the defect processes that take placed due to X-ray irradiation are reversed with heating.

It is difficult to understand the origin of the TL peaks in CaF_2 doped with Gd or Sm from the present work. However, from their detailed investigations, earlier workers attempted a discussion of the mechanisms responsible for the various TL peaks in RE-doped CaF_2 irradiated with X-rays[4,5,13]. Our results seem to indicate that the TL pattern in CaF_2 doped with Gd or Sm is not appreciably different— in general agreement with earlier findings[4]. The shift in the glow peak temperatures is probably connected with the lattice distortions occurring in CaF_2 with the two dopants.

Comparing the data of the present work (in which X-ray irradiation of the Gd- or Sm-doped CaF_2 crystals was carried out at RT) with that of the earlier workers where X-ray irradiation of the samples was carried out at LT, the following results of our measurements are important: (i) formation of the absorption band at 370 nm (which is similar to the F-band in alkali halides) in CaF_2:Gd (0.2 mol %) which was never reported by others, (ii) the absorption spectrum is simpler, e.g., having only two absorption bands at 370 and 540 nm in CaF:Gd (0.2 mol %) and two prominent absorption bands at 412 and 630 nm and also two weak

absorption bands at 240 and 300 nm in CaF_2 : Sm (0.2 mol %) whereas when irradiation was done at LT, the absorption spectrum of these samples was more complex containing six absorption bands and (iii) the TL pattern contains only three peaks whereas earlier workers reported 4 to 6 TL peaks, the peak temperatures being considerably different compared to those of the present work.

References

1 Arends J, *Phys Status Solidi* (*Germany*), **7** (1964) 805.

2 Beaumont J H & Hayes W, *Proc R Soc* (*London*) *A* (*GB*), **309** (1969) 41.

3 Bhola V P, *J Lumin* (*Netherlands*), **9** (1974) 121.

4 Merz J L & Pershan P S, *Phys Rev* (*USA*), **162** (1967) 217.

5 Becker M, Kiessling J & Scharmann A, *Phys Status Solidi* (*a*) (*Germany*), **15** (1973) 515.

6 Bose H N, *Proc Phys Soc* (*London*) *Ser B* (*GB*), **68** (1955) 249.

7 Heist R H & Fong F K, *Phys Rev B* (*USA*), **31** (1970) 2970.

8 Nauta-Leeffers Z C & den Hartog H W, *Phys Rev B* (*USA*), **19** (1979) 4162.

9 Franklin A D, Crissman J M & Young K F, *J Phys C* (*GB*), **8** (1975) 1244.

10 Capelletti R, Okuno E, Mathews G E & Crawford J H (Jr), *Phys Status Solidi* (*a*) (*Germany*), **47** (1978) 617.

11 Andeen C & Fontanella J, *J Phys & Chem Solids* (*GB*), **38** (1976) 237.

12 Chaudhary R K, Rao A V Krishna & Rao K V, *Phys Status Solidi* (*a*) (*Germany*), **77** (1983), in press.

13 Pai S T & Lee K C, *Phys Rev B* (*USA*), **23** (1981) 2022.

Indian Journal of Pure & Applied Physics
Vol. 21, November 1983, pp. 631-634

EPR of Mn^{2+} in $Cs_2Zn(SeO_4)_2.6H_2O$ and $(NH_4)_2Fe(SeO_4)_2.6H_2O$ Single Crystals

S K YADAV, V P SETH & R K MALHOTRA
Department of Physics, Maharshi Dayanand University, Rohtak

Received 24 *December* 1982; *revised received* 18 *July* 1983

EPR investigations have been carried out in Mn^{2+}-doped $Cs_2Zn(SeO_4)_2.6H_2O$ and $(NH_4)_2Fe(SeO_4)_2.6H_2O$ single crystals at room temperature and at X-band frequency. Mn^{2+} has been found to substitute for Zn^{2+} or Fe^{2+} exhibiting two magnetically inequivalent complexes. The EPR spectra have been analyzed using spin-hamiltonian of orthorhombic symmetry. Spin-hamiltonian parameters are determined.

1 Introduction

Tutton salts with the general formula $M'_2M''(XO_4)_2.6H_2O$, where M'' is a divalent cation (Zn, Fe or an ion of the 3*d* group), M' is a monovalent cation (K, Rb, Cs, Tl or NH_4) and X = S, Se, form an isomorphous series of compounds. Therefore, it is easy to prepare solid solutions of paramagnetic Tutton salts in diamagnetic ones over a wide range of relative concentrations from 0 to 100%. In the present paper, we report results of our EPR study at 298 K of Mn^{2+} incorporated into $Cs_2Zn(SeO_4)_2.6H_2O$ (CZSeH) and $(NH_4)_2Fe(SeO_4)_2.6H_2O$ (AFSeH) single crystals, for the first time.

2 Crystal Structure

CZSeH and AFSeH belong to a series of isomorphous salts called Tutton salts. The crystal structure of Tutton salts[1] is known to be monoclinic with space group $P(2_1/a)$. The crystallographic axes (a, b, c) are approximately in the ratio 3:4:2 and the angle β is about 105°. There are two formula units per unit cell. The two inequivalent divalent cations in the unit cell are situated at the points, (0, 0, 0) and (1/2, 1/2, 0) and all others are in general positions. Each divalent cation is surrounded by a slightly distorted octahedron of water molecules.

3 Experimental Details

Single crystals of $Cs_2Zn(Se\,O_4)_2.6H_2O$ and $(NH_4)_2Fe(SeO_4)_2.6H_2O$ doped with Mn^{2+} were grown by slow evaporation of aqueous solutions at room temperature. The Mn^{2+} ion impurities were introduced into the lattice by adding a small amount (0.1% by weight) of manganese sulphate. EPR measurements were carried out at 298 K using a JEOL JES-FE 3X homodyne X-band spectrometer equipped with TE_{011} −cylindrical cavity and 100 kHz field modulation. As a reference for magnetic field strength, the resonance line of DPPH with $g = 2.0036$ is used. The crystals were mounted on quartz rods. The angular variation studies were done using JES-UCR-2X sample angular rotating device.

4 Results and Discussion

For an arbitrary orientation of the crystal, a complex spectrum corresponding to two identical but differently oriented Mn^{2+} complexes is observed in CZSeH and AFSeH. When the magnetic field is varied in the *ac* plane, the EPR spectrum shows only one set of sextets ($\Delta M = \pm 1$, $\Delta m = 0$ transitions). This is in confirmation of the fact that the *ac* plane is a mirror plane perpendicular to the *b* axis, in which two divalent sites become equivalent. The Mn^{2+} ions substitute for divalent cations and consequently $[Mn(H_2O)_6]^{2+}$ complexes are obtained in CZSeH and AFSeH. The principal axes of the two inequivalent Mn^{2+} complexes were obtained by locating the extreme in the fine structure spread. As an illustration, the spectrum taken at 298 K with the magnetic field along the principal z axis of one set of equivalent Mn^{2+} complexes in CZSeH is shown in Fig. 1. Fig. 2 shows the relative orientation of the susceptibility, rhombic crystalline field and crystallographic axes. The direction cosines of the principal axis (z-axis) of the spin-hamiltonian with respect to a', b and c axes (a' axis perpendicular to c axis in *ac* plane) are respectively 0.21, 0.56 and 0.80. The angular variation studies indicate that the observed spectrum has orthorhombic symmetry. Since EPR, in general, does not distinguish between orthorhombic and lower symmetries[2], and as the site symmetry of the divalent ion is C_i, the crystal field symmetry at the Mn^{2+} site may be either orthorhombic or more probably lower. Fig. 3 shows the angular variation of the fine structure transitions ($\Delta M = \pm 1$) in the z-x plane of one of the Mn^{2+} complexes in CZSeH. Similar curves have been found for AFSeH.

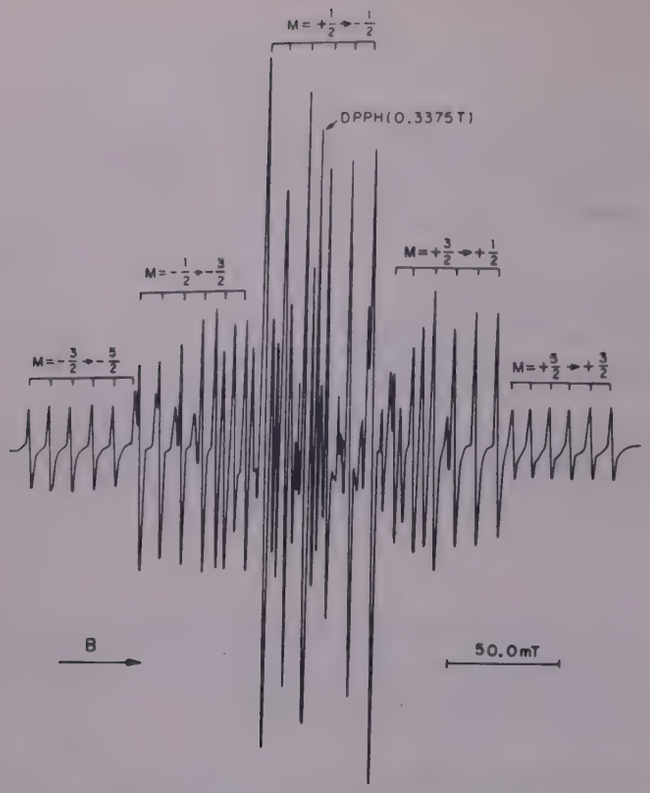

Fig. 1—EPR spectrum of $Cs_2Zn(SeO_4)_2.6H_2O:Mn^{2+}$ single crystals at 298 K and at X-band frequency ($\nu = 9.45$ GHz) with B parallel to the z-axis of one of the magnetic complexes of Mn^{2+}

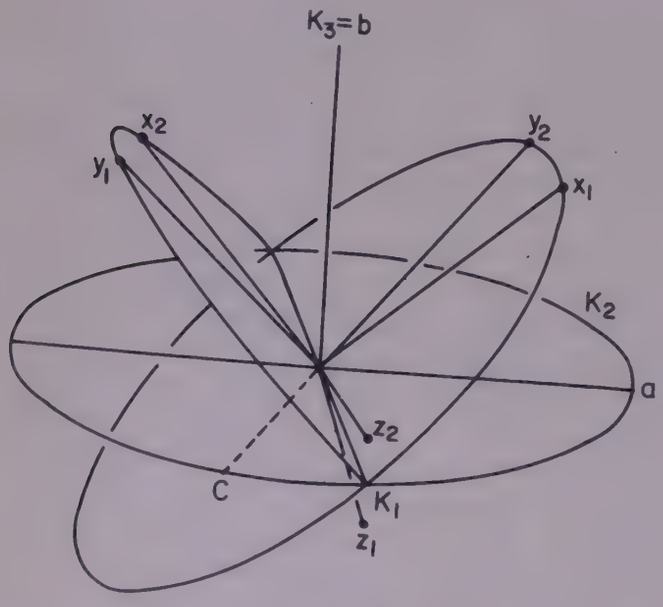

Fig. 2—Relative directions of the axes in crystals like $Cs_2Zn(SeO_4)_2.6H_2O$ [a, b, c, crystallographic axes; K_1, K_2, K_3, susceptibility axes: x, y, z, axes of rhombic crystalline field. z_1, z_2 lie in K_1K_3 plane, so that x_1y_2 lies very nearly in 45° plane, angle x_1oy_2 (45° plane) = 0°, angle z_1oz_2 (K_1K_3 plane) = 68° ± 1°. The angle ψ between K_1 and c is such that $\psi = 15°$]

The linewidths in the EPR spectra of Mn^{2+} in CZSeH at 298 K are about 0.7 mT and 0.6 mT along the x- and z-axes, respectively, whereas in AFSeH at the same temperature these values are respectively 3.0 mT and 25 mT. The linewidth is mainly due to the local magnetic field of the proton nuclear moments in water

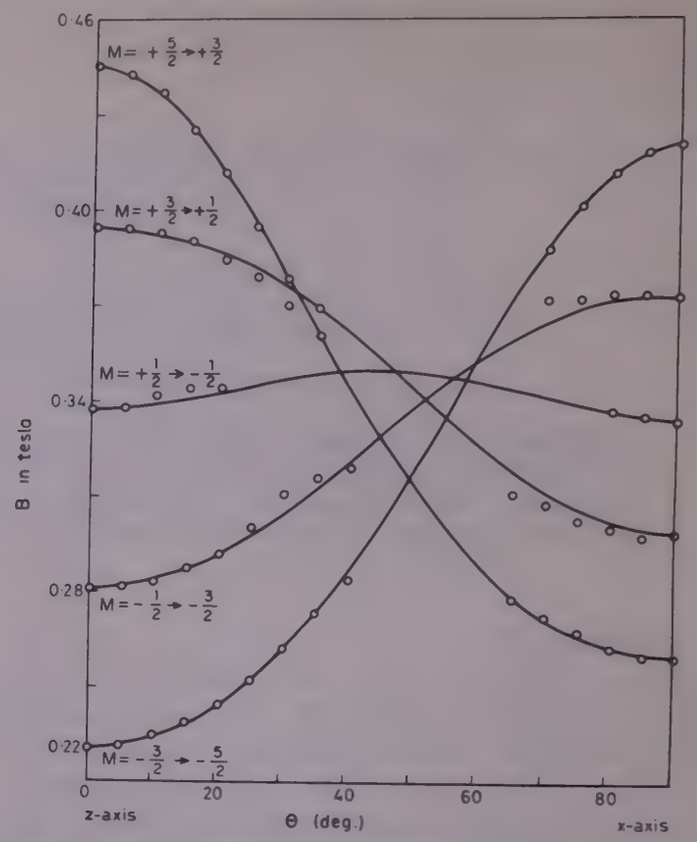

Fig. 3—Angular variation of the allowed fine structure transitions in the zx plane of one of the magnetic complexes of Mn^{2+} in $Cs_2Zn(SeO_4)_2.6H_2O$ single crystal at 298 K. Continuous curves represent the theoretical values whereas experimental values are shown by open circles

molecules surrounding the magnetic ion in the form of a distorted octahedron. The large value[3] of the linewidth in case of ferrous lattice is probably due to Fe^{2+} ion.

The spectra observed at room temperature have been analyzed using the spin-hamiltonian appropriate to Mn^{2+} in orthorhombic (or lower) symmetry[4]:

$$H = \beta[S_z g_z B_z + g_x(S_x B_x + S_y B_y)] + \tfrac{1}{3}b_2^0 O_2^0 + \tfrac{1}{3}b_2^2 O_2^2 + \tfrac{1}{60}(b_4^0 O_4^0 + 5b_4^2 O_4^2 + b_4^4 O_4^4) + [S_z A_z I_z + A_x(S_x I_x + S_y I_y)] \quad \ldots (2)$$

where the first term represents the electronic Zeeman interactions; second and third terms represent, respectively, the axial and rhombic parts of fine structure; the fourth term represents fourth-order part of the crystal field and the last term represents the hyperfine interaction term $S = I = 5/2$ for Mn^{2+}.

Magnetic field measurements were made for the allowed lines with B parallel to the z- and x-axes, respectively. No measurement could be made for B parallel to y-axis since the lines got mixed up and consequently the various fine structure transitions could not be distinguished. Therefore, it was necessary to assume that $A_x = A_y$ and $g_x = g_y$ in the calculations (the hyperfine and g-tensors are normally isotropic for the Mn^{2+} ion). Using the expression for the resonance

Table 1—Spin-Hamiltonian Parameters and the Angle (α) Between the z Axes of two Inequivalent Magnetic Mn^{2+} Complexes in some Tutton Salt Single Crystals

[All the crystal field and hyperfine parameters are in units of $10^{-4}cm^{-1}$]

Crystal	g_z	g_x	A_z	A_x	b_2^0	b_2^2	b_4^0	b_4^2	b_4^4	α deg	Ref.
$(NH_4)_2Mg(SeO_4)_2.6H_2O$	2.004 ±0.001	2.006 ±0.002	−88.0 ±1.0	−88.0 ±1.0	248.6 ±1.0	−182.4 ±6.0	2.9 ±0.5	—	—	66±4	13
$(NH_4)_2Fe(SeO_4)_2.6H_2O$	2.0018 ±0.0005	1.9906 ±0.0005	−86.6 ±2.0	−87.6 ±2.0	252.2 ±0.5	−178.7 ±9.0	3.0 ±0.5	−3.74 ±3.0	15.0	67±1	PS
$(NH_4)_2Zn(SeO_4)_2.6H_2O$	2.005 ±0.001	2.007 ±0.002	−88.6 ±1.0	−87.0 ±1.0	264.9 ±1.0	−154.5 ±6.0	2.65 ±0.5	— —	— —	68±4	13
$(NH_4)_2Fe(SO_4)_2.6H_2O$	2.004 ±0.001	— —	−87.8 —	90.8 —	−245.8 —	203.4 —	2.9 ±0.5	— —	— —	70±5	14
$Cs_2Mg(SeO_4)_2.6H_2O$	2.0069 ±0.0005	2.0061 ±0.0008	−89.0 ±1.0	−88.0 ±1.0	−249.5 ±1.0	129.0 ±6.0	3.15 ±0.5	—	—	66±2	15
$Cs_2Zn(SeO_4)_2.6H_2O$	2.0000 ±0.0005	2.0024 ±0.0005	−87.9 ±1.0	−86.9 ±1.0	−254.4 ±0.6	115.0 ±2.0	3.71 ±0.1	46.7 ±10.0	66.4 ±10.0	68±1	PS
$Cs_2Zn(SO_4)_2.6H_2O$	2.0081 ±0.0005	2.0114 ±0.0015	−89.5 ±1.0	−88.6 ±1.0	−265.7 ±2.0	96.0 ±12.0	2.275 ±0.5	—	—	70±2	16

PS = Present study

field positions up to second-order perturbation[4] for the above spin-hamiltonian, the best fit parameters were obtained and are listed in Table 1. The signs of the parameters (given in Table 1) are only relative. The relative signs of the parameters b_2^0 and A_z were obtained by comparing the second-order shifts in the separation between the hyperfine components for the various electronic transitions[5]. The sign of b_2^0 is then obtained by assuming A_z to be negative as, in all the materials where the signs have been determined, A_z has been found to be negative[6]. The sign of b_2^2 results from the sign of b_2^0 and the choice of x- and y-axes. Table 1 also includes the parameters of other Tutton salts for comparison. It is found that the sign of b_2^0 in AFSeH is positive whereas in CASeH it is negative.

The g value, which deviates slightly from the free-spin value, shows a small anisotropy. The anisotropy of g is within the experimental error. The facts that the crystal field parameters have non-zero values, and that g departs slightly from the free-spin value, show that the ground state is not exactly $^6S_{5/2}$. Because of this, g may show an anisotropy. The deviation from the free-spin value may be attributed to the effects of covalent bonding[4]; although we cannot extract any meaningful covalency parameter out of it.

The value of the hyperfine splitting constant is nearly isotropic within the experimental error. It was recognized that the nearest neighbour interactions are dominating for hyperfine splitting in contrast to other parameters like b_n^m and g values where long range interactions may be important[7]. Therefore, the determination of hyperfine splitting constant in EPR spectra of Mn^{2+} makes it possible to evaluate the nature of bond between Mn^{2+} ion and its immediate surroundings. Van Wieringen[8] has shown that the hyperfine splitting of Mn^{2+} decreases with increasing covalency of the magnetic complex. The relation between A and the local bonding of the Mn^{2+} and the nearest-neighbour ligands was put phenomenologically on a more quantitative basis by plotting A versus the Pauling covalency parameter[9-12]. Here the covalency parameter c/n is derived from the electronegativity of Mn^{2+} and the ligands and the number of ligands, using the expression developed by Hannay and Smyth[13]. A in this plot is obtained experimentally from a series of crystals in which Mn^{2+} is surrounded by the same type of ligands. This curve (A versus c/n) can be used to determine the immediate surrounding of the Mn^{2+} in AFSeH and CZSeH.

The average hyperfine splitting values of Mn^{2+} when it is surrounded by six oxygens[14-16] by six water molecules[17-27] respectively are 81.7×10^{-4} cm^{-1} and 89.1×10^{-4} cm^{-1}. The corresponding covalency parameter can be obtained from A versus c/n plot given by Simanek and Muller[12]. The c/n values for Mn^{2+}-6 O_2^- and $[Mn(H_2O)_6]^{2+}$ complexes are found to be 11.2% and 7.0%, respectively. In the present study, the measured values of A are $(87.1 \pm 2.0) \times 10^{-4}$cm^{-1} and $(87.4 \pm 1.0) \times 10^{-4}$ cm^{-1} for AFSeH and CZSeH, respectively. The corresponding values of c/n from the A versus c/n plots are 8.4% and 8.2% respectively. Within the experimental error, these values of A and c/n are close to the average value of A and c/n of Mn^{2+} when it is surrounded by six water molecules. This indicates that Mn^{2+} in these systems is also surrounded by six water molecules.

From Table 1 it is seen that the values of α (the angle between the z axes of two inequivalent manganese complexes) and of the parameter b_2^0 are about the same range for many crystals. Value of the parameter b_2^2 differs from the trend for ammonium and cesium compounds. However, it is observed that the value of b_2^2 is very nearly of the same magnitude in series of ammonium and also in series of cesium Tutton salts separately. This gives a qualitative idea of the local symmetry of the divalent cation sites, especially in the systems where no detailed crystal structure is available. Qualitatively it can be concluded that the coordination of the octahedron of water molecules at the divalent cation is nearly the same for all the systems, as regards either symmetry or the distance from the divalent cation. It is also noticed from Table 1 that the value of b_2^0 is larger for Zn Tutton salt than for Mg salt. The lattice parameters of the Tutton salts studied are not known. However, the lattice parameters of the Zn Tutton salt are expected to be slightly greater than those for Mg salt, because Zn has a larger atomic radius than Mg. In the same way, one expects the values of b_2^2, b_2^0, etc. parameters of the Zn salt to be larger[28], than those of Mg.

Acknowledgement

This work was supported partly by CSIR, New Delhi, under Project 3(502)/81-EMR II. The authors wish to thank Prof. T S Jaseja for his interest and encouragement.

References

1 Hoffmann W, *Z Kristallogr (Germany)*, **78** (1931) 279.
2 Bowers K D & Owen J, *Rep Prog Phys (GB)*, **18** (1955) 304.
3 Saraswat R S & Upreti G C, *Chem Phys (USA)*, **23** (1977) 97.
4 Vinokurov V M, Zaripov M M & Stepanov V G, *Sov Phys Solid State (USA)*, **6** (1964) 870.
5 Low W, *Paramagnetic resonance in solids*—Solid State Physics Supplement 2 (Academic Press, New York and Lodnon) 1960, 72.
6 Abragam A & Bleaney B, *Electron paramagnetic resonance of transition ions* (Clarendon Press, Oxford) 1970, Ch. 7.
7 Muller K A, *Proc 16th AMPERE Congress Bucharest*, edited by I Ursu (Bucharest Publishers, House of the Academy of the Socialist Republic of Rumania, Bucharest) 1970.
8 Van Wieringen J S, *Discuss Faraday Soc (GB)*, **19** (1955) 118.
9 Matumura O, *J Phys Soc Jpn (Japan)*, **14** (1959) 108.
10 Title R S, *Phys Rev (USA)*, **131** (1963) 623.
11 Henning J C M, *Phys Lett A (Netherlands)*, **24** (1967) 40.
12 Simanek K & Muller K A, *J Phys & Chem Solids (GB)*, **31** (1970) 1027.
13 Hanny N B & Smyth C F, *J Am Chem Soc (USA)*, **68** (1947) 171.
14 Low W, *Phys Rev (USA)*, **105** (1957) 793.
15 Danilov A G & Manoogian A, *Can J Phys (Canada)*, **47** (1969) 839.
16 Chatelain A & Weeks R A, *J Chem Phys (USA)*, **51** (1970) 5862.
17 Vinokurov V M & Tukhvatulliu R S, *Geokhimiya (USSR)*, **4** (1968) 496.
18 Fritz I J & Yarmus L, *Phys Rev (USA)*, **47** (1968) 839.
19 Milsch B & Windsch W, *Phys Status Solidi (Germany)*, **31** (1969) K 79.
20 Jain V K, *Electron paramagnetic resonance studies of* Mn^{2+} *and* VO^{2+} *in single crystals*, Ph D thesis, Indian Institute of Kanpur, 1976.
21 Jain V K & Srinivasan T M, *Z Naturforsch a (Germany)*, **32** (1977) 665.
22 Jain V K & Srinivasan T M, *Pramana (India)*, **10** (1978) 155.
23 Saraswat R S & Upreti G C, *Chem Phys (USA)*, **23** (1977) 97.
24 Jain V K, Srinivasan T M & Venkateswarlu P, *Indian J Phys Part A (India)*, **53** (1979) 318.
25 Janakiraman R & Upreti G C, *Chem Phys Lett (Netherlands)*, **4** (1970) 550.
26 Jain V K & Srinivasan T M, *Acta Phys Pol A (Poland)*, **53** (1978) 779.
27 Jain V K, *Z Naturforsch a (Germany)*, **32** (1977) 1364.
28 Ochi J, Sano W, Isotani S & Hennies C E, *J Chem Phys (USA)*, **62** (1975) 2115.

Indian Journal of Pure & Applied Physics
Vol. 21, November 1983, pp. 635-637

^{1}H NMR & EPR Studies on Copper Complexes: $Cu(Pyrazole)_2Br_2.H_2O$ & $Cu(Benzoxazole)_2Br_2.2H_2O$

K V G REDDY, K V R CHARY* & B A SASTRY
Solid State & Molecular Physics Laboratory, Department of Physics, Osmania University, Hyderabad 500 007
and
G PONTICELLI & R PINNA
Istituto Di Chemical Generale, Inorganica Ed Analitica, Universita Di Cagliari, Via Ospedale 72, 09100 Cagliari, Italy

Received 21 *December* 1982; *revised received* 28 *May* 1983

The ^{1}H NMR and EPR studies have been carried out on $Cu(Pyrazole)_2Br_2.H_2O$ and $Cu(Benzoxazole)_2Br_2.2H_2O$ at different temperatures. From the variation of the second moment with temperature, it is found that $Cu(Pyrazole)_2Br_2.H_2O$ undergoes a general molecular reorientation and this is found to be associated with an activation energy of 9.94 kcal mole. The EPR spectra of these complexes in N, N'-dimethylformamide indicate strong solute-solvent interaction.

1 Introduction

A large number of copper(II) complexes of benzoxazole(BO) and pyrazole(PY) were synthesized and studied by different techniques, viz. visible spectroscopy, infrared spectroscopy, conductivity, magnetic moments and X-ray structural analysis[1-7] to obtain further information about their crystal and molecular structures. So far, to the best of the knowledge of the authors, no detailed magnetic resonance studies were performed on any of the above complexes. In the present investigation, an attempt has been made to get information regarding the molecular structure and molecular motion in $Cu(Pyrazole)_2Br_2.H_2O$ and $Cu(Benzoxazole)_2Br_2.2H_2O$ hereinafter referred to as $Cu(PY)_2Br_2.H_2O$ and $Cu(BO)_2Br_2.2H_2O$ (or simply as complexes I and II) respectively. ^{1}H NMR and EPR studies in polycrystalline samples and in N, N'-dimethylformamide(DMF) solutions were carried out on these two samples.

2 Experimental Details

2.1 Preparation of the Samples and Earlier Studies

These complexes were prepared by the general procedure described earlier[1,2]. The compositions of these complexes are checked by the chemical analysis. From the IR and other spectroscopic studies[2], it is found that the geometry around the copper(II) in I is distorted octahedral formed with four bromine atoms and two nitrogen atoms from the pyrazole ligands. Bromine acts as a bridging bidentate ligand. In the case of II, using the above techniques[8], it is found that the geometry around copper is square planar formed with two bromines and two nitrogens of the two benzoxazole molecules. Except for the above data, no other information regarding the structure is known.

*Present address: FT-NMR Centre, Tata Institute of Fundamental Research, Bombay 400 005

2.2 Experimental Procedure

^{1}H NMR spectra in polycrystalline samples were recorded in the temperature range 77-350 K on a home-made CW NMR spectrometer whose details are given elsewhere[9].

The EPR spectra of these complexes in polycrystalline and DMF solutions were recorded using a Varian E-4, *X*-band spectrometer. The modulation frequency of the magnetic field is 100 kHz. The errors in *g* and *A* (hyperfine line separation) measurements are about ± 0.001 and ± 2.0 G respectively.

3 Results and Discussion

3.1 ^{1}H NMR Studies

From the first derivative signals of these complexes in the temperature range 77-350 K for I and 77-300 K for II, second moment(S_2) values were calculated using the standard procedure[10]. In the case of II, the ^{1}H NMR signals could not be recorded beyond the room temperature, since the complex was losing its water of hydration. The variation of the second moment(S_2) with temperature for both the samples are shown in Figs. 1 and 2.

From Fig. 1 it is found that the second moment value of I is constant at 5.55 ± 1 G^2 in the temperature range 77-285 K and a rapid fall in the second moment from 5.55 ± 1 G^2 to 1.1 ± 1 G^2 is noticed in the range 285-300 K. Beyond 300 K, it is found that it remains constant. From Fig. 2 it can be observed that the value of second moment for II is practically constant at 3.7 ± 1 G^2 in the temperature range 77-300 K.

3.2 Rigid Lattice Second Moment

In the present case it is not possible to calculate the theoretical value of the second moment (S_{2rig}) since the hydrogen atom positions are not available for both these complexes. From the structural formula it is seen,

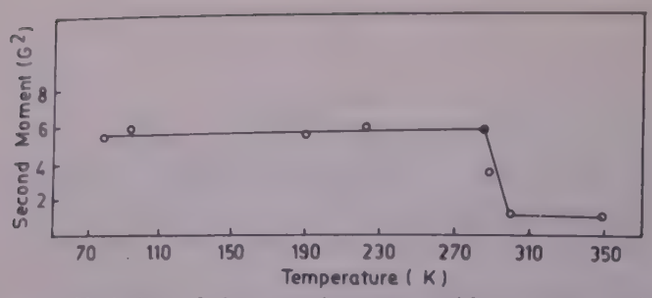

Fig. 1—Variation of the second moment with temperature for $Cu(Py)_2Br_2.H_2O$

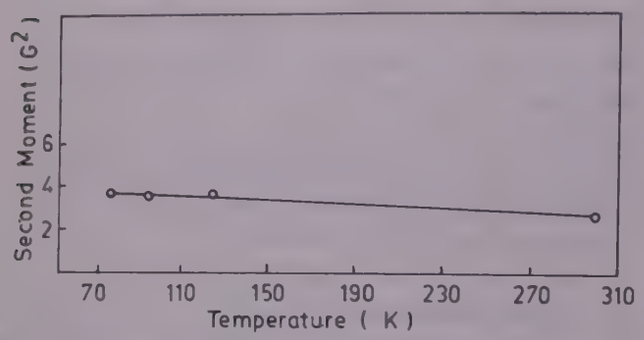

Fig. 2—Variation of the second moment with temperature for $Cu(BO)_2Br_2.2H_2O$

that there is no functional group existing in both the complexes to contribute the major part to the second moment and also the H-H distances in pyrazole and benzoxazole ligands should be definitely more than 2.5 Å similar to benzene molecule[11]. The low value of the second moment appears to be reasonable for a rigid lattice. This is supported by the fact that in $Cu(PY)_4Cl_2$[12], the calculated rigid lattice second moment is found to be $3.7\,G^2$.

The second moment fall observed in the case of I in the temperature range 285-300 K (Fig. 1) may arise due to some type of molecular motion. Since the value of the second moment at higher temperatures is low ($1.1 \pm 1\,G^2$), it appears that the molecule is undergoing general molecular reorientation. It is not possible to rule out hindered molecular motion also. In order to decide the appropriate type of molecular motion, one requires accurate hydrogen atom positions which are not available for this complex. This prevents unambiguous interpretation of the anomalous change of the second moment in terms of correct molecular motion.

The modified Bloembergen *et al.* equation[13,14] is used to calculate the correlation frequencies associated with the second moment transition. These re-orientation frequencies are assumed to fit in Arrhenius equation $\nu_c = \nu_0 \exp[-E_a/RT]$. A plot between ln ν_c versus $1000/T\,(K^{-1})$ in the case of I yields a straight line (Fig. 3), whose slope gives the activation energy value as 9.94 kcal/mol.

3.3 EPR Studies

Fig. 4 shows the EPR spectra of these two complexes I and II in polycrystalline and solution forms. From the

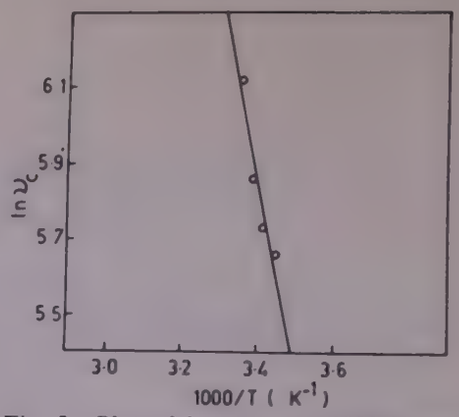

Fig. 3—Plot of ln ν_c versus $1000/T$ for $Cu(Py)_2Br_2.H_2O$

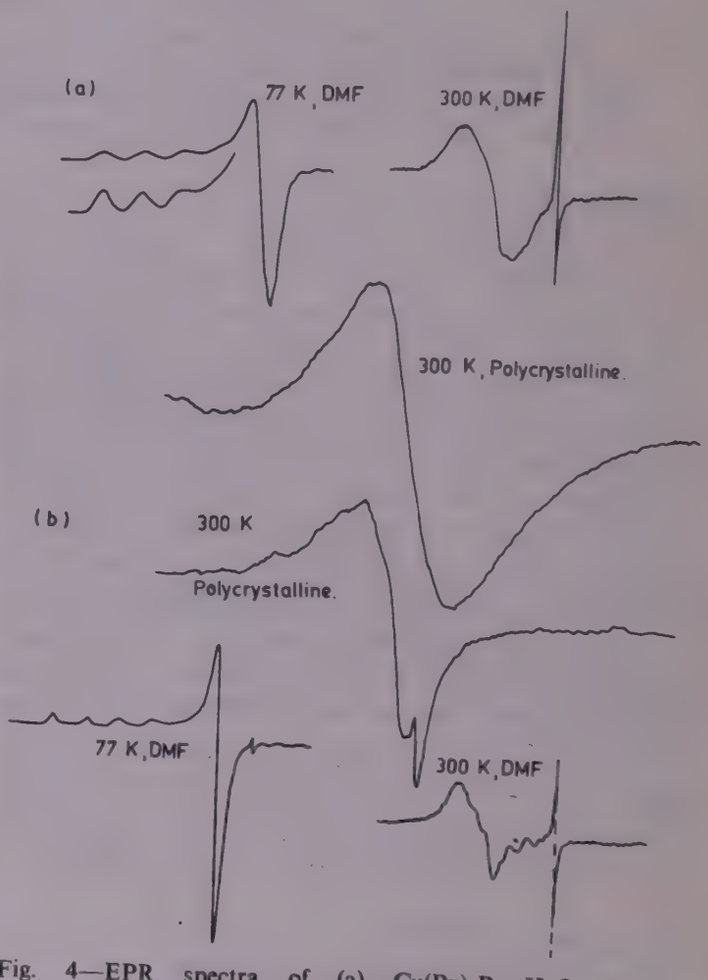

Fig. 4—EPR spectra of (a) $Cu(Py)_2Br_2.H_2O$ and (b) $Cu(BO)_2Br_2.2H_2O$ in polycrystalline and DMF solutions

X-band EPR spectra, no information about their molecular structures is obtained as single lines without hyperfine structure are observed. As is evident from Fig. 3, the correlation frequencies are very much less than the *X*-band microwave frequencies employed to record the EPR spectrum. Because of the above fact, since the molecular motions cannot influence the EPR spectrum in the temperature range 285-300, no attempt has been made to record the EPR spectra in the above temperature range to confirm molecular motion. Since no information is obtained from polycrystalline samples, the EPR spectra have been recorded in DMF solutions both at room and liquid nitrogen

temperatures to study the chromophore around copper(II). The frozen solution spectra of both the complexes are indicating clearly one species. The approximate g and A values from these spectra are calculated using the methods given in the literature[15] and are given below:

I. $Cu(PY)_2Br_2.H_2O$

$g=2.148$	$A=61.6$ G
$g_{\parallel}=2.338$	$A_{\parallel}=142.5$ G
$g_{\perp}=2.05$	$A_{\perp}=21$ G

II. $Cu(BO)_2Br_2.2H_2O$

$g=2.165$	$A=45.8$ G
$g_{\parallel}=2.374$	$A_{\parallel}=115$ G
$g_{\perp}=2.061$	$A_{\perp}=11$ G

The above values of g and A indicate the oxygen coordination similar to the isoxazole complexes of copper(II)[16-18] and are very much different from some of the pyrazole complexes studied earlier in polycrystalline form[2]. Therefore, it appears here also, as in isoxazole complexes, that the DMF must be interacting strongly[4-6] to give complexes of the type $(DMF)^{2+}$.

4 Conclusions

1 The values of the second moment of these complexes, in the temperature range 77-300 K, indicate that the H-H distances are larger than 2.5 Å.

2 The low value of the second moment (1.1 ± 1 G^2) obtained in the case of $Cu(Py)_2Br_2.H_2O$ at high temperatures is indicating a general molecular reorientation.

3 The activation energy associated with the second moment fall in the case of $Cu(Py)_2Br_2.H_2O$ is found to be 9.94 kcal/mol.

4 The g and A values indicate an elongated octahedral coordination around copper(II) and the unpaired electron is in $|x^2-y^2\rangle$ orbital. The EPR results in frozen DMF solution clearly indicate that the unpaired electron is in $|x^2-y^2\rangle$ orbital implying nearly an elongated octahedral coordination around copper(II) in both the cases.

Acknowledgement

The authors thank the Head, Department of Physics, Osmania University, Hyderabad, and are also grateful to the University Grants Commission, New Delhi, for the financial assistance.

References

1 Duff E J & Hughes M N, *J Chem Soc A (GB)*, (1968) 2144.
2 Reedijk J, Windhorst J C A, Van Ham N H M & Groeneveld W L, *Recueil (France)*, **111** (1971) 234.
3 Reedijk J & Smith J A, *Recueil (France)*, **90** (1971) 117, 1135.
4 Duff E J, *J Inorg & Nucl Chem (GB)*, **32** (1970) 3103.
5 Daugherty N A & Swisher J H, *Inorg Chem (USA)*, **7** (1968) 165.
6 Mighell A D, Reimann C W & Santoro A, *Acta Crystallogr, Sect B (Denmark)*, **25** (1969) 595.
7 Mighell A, Santoro A, Prince E & Reimann C, *Acta Crystallogr. Sect B (Denmark)*, **31** (1975) 2479.
8 Ponticelli G, Istituto Di Chemica Generale, Inorganica Ed Analytica, Universita Di Cagliari, Via Ospedale 72, 09100 Cagliari, Italy, (Private communication) 1982.
9 Reddy K V G, Chary K V R & Sastry B A, *Aust J Chem (Australia)*, **35** (1982) 2367.
10 Andrew E R, *Phys Rev (USA)*, **91** (1953) 425.
11 Slichter C P, *Principles of nuclear magnetic resonance* (Harper and Row, New York), 1961, 61.
12 Reddy K V G, Chary K V R & Sastry B A, *Physica (Netherlands)*, Communicated, 1982.
13 Bloembergen N, Purcell E M & Pound R V, *Phys Rev (USA)*, **73** (1948) 679.
14 O'Reilly D E & Tsang T, *J Chem Phys (USA)*, **46** (1967) 1298.
15 Sastry B A, Asadullah S Md, Ponticelli G & Massacessi M, *J Chem Phys (USA)*, **70** (1979) 2834.
16 Sastry B A, Asadullah S Md, Reddy K V G, Ponticelli G & Massacessi M, *J Mol Struct (Netherlands)*, **55** (1979) 143.
17 Sastry B A, Asadullah S Md, Ponticelli G & Massacessi M, *J Inorg & Nucl Chem (GB)*, **42** (1980) 833.
18 Ponticelli G, Pelizzi G, Sastry B A, Asadullah S Md & Chary E S, *Indian J Pure & Appl Phys*, **18** (1980) 212.

Indian Journal of Pure & Applied Physics
Vol. 21, November 1983, pp. 638-643

Non-Abelian Gauge Theory of Fields Associated with Dyons for Non-zero Mass System

B S RAJPUT, SATYARAJ KUMAR & O P S NEGI
Department of Physics, Kumaun University, Naini Tal 263002

Received 15 *June* 1982

Non-Abelian gauge theory of fields associated with dyons for non-zero mass system has been carried out by using the reduced expansions of generalized fields produced by spin-1/2 dyons and it has been shown that in this theory the particle current is gauge covariant but not conserved. It has also been shown that in this theory the gauge invariance of generalized field equations requires local gauge changes in generalized field and current and that there is no need of extra constraint to maintain the dual symmetry. The non-Abelian gauge term in interaction Hamiltonian has been shown to contain the product of number operators of spin-1 and spin-0 particles and it reveals an additional character of dyons that they behave as composite sites of multiple spins in the non-Abelian gauge space.

1 Introduction

Recent interest in the subject of monopoles has been enhanced by the observations of t'Hooft[1] that the classical solutions having the properties of magnetic monopoles may be found in Yang-Mills[2] theory, and also by an extension of this idea by Julia and Zee[3] who showed that it is possible to construct the classical solution having both the magnetic and electric charges on the same particles. In the mean time, it became clear that the monopoles can better be understood in non-Abelian theories in which they appear as classical solutions of the system[4], which have topological meaning. The Wu-Yang formalism[5] offers some hope for more convenient treatment of monopoles but it too appeared cumbersome[6] for problems involving many monopoles. More recently, Brandt *et al.*[7] showed that it is impossibly difficult to extend Wu-Yang programme[5] for full quantum field theory. On the other hand, Mc Keon[8] developed the idea of Cabibbo and Ferrari[9] in strict analogy with Mandelstam[10], and Ezwa and Tze[11] presented a Lagrangian theory of monopoles with a non-Abelian gauge symmetry and free from Dirac vito[12]. The latter theory[11] lacks in action principle in the presence of particles carrying both electric and magnetic fields (dyons)[13].

Starting with the idea of Cabibbo and Ferrari[9] of two four-potentials, we have made attempts[14-17] to develop the consistent quantum field theory of generalized electromagnetic fields produced by particles (dyons) each carrying the generalized charge as a complex quantity with electric and magnetic charges as its real and imagninary parts.

In the present paper, using the reduced expansions[16] of generalized fields produced by dyons of spin 1/2, it has been shown that these fields cannot be described in Abelian gauge theory and that the sensible gauge theory for the fields of dyons of non-zero mass is non-Abelian one Non-Abelian gauge theory of fields associated with particles of non-zero mass system, each of which carries the generalized charge, has been constructed and it has been shown that the generalized particle current is gauge covariant but not conserved in non-Abelian theory. It has also been shown that, in non-Abelian theory, the gauge invariance of the generalized field equations requires the local gauge changes in generalized field and current. It has also been shown that, in contrast to the results of Brandt *et al.*[7], no extra constraint except the consistency condition is required to maintain the dual symmetry in non-Abelian theory of dyons carrying generalized charges.

The field Hamiltonian has been obtained by using the second quantized reduced expansions of generalized four-potentials, and it has been shown that the coupling between the generalized charges is increased in non-Abelian theory, as also that the non-Abelian term in the interaction Hamiltonian consists of the product of number operators of spin-1 and spin-0 particles with positive and negative energies. It reveals an additional character of the dyons that in non-Abelian gauge space (i.e. internal group space) they behave as composite states of multiple spins.

2 Generalized Electromagnetic Fields

A consistent quantum field of the generalized electromagnetic fields produced by spin-1/2, non-zero mass particles, carrying generalized charges, represented by

$$q_j = e_j - ig_j \qquad \ldots (1)$$

where generalized charge on jth particle has been written in terms of its electric and magnetic charges e_j

and g_j, has been constructed[16] by introducing two four-potentials $\{A_\mu\} \equiv (A^T, i\varphi_e)$ and $\{B_\mu\} \equiv (B^T, i\varphi_g)$ in order to avoid the occurrence of controvertial[18,19] arbitrary string variables in the solutions of generalized field equations. In the presence of these two four-potentials, the dual invariance of the theory leads to chirality quantization conditions[20].

These electric and magnetic four-potentials have been combined in the following manner to define the generalized four-potential $\{V_\mu\}$, as

$$\{V_\mu\} = \{A_\mu\} - i\{B_\mu\} \qquad \ldots (2)$$

the reduced expansions for which may be written as follows[16], in terms of Foldy[21] and Shirokov[22] realization of irreducible representations of Poincare group for non-zero mass system;

$$V_0(x) = \frac{q}{(2\pi)^3} \int \frac{d\mathbf{p}}{\omega'^3} [f(m', \mathbf{p}) \exp\{i(\mathbf{p}.\mathbf{x} - \omega' t)\} + h^*(m', \mathbf{p}) \exp\{-i(p.x - \omega' t)\}] \qquad \ldots (3a)$$

$$\mathbf{V}(x) = \frac{1}{4\pi^{3/2}} \int d\mathbf{p} \left[\left\{ \frac{\mathbf{f}(m, \mathbf{p})}{\omega} - \frac{i\mathbf{p}X\mathbf{f}(m, \mathbf{p})}{p^2} \exp\{i(\mathbf{p}.\mathbf{x} - \omega t)\} + \left\{ \frac{\mathbf{h}^*(m, \mathbf{p})}{\omega} - \frac{i\mathbf{p}X\mathbf{h}^*(m, \mathbf{p})}{p^2} \right\} \exp\{-i(p.x - \omega t)\} \right] \qquad \ldots (3b)$$

where amplitudes $f(m', \mathbf{p})$, $h^*(m', \mathbf{p})$ and $\mathbf{f}(m, \mathbf{p})$, $\mathbf{h}^*(m, \mathbf{p})$ are the representations of wavefunctions for spin-zero (scalar part) of mass m' and spin-1 (transverse part) of mass m respectively in the basis characterized in the Hilbert space upon which the infinitesimal generators of inhomogeneous Lorentz group operate. The scalar part $V_0(x)$ of the generalized four-potential leads to the non-zero longitudinal components of both generalized electric and magnetic fields. In the absence of electric and magnetic charge source density, the longitudinal part of the corresponding field vanishes. It has been shown earlier[23] that it is not possible to reduce the purely transverse electromagnetic fields which satisfy the Maxwell's equations without source for non-zero mass system. This reduction is possible only either in the presence of charge source or current source or both. This conclusion lead us[23] to assume the presence of an intrinsic current source density $j_1(x)$ associated with transverse parts of generalized electromagnetic field. The reduced expansion of this intrinsic current may be written as[23];

$$j_1(x) = -\frac{m^2}{4\pi^{3/2}} \int \frac{dp}{\omega} [f(m, \mathbf{p}) \exp\{i(\mathbf{p}.\mathbf{x} - \omega t)\} + h^*(m, \mathbf{p}) \exp\{-i(\mathbf{p}.\mathbf{x} - \omega t)\}] \qquad \ldots (4)$$

From the generalized four-potential given by Eq. (2), the generalized four-current density (J_μ) may also be written as the complex quantity with electric and magnetic four-currents as its real and imaginary parts;

$$J_\mu = j_\mu - ik_\mu \qquad \ldots (5)$$

the reduced expansions of which may be written as follows[16];

$$\mathbf{J} = \frac{q}{(2\pi)^3} \int \frac{d\mathbf{p}}{\omega^2} \mathbf{p} [f(m', \mathbf{p}) \exp\{i(\mathbf{p}.\mathbf{x} - \omega' t)\} + h^*(m', \mathbf{p}) \exp\{-i(\mathbf{p}.\mathbf{x} - \omega' t)\}] \qquad \ldots (6a)$$

and

$$J_0 = \frac{q}{(2\pi)^3} \int \frac{p^2}{\omega'^3} d\mathbf{p} [f(m', \mathbf{p}) \exp\{i(\mathbf{p}.\mathbf{x} - \omega' t)\} + h^*(m', \mathbf{p}) \exp\{-i(\mathbf{p}.\mathbf{x} - \omega' t)\}] \qquad \ldots (6b)$$

The components of generalized four-current $\{\mathcal{J}_\mu\}$ may then be written as follows in terms of intrinsic current density $j_1(x)$ given by Eq. (4) and the generalized four-current density $\{J_\mu\}$ given by Eq. (5):

$$\{\mathcal{J}_\mu\} = (j_1 + \mathbf{J}, iJ_0) \qquad \ldots (7)$$

where

$$(\mathbf{J}, iJ_0) = \{J_\mu\} \qquad \ldots (8)$$

Generalized electromagnetic field tensor describing the generalized electromagnetic fields associated with dyons may be written as

$$F_{\mu\nu} = \mathcal{E}_{\mu\nu} - \mathcal{H}^d_{\mu\nu} \qquad \ldots (9)$$

where superscript d denotes the dual tensor defined as:

$$\mathcal{H}^d_{\mu\nu} = \tfrac{1}{2} \varepsilon_{\mu\nu\gamma\rho} \mathcal{H}^{\gamma\rho} \qquad \ldots (10)$$

In Eq. (10), $\mathcal{E}_{\mu\nu}$ and $\mathcal{H}_{\mu\nu}$ are the electric and magnetic contributions of generalized electromagnetic field tensor. These tensors may be written as follows in terms of electric and magnetic four-potentials respectively:

$$\mathcal{E}_{\mu\nu} = A_{\mu,\nu} - A_{\nu,\mu} \qquad \ldots (11a)$$

and

$$\mathcal{H}_{\mu\nu} = B_{\mu,\nu} - B_{\nu,\mu} \qquad \ldots (11b)$$

Dual of generalized tensor may be written as

$$F^d_{\mu\nu} = \mathcal{H}_{\mu\nu} + \mathcal{E}^d_{\mu\nu} \qquad \ldots (12)$$

Classical Abelian Lorentz-invariant, generalized Maxwell equations may then be written in the following form:

$$F_{\mu\nu,\nu} = \mathcal{E}_{\mu\nu,\nu} = j_\mu$$

and

$$F^d_{\mu\nu,\nu} = \mathcal{H}_{\mu\nu,\nu} = k_\mu$$

since $\mathcal{E}^d_{\mu\nu,\nu} = \mathcal{H}^d_{\mu\nu,\nu} = 0$

These field equations may be combined in the following form:

$$G_{\mu\nu,\nu}=J_\mu \qquad \ldots (14)$$

where

$$G_{\mu\nu}=F_{\mu\nu}-iF^d_{\mu\nu} \qquad \ldots (15)$$

and J_μ is the generalized four-current density defined by Eqs (7) and (8).

The generalized four-current [Eq. (5)] and field equation [Eq. (14)] do not have path dependence in Abelian theory though the former may be written in the following manner in terms of the trajectory Γ_i of dyons carrying generalized charges:

$$\mathbf{J}(x)=\sum_{i=1}^{N} q_i \int_{\Gamma_i} dz_i \delta^4(x-z)=Q(x)L(x) \qquad \ldots (16)$$

where the particle trajectories Γ_i are given by the functions $z_{i\mu}(s)(i=1.... N$ for N dyons) of proper time S; $dz_\mu=\dot{z}_\mu ds$, $\dot{z}=dz/ds$ and

$$L(x)=\sum_{i=1}^{N} \int_{\Gamma_i} ds\, \delta^4(x-z) \qquad \ldots (17)$$

is the conserved particle number; $Q(x)$ is constant on each trajectory.

In terms of generalized electromagnetic field tensor $G_{\mu\nu}$, the equation of motion for any particle carrying generalized charge becomes;

$$m\ddot{x}_\mu=\mathrm{Re}(q^*G_{\mu\nu})\dot{x}^\nu \qquad \ldots (18)$$

and the classical Lorentz force may be written as

$$\mathscr{F}_{\mu\nu}(x)=\mathrm{Re}[Q^*(x)G_{\mu\nu}] \qquad \ldots (19)$$

where Re denotes the real part.

The generalized field equations [Eq. (14)], the Lagrangian density yielding these equations, equation of motion [Eq. (18)] and Lorentz force given by Eq. (19) are invariant under the duality transformations:

$$(F,F^d)\rightarrow(F\cos\theta+F^d\sin\theta,\ F\sin\theta-F^d\cos\theta)$$

$$(j_\mu,k_\mu)\rightarrow(j_\mu\cos\theta+k_\mu\sin\theta,\ j_\mu\sin\theta-k_\mu\cos\theta) \qquad \ldots (20)$$

provided that we impose the following condition on the electric and magnetic constituents of generalized fields, potentials and current densities:

$$\frac{B_\mu}{A_\mu}=\frac{k_\mu}{j_\mu}=-\frac{g}{e}=-\cot\theta \qquad \ldots (21)$$

It has already been shown in our earlier paper[24] that a pure rotation in charge space or its arbitrary combination with a transformation containing simultaneously the space and time reflections is an invariant transformation of field equation [Eq. (14)], corresponding Lagrangian density and the equation of motion [Eq. (18)] and that these equations are also invariant under the combination of pure reflection in charge space with space reflection or time reflection (not both).

3 Abelian Gauge Theory

Equations (14), (18) and (19) are Poincare invariant under duality transformations and there is no non-trivial gauge group but the electric and magnetic conservations are explicit and follow from the antisymmetry of $F_{\mu\nu}$ and $F^d_{\mu\nu}$. Because of the explicit conservations of current given by Eq. (6), the Lagrangian and field equations are invariant to the enlarged group of non-singular local gauge transformation; hence we may write

$$V_\mu\rightarrow V_\mu+\partial_\mu\Lambda_q(x) \qquad \ldots (22)$$

where $\Lambda_q(x)=\Lambda_e(x)-i\Lambda_g(x)$

In case the particles are singly charged (electrically), we need only one four-potential and then the field equations in quantum electrodynamics are invariant under an Abelian group of gauge transformations where the gauge group is $U(1)$ and $\Lambda_e(x)$ is space-time dependent. In the presence of dyons, the introduction of second four-potential is actually compensated by an enlargement of the group of gauge transformations given by Eq. (22). It is therefore possible to develop the Abelian theory which maintains the elegant electromagnetic symmetry and enlarges the gauge group $U(1)$.

If dyon be considered as having extended structure so that its electric and magnetic charges are situated at two different points in the space-time manifold, then it may be possible, in agreement with the idea of Wu and Yang[5], to divide the space-time manifold into two overlapping regions R_1 and R_2 such that R_μ vanishes in R_1 and A_μ vanishes in R_2. In such a case the points of region R_1 will observe vanishing field tensor $\mathscr{H}_{\mu\nu}$ and the field will be described only by the field tensor $\mathscr{E}_{\mu\nu}$ given by Eq. (11a) and the gauge transformation [Eq. (22)] will satisfy the condition:

$$\partial_\mu\partial_\nu\Lambda_e(x)-\partial_\nu\partial_\mu\Lambda_e(x)=0 \qquad \ldots (23)$$

On the other hand, in the region R_2 the field tensor $\mathscr{E}_{\mu\nu}$ will vanish and gauge Λ_g will satisfy the condition (23). When the dyons carrying generalized charges are the point particles, such a splitting of the space into the overlapping regions will not be possible and then the generalized fields will be described everywhere by the generalized four-potential V_μ.

It has already been shown in our earlier paper[25] that for the fields associated with massless dyons the introduction of the second potential does not cause an increase of the number of independent variables which describe the free field and that no axial gauge in

Abelian theory is possible for generalized four-potential V_μ. It has also been shown that it is not possible to make the Abelian gauge a temporal one for the generalized fields associated with massless dyons.

In order to carry out similar studies of Abelian gauge terms for the generalized fields associated with dyons of non-zero mass, let us consider the operation of any operator $\hat{A}$, out of the infinitesimal generators of Poincare group on the reduced expansions (3) of generalized four-potential for non-zero mass system. We observe that it leads to similar reduced expansions except that $f(p)$ and $k(p)$ are replaced by $\hat{A}f(p)$ and $\hat{A}k(p)$, where $\hat{A}$ is the corresponding finite spin infinitesimal generator of unitary ray representation of Poincare group and no gauge term appears while in this case the introduction of two four-potentials to describe the generalized electromagnetic fields completely removes the unphysical and controversial string variables. In other words, a singular transformation which removes the Dirac string from the description for generalized electromagnetic fields for non-zero mass system is not an Abelian gauge transformation. As such, the generalized fields associated with non-zero mass system cannot be described by Abelian gauge theory. Such a theory can describe the field associated with massless dyons, but such dyons constitute the most unphysical system because, if at all any type of system of particles each carrying electric and magnetic charge exists physically, it will be the system of dyons of non-zero mass system. It may, therefore, be concluded that the suitable theory to describe the non-zero mass dyons is the non-Abelian one.

4 Non-Abelian Gauge Theory

The non-Abelian gauge theory can be viewed as Einstein's theory of gravitation in a higher-dimensional unifed space[26] which consists of four-dimensional space-time and n-dimensional internal group space. In such a theory, the field has n-fold internal multiplicity and the multiplet $F^j(j=1.... n)$ of the gauge field transforms as a basis of adjoint representation of n-dimensional non-Abelian gauge symmetry group. The generalized field Eq. (14) may then be written as follows in non-Abelian gauge theory:

$$(\partial^\nu \delta^{jk} + q f^{jkl} V^{1\nu *}) G^k_{\mu\nu} \qquad \ldots (24)$$

where we have imposed the following condition

$$e^2 f^{jkl} B^1_\mu F^{(d)k}_{\mu\nu} = -g^2 f^{jkl} A^1_\mu F^k_{\mu\nu}$$

or

$$e^2(\vec{B} \times \vec{F}^{(d)}_\mu) = -g^2(\vec{A} \times \vec{F}_{\mu\nu}), \qquad \ldots (25)$$

where A stands for $A^j(j=1...n)$ and the cross product $\times$ is written in n-dimensional internal group space and μ, $\nu=0, 1, 2, 3$ are the variables representing the external degree of freedom; f^{jkl} are group structure constants and $G^j_{\mu\nu}$ is given by

$$G^j_{\mu\nu} = F^j_{\mu\nu} - F^{(d)j}_{\mu\nu} + q f^{jkl} V^k_\mu V^1_\nu \qquad \ldots (26)$$

where $F^j_{\mu\nu} = \partial_\nu V^j_\mu - \partial_\mu V^j_\nu$

and

$$F^{(d)}_{\mu\nu} = 1/2 \varepsilon_{\mu\nu\gamma\rho} F^{\gamma\rho j}$$

With the generalized field equation [Eq. (24)] the locking of external four-dimensional space with internal charge is not essential in contrast to the results of Boulware *et al.*[27] and it defines a suitable theory of dyons. Further, it is Lorentz- and gauge-invariant and reduces to the field equation [Eq. (14)] in the Abelian limit (for $n=1$). The generalized four-current may then be written as:

$$J^j_\mu(x) = q \frac{p^2}{\omega'^2} \bar{\psi}_{1/2}(x) \gamma_\mu T^j \psi_{1/2}(x) \qquad \ldots (27)$$

where the matrices T satisfy the following commutation relation in group space:

$$(T^j, T^k) = f^{jkl} T^l \qquad \ldots (28)$$

and $\psi_{1/2}(x)$ is the wavefunction of massless fermions. This generalized current is not conserved in the ordinary space contrary to Abelian case but the generalized conservation law of this current may be written in terms of gauge covariant derivative defined as:

$$\nabla^\nu = \partial^\nu + q \vec{V}^\nu X \qquad \ldots (29)$$

such that Eq. (24) may be written as

$$\nabla^\nu \vec{G}_{\mu\nu} = \vec{\mathscr{J}}_\mu,$$

which gives the required conservation as

$$\nabla^\mu \vec{\mathscr{J}}_\mu = 0 \qquad \ldots (30)$$

In Eqs (29) and (30) the vector sign $\rightarrow$ and cross product $\times$ are denoted in the internal group space.

In non-Abelian theory, the local gauge transformations may be generalized in the following form:

$$\vec{V}_\mu(x) \rightarrow \vec{V}_\mu(x) + \vec{V}'_\mu(x) \qquad \ldots (31)$$

where

$$\vec{V}'_\mu(x) = (\vec{\partial}_\mu + q \vec{V}^*_\mu(X) \vec{\Lambda}_q = \nabla_\mu \vec{\Lambda}_q$$

i.e. $V'^j_\mu = q f^{jkl} V^{*k}_\mu(x) \Lambda^l_q(x) + \partial_\mu \Lambda^j_q(x)$

and the gauge term $\Lambda^j_q(x)$ is given by the following equation in terms of electric and magnetic gauge constituents:

$$\Lambda^j_q(x) = \Lambda^j_e(x) - i \Lambda^j_g(x)$$

From these results it readily follows that the local gauge changes in the generalized fields and current for the invariance of field equation in the non-Abelian gauge theory are given as follows in the group space:

$$\vec{\tilde{G}}'_{\mu\nu}(x)=q[\vec{\tilde{G}}^{*}_{\mu\nu}\times\vec{\tilde{\Lambda}}_{q}(x)]$$

and

$$\vec{\tilde{\mathscr{J}}}_{\mu}(x)=q[\vec{\tilde{\mathscr{J}}}_{\mu}(x)\times\vec{\tilde{\Lambda}}_{q}(x)]$$

from which we get

$$\nabla^{\mu}\mathscr{J}'_{\mu}=0 \qquad \ldots (33)$$

which ensures the gauge covariance of the generalized current. In other words, the generalized particle current, though not conserved in non-Abelian theory, is gauge covariant and, consequently, the field equation [Eq. (24)] is invariant to a non-trivial local gauge group. Furthermore, we do not need any extra constraint to maintain the dual symmetry of Eq. (24) in non-Abelian theory in contrast to the result of Brandt and Neri[28]. Rather, the following condition, which has been used to derive Eqs (24) and (32), is sufficient to maintain the dual symmetry:

$$\frac{B^{j}_{\mu}}{A^{j}_{\mu}}=\frac{\Lambda^{j}_{q}}{\Lambda^{j}_{c}}=\frac{k^{j}_{\mu}}{j^{j}_{\mu}}=-\frac{g}{e} \qquad \ldots (34)$$

This condition is not a strange one but the generalization of condition (21) which is needed for dual invariance of the generalized field equation in the absence of non-Abelian gauge fields.

The suitable Lagrangian density yielding field equation [Eq. (24)] of the non-Abelian theory can be written in the following form:

$$\mathscr{L}=\frac{1}{4}G^{j2}_{\mu\nu}-i\psi^{j}_{1/2}\gamma\mu(\partial_{\mu}-iqV^{j}_{\mu}T^{j})\psi^{j}_{1/2}$$

$$+j_{1}V_{\mu}+m\psi^{j}\psi^{j} \qquad \ldots (35)$$

which shows that the generalized source density couples with the electric and magnetic four-potentials in the symmetric way. This Lagrangian is dual invariant subject to the constraint (34).

The Hamiltonian density of second-quantized, generalized electromagnetic fields may be calculated in the following form:

$$H(x)=\sum_{\alpha=1}^{5}\left[\frac{1}{2}G^{j2}_{\alpha,0}-\psi^{\dagger}_{1/2}i\gamma^{\alpha}(\partial_{\alpha}-iqV^{j}_{\alpha}T^{j})\psi^{\dagger}_{1/2}+j_{1}V_{\mu}\right] \qquad \ldots (36)$$

Substituting the second-quantized reduced expansions (3), (4) and (6) in Eq. (36) and carrying out the volume integration, we get the following form of the total field Hamiltonian operator:

$$\mathscr{H}=\mathscr{H}_{0}+\mathscr{H}_{\gamma}+\mathscr{H}_{m}+\mathscr{H}_{I} \qquad \ldots (37)$$

where $\mathscr{H}_{\gamma 0}=I_{1}+I_{1}^{\dagger}$, is the free-field Hamiltonian due to the longitudinal part of electromagnetic field associated with spin-1 particles; $\mathscr{H}_{\gamma}$, $\mathscr{H}_{m}$, $\mathscr{H}_{I}$ are the electromagnetic free-field Hamiltonian, Dirac free-field Hamiltonian and the interaction Hamiltonian respectively. In the internal group space, these constituents of the total Hamiltonian have the following form:

$$\mathscr{H}_{\gamma 0}=\frac{q}{4\pi^{3/2}}\int\frac{dp}{\omega'^{3}}[\{f^{j*}(m,p).p\}f^{j}(m',p)$$

$$+\{h^{j}(m,p).p\}h^{j*}(m',p)]$$

$$+\frac{q}{4\pi^{3/2}}\int\frac{dp}{\omega'^{3}}[\{p.f^{j}(m,p)\}f^{j*}(m',p)$$

$$+\{p.h^{j*}(m,p)\}h^{j}(m',p)] \qquad \ldots (38a)$$

$$\mathscr{H}_{\gamma}=\int dp[f^{j*}(m,p)f^{j}(m,p)$$

$$=+h^{j}(m,p)h^{j*}(m,p)] \qquad \ldots (38b)$$

$$\mathscr{H}_{m}=\int dp[f^{j*}(m',p)f^{j}(m',p)$$

$$+h^{j}(m',p)h^{j*}(m',p)] \qquad \ldots (38c)$$

$$\mathscr{H}_{I}=\frac{q^{*}q}{(2\pi)^{3}}\int\frac{dp}{\omega'^{4}}[f^{j*}(m',p)f^{j}(m',p)+h^{j}(m',p)h^{j*}(m',p)]$$

$$+\frac{q^{2}q^{2*}}{16\pi^{3}}f^{jkl}\int\frac{dp}{\omega'^{6}}\left(\frac{1}{\omega^{2}}+\frac{1}{p^{2}}\right)[f^{l}(m',p)$$

$$\times f^{l*}(m',p)\{f^{k*}(m,p).f^{k}(m,p)\}$$

$$+h^{l*}(m',p)h^{l}(m',p)\{h^{k}(m,p).h^{k*}(m,p)\}]$$

$$+\frac{m^{2}}{2}\int\frac{dp}{p^{2}}[f^{j*}(m,p)f^{j}(m,p)+h^{j}(m,p)h^{j*}(m,p)]$$

$$\ldots (38d)$$

The free-field Hamiltonian given by Eq. (38b) and Dirac free-field Hamiltonian given by Eq. (38c) have the usual form as derived earlier[15] for non-zero mass system.

The interaction Hamiltonian (38d) consists of three terms. The first term is due to $q^{*}q$ which leads to the fact that the coupling between two generalized charges q_{i} and q_{j} depends on electric and magnetic coupling parameters:

$$\alpha_{ij}=e_{i}e_{j}+g_{i}g_{j} \text{ and } \mu_{ij}=e_{i}g_{j}-e_{j}g_{i} \qquad \ldots (39)$$

respectively and contains the quanta of fields associated with spin-0 particles. The second term in Eq. (38d) is the only contribution of non-Abelian gauge theory and contains the product of two particle number operators for spin-1 and spin-0. This mixing of transverse and scalar part is the only factor which gives the additional character to the dyon and due to which dyons will behave as the composite states having multiple spins in non-Abelian theory. Due to this term,

the coupling parameters (electric and magnetic) are also changed as follows:

$$\alpha'_{ij} \to \alpha_{ij}^2 - \mu_{ij}^2, \text{ and } \mu'_{ij} \to 2\alpha_{ij}\mu_{ij} \quad \ldots (40)$$

which shows that the coupling in non-Abelian theory is stronger than in the Abelian gauge theory of dyons. This coupling of charges is mainly in the group space. We[25] have already shown that, in non-Abelian theory, the term μ_{ij} is responsible for the interaction of generalized charges in angular momentum basis and is solely responsible for chirality quantization, allowing the integer and half-integer values of magnetic coupling parameter. As such, in non-Abelian theory, the term μ'_{ij} will be responsible for the product of rotational invariance in charge space and for the chirality quantization.

If the structure constant vanishes, the theory reduces to the Abelian one. The present gauge theory of non-Abelian monopoles has a built-in dual structure and may describe the dual dynamics between colour isocharges and topological charges of non-Abelian symmetry in terms of two four-potentials in a dual symmetric way.

Acknowledgement

One of the authors (S R K) is grateful to the Department of Science and Technology, New Delhi for financial assistance.

References

1 t'Hooft F, *Nucl Phys B (Netherlands)*, **79** (1974) 276.
2 Yang C N & Mills R N, *Phys Rev (USA)*, **96** (1954) 191.
3 Julia B & Zee A, *Phys Rev D (USA)*, **11** (1975) 2227.
4 t'Hooft G, *Nucl Phys B (Netherlands)*, **138** (1978) 1.
5 Wu T T & Yang C N, *Phys Rev D (USA)*, **14** (1976) 437.
6 Banks T & Tombolis E, *Phys Rev D (USA)*, **20** (1979) 501.
7 Brandt R A, Neri F & Zwanziger D, *Phys Rev D (USA)*, **19** (1979) 1153.
8 Mc Keon G, *Phys Rev D (USA)*, **17** (1977) 557.
9 Cabibbo N & Ferrari E, *Nuovo Cimento (Italy)*, **23** (1962) 147.
10 Mandelstam S, *Phys Lett B (Netherlands)*, **53** (1975) 476.
11 Ezwa Z F & Tze H C, *Phys Rev D (USA)*, **15** (1977) 1647.
12 Brandt R A & Primack J R, *Phys Rev D (USA)*, **15** (1977) 1798.
13 Zwanziger D, *Phys Rev (USA)*, **176** (1968) 1480, 1489.
14 Rajput B S & Prakash Om, *Indian J Phys*, **50** (1976) 929; **53A** (1979) 274.
15 Rajput B S & Prakash Om, *Indian J Pure & Appl Phys*, **16** (1978) 593.
16 Rajput B S & Joshi D C, *Indian J Pure & Appl Phys*, **18** (1980) 988.
17 Rajput B S & Joshi D C, *Pramana* (India), **13** (1979) 637.
18 Peres A, *Phys Rev (USA)*, **167** (1969) 1449.
19 Peres A, *Phys Rev Lett (USA)*, **13** (1967) 50.
20 Prakash Om & Rajput R S, *Indian J Phys*, **48** (1974) 152.
21 Foldy L L, *Phys Rev (USA)*, **102** (1956) 568.
22 Shirokov Yu M, *Soviet Phys JETP (USA)*, **13** (1961) 240.
23 Rajput B S, *Nuovo Cimento, Lett (Italy)*, **2** (1971) 712.
24 Joshi D C & Rajput B S, *Indian J Phys Sec A*, **54** (1980) 11.
25 Rajput B S & Joshi D C, *Had J (USA)*, **4** (1981) 1805.
26 Cho Y M, *J Math Phys (USA)*, **16** (1975) 2029.
27 Boulware D G, Brown L S, Cahn R N *et al.*, *Phys Rev D (USA)*, **14** (1976) 2708.
28 Brandt R A & Neri F, *Nucl Phys B (Netherlands)*, **145** (1978) 221.

Indian Journal of Pure & Applied Physics
Vol. 21, November 1983, pp. 644-650

Meson Spectroscopy for the Superposition of Linear-cum-Logarithmic Potential with a Modified Coulomb Potential

ANURADHA BHARGAVA & L K SHARMA
Department of Applied Physics, Government Engineering College, Jabalpur 482011

Received 18 *February* 1983

Explicit and complete series solution of the Schrödinger equation for a quark-confining linear-cum-logarithmic potential with a weak modified Coulomb component has been obtained. This solution and eigenvalues have been used in studying the behaviour of Regge trajectories. Finally, the relevance of these investigations to the spectroscopy of heavy quark composites is discussed in detail.

1 Introduction

Considerable experimental evidence has accumulated in recent years in support of the idea that hadrons are composite. The most popular model of composite hadrons, the quark model, has been successful in explaining several high-energy phenomena. Yet all attempts to isolate and observe the quarks have failed todate. The charmonium model[1-7] has been quite successful in interpreting ψ and ψ' as charmed-quark-antiquark ($c\bar{c}$) bound-states and other subsequently observed phenomena.

The interaction between quarks is mediated by gluons. From the asymptotic freedom arguments, it is known that if the distance between quarks gets small (the interaction energy being very high), the strong coupling constant $\alpha_s < 1$ and one has a similar situation as in QED. One gluon exchange prevails and perturbation theory can be applied. At large distances, however, the interaction energy being small, α_s gets large and this coupling prevents the liberation of quarks since the production of $q\bar{q}$ pair is more likely.

The large masses of ψ resonances and charmed mesons led to the assumption that the charmed quarks are so heavy that they may be treated nonrelativistically[1]. No one has yet been successful in calculating the effective form of the interquark interaction from quantum chromodynamics (QCD) in the non-relativistic limit[8-12]. Most of the attempts, therefore, at understanding the level spacing and the decay rates of heavy mesonic states in the ψ, γ (9.4 GeV/c^2) and γ' (10.0 GeV/c^2) regions start from a nonrelativistic consideration of the bound state problems for a vector (or scalar) interaction and utilize numerical techniques for solving the wave equation[13-15]. The spin-orbit coupling, tensor forces and hyperfine structure are treated as additional corrections. In spite of the fact that different models have been able to provide most of the important features of meson spectroscopy, a comparison of the results so obtained, however, shows that various parameters involved in these models differ appreciably in their values. This fact indicates a certain range of uncertainty in their values. Although numerical methods have proved to be indispensable in this type of study it would be worthwhile to derive theoretically relations for level spacings, leptonic decay widths, etc. For understanding various aspects, therefore, different potential models have been developed[16-22].

In the following we undertake to study the charmonium spectroscopy for a potential which is the superposition of a quark-confining linear potential, a logarithmic potential and a weak short-range gluon exchange modified Coulomb potential $-g_3/r\log(r/r_0)$. This modified Coulomb potential has been suggested by asymptotic freedom arguments[13,24]. In section 2, we have obtained the asymptotic expansions for eigenenergies and Regge trajectories. In Section 3, we investigate the physical implication of these asymptotic expansions of eigenenergies and Regge trajectories. In this section, we have also evaluated the quark masses in S and P states along with the leptonic decay widths; the results obtained are given in Tables 1 and 2. We also consider the spin-dependent corrections (spin-orbit, tensor, spin-spin) and calculate the splitting of the $3P_J$ levels of charmonium. Finally, in Section 4 we give a brief discussion of our results.

2 Asymptotic Eigensolutions

We consider the Schrödinger equation for the following potential

$$V(r)=g_1 r-g_2\log\left(\frac{r}{r_0}\right)-\frac{g_3}{r\log(r/r_0)}-V_0 \qquad \ldots (1)$$

where $g_1>g_2>g_3$ and V_0 is the scaling parameter. Separating off the motion of the centre of mass in the usual way, we obtain the radial wave equation for the

Table 1—Lowest S and P States of Charmonium Obtained for the Potential (1)

(The input value is underlined. The quark mass m in each case has been chosen to be equal to 1.65 GeV)

State	Mass calculated for potential (1) GeV	Mass observed GeV
1^3S_1	<u>3.096</u>	3.096
1^3P	3.465	—
2^3S_1	3.702	3.684
2^3P	3.95	—
3^3S_1	4.19	4.16

Parameter	Input value used for potential (1)
β, GeV^3	0.4
η, GeV^3	0.1
δ, GeV	0.00215
r_0, GeV^{-1}	1.0
m, GeV	1.65

Table 2—Leptonic Decay Widths for Potential (1)

(All parameters are as given in Table 1)

State	Decay width calculated for potential (1) keV	Decay width observed (Ref. 14) keV
1^3S_1	4.981	4.8 ± 0.6
2^2S_1	1.903	2.1 ± 0.3
3^3S_1	0.955	0.77 ± 0.1

relative motion of the two particles of masses m_1 and m_2, i.e.

$$\frac{d^2\psi}{dr^2}+\frac{2\mu}{\hbar^2}\left[E-\frac{l(l+1)\hbar^2}{2\mu r^2}-V(r)\right]\psi=0 \qquad \ldots (2)$$

where

$$\psi=\left(\frac{1}{r}\right)\psi(r)\,\rho_l^m(\cos\theta)e^{im\varphi}$$

$\mu[=m_1m_2/(m_1+m_2)]$ is the reduced mass of the two particles and r is their separation.

Setting

$$\alpha=2\mu(E+V_0)/\hbar^2$$
$$\beta=2\mu g_1/\hbar^2$$
$$\eta=2\mu g_2/\hbar^2 \qquad \ldots (3)$$
$$\delta=2\mu g_3/\hbar^2$$

and

$$\gamma=l(l+1)$$

Eq. (2) can be written as

$$\frac{d^2\psi}{dr^2}+\left[\alpha-\beta r+\eta\log(r/r_0)+\frac{\delta}{r\log(r/r_0)}-\frac{\gamma}{r^2}\right]\psi=0 \qquad \ldots (4)$$

Next setting

$$r=e^Z(-\infty<Z<\infty)$$

and

$$\psi=e^{Z/2}\varphi \qquad \ldots (5)$$

we obtain the following basic equation

$$\frac{d^2\varphi}{dZ^2}+\{-L^2+v(Z)\}\varphi=0 \qquad \ldots (6)$$

where

$$v(Z)=\alpha e^{2Z}-\beta e^{3Z}+\eta e^{2Z}(Z-C)+\frac{\delta e^Z}{(Z-C)}$$

$$L^2=\gamma+\frac{1}{4} \qquad \ldots (7)$$

and $C=\log r_0$

Now such value of Z say Z_0 is determined for which $v(Z)$ becomes maximal. In the vicinity of this maximum, $[v(Z)-L^2]$ may become positive, thereby making the solutions oscillatory as needed for the existence of eigenvalues. Thus setting $(dv/dZ)_{Z=Z_0}=0$, and solving for Z_0, one gets

$$Z_0=\log\frac{2\alpha}{3\beta}\left[1+\frac{\eta(2k+1)}{2\alpha}+\frac{3\beta\delta(k-1)}{4\alpha^2k^2}\right] \qquad \ldots (8)$$

for $\alpha>0$, $\beta>0$

Expanding $v(Z)$ in the vicinity of the maximum at Z_0, gives

$$v(Z)=v(Z_0)+\sum_{i=2}^{\infty}\frac{(Z-Z_0)^i}{i!}v^{(i)}(Z_0) \qquad \ldots (9)$$

where for $i=0, 1, 2\ldots$

$$\begin{aligned}v^{(i)}(Z_0)=&[2^i\alpha+2^{i-1}\eta\{2(Z_0-C)+i\}]e^{2Z_0}\\&-3^i\beta e^{3Z_0}+\delta e^{Z_0}[(Z_0-C)^{-1}-i(Z_0-C)^{-2}\\&+i(i-1)(Z_0-C)^{-3}-i(i-1)(i-2)(Z_0-C)^{-4}\\&+i(i-1)(i-2)(i-3)(Z_0-C)^{-5}-\ldots]\end{aligned} \qquad \ldots (10)$$

For $i=0$, this expression is positive; for $i=1$, it is zero; and for $i>1$, it is negative (as required for a maximum of $v(Z)$ at $Z=Z_0$, for $\alpha>0$).

Now setting

$$h=[-2v^{(2)}(Z_0)]^{1/4}$$

i.e.

$$h^2=\frac{4\alpha^{3/2}}{3\beta}\left[1+\frac{\eta(6k+1)}{4\alpha}+\frac{15\beta\delta(k-1)}{8\alpha^2k^2}-\frac{3\beta\delta[a]}{8\alpha^2}\right]+O(\beta^2) \qquad \ldots (11)$$

where $k=\log(2\alpha/3\beta r_0)$

and

$$[a]=[2(Z_0-C)^{-3}-2(Z_0-C)^{-2}+(Z_0-C)^{-1}] \quad \ldots (12)$$

Further, changing the independent variable in Eq. (6) to

$\omega=h(Z-Z_0)$ transforms the equation to

$$\frac{d^2\varphi}{d\omega^2}+\left[\frac{-L^2+v(Z_0)}{h^2}-\frac{\omega^2}{4}\right]\varphi=\sum_{i=3}^{\infty}\left(\frac{v^{(i)}(Z_0)}{2v^{(2)}(Z_0)}\right)\frac{\omega^i}{i!h^{i-2}}\varphi \quad \ldots (13)$$

where

$$\frac{v^{(i)}(Z_0)}{v^{(2)}(Z_0)}=\frac{P}{Q} \quad \ldots (14)$$

where $P=[2^i\alpha+2^{i-1}\eta\{2(Z_0-C)+i\}]e^{2Z_0}-3^i\beta e^{3Z_0}+\delta e^{Z_0}[f]$ and $Q=[2^2\alpha+2\eta\{2(Z_0-C)\}]e^{2Z_0}-3^2\beta e^{3Z_0}+\delta e^{Z_0}[a]$

and

$$[f]=[(Z_0-C)^{-1}-i(Z_0-C)^{-2}+i(i-1)(Z_0-C)^{-3}-i(i-1)(i-2)(Z_0-C)^{-4}+\ldots] \quad \ldots (15)$$

In particular, we have for $i=3, 4$

$$\frac{v^{(3)}(Z_0)}{v^{(2)}(Z_0)}=\left[5+\frac{\eta}{\alpha}-\frac{9\beta\delta(k-1)}{2\alpha^2k^2}+\frac{15\beta\delta[a]}{4\alpha^2}-\frac{3\beta\delta[b]}{4\alpha^2}\right] \quad \ldots (16)$$

and

$$\frac{v^{(4)}(Z_0)}{v^{(2)}(Z_0)}=\left[19+\frac{7\eta}{\alpha}-\frac{45\beta\delta(k-1)}{2\alpha^2k^2}+\frac{57\beta\delta[a]}{4\alpha^2}-\frac{3\beta\delta[C]}{4\alpha^2}\right] \quad \ldots (17)$$

where

$$[b]=[(Z_0-C)^{-1}-3(Z_0-C)^{-2}+6(Z_0-C)^{-3}-6(Z_0-C)^{-4}] \quad \ldots (18)$$

and

$$[C]=[(Z_0-C)^{-1}-4(Z_0-C)^{-2}+12(Z_0-C)^{-3}-24(Z_0-C)^{-4}+24(Z_0-C)^{-5}] \quad \ldots (19)$$

For large values of h, the right hand side of Eq. (13) can, to a first approximation, be neglected. The corresponding behaviour of the eigenvalues $(1/h^2)[-L^2+v(z_0)]$ can then be determined by comparing the equation with the equation of parabolic cylinder functions. The solutions are square integrable only if

$$\frac{1}{h^2}[-L^2+v(Z_0)]=\frac{1}{2}q$$

where $q=2n+1$, $n=0, 1, 2\ldots$ (provided the wavefunction is required to vanish at infinity; otherwise it is only approximately an odd integer). For the complete solution, we get

$$\frac{1}{h^2}[-L^2+v(Z_0)]=\frac{1}{2}q+\frac{\Delta}{h} \quad \ldots (20)$$

The value of Δ in Eq. (20) remains to be determined. Now substituting Eq. (20) into Eq. (13) one gets

$$\mathscr{D}_q\varphi=\frac{2\Delta}{h}\varphi-\sum_{i=3}^{\infty}\left\{\frac{v^{(i)}(Z_0)}{v^{(2)}(Z_0)}\right\}\frac{\omega^i}{i!h^{i-2}}\varphi \quad \ldots (21)$$

where

$$\mathscr{D}_q=-2\frac{d^2}{d\omega^2}-q+\frac{1}{2}\omega^2 \quad \ldots (22)$$

Eq. (21) is now in a form suitable for the application of our perturbation method. The first approximation $\varphi=\varphi^{(0)}$ is simply a parabolic cylinder function $D_{(q-1)/2}(\omega)$, i.e.

$$\varphi^{(0)}=\varphi_q=D_{(q-1)/2}(\omega), \mathscr{D}_q\varphi_q=0 \quad \ldots (23)$$

where

$$D_{(q-1)/2}(\omega)=2^{(q-3)/4}e^{-\omega^2/4}\psi\left(\frac{3-q}{4}\ \frac{3}{2};\ \frac{\omega^2}{2}\right)$$

ψ being a confluent hypergeometric function. The function φ_q is well known to obey the recursion formula

$$\omega\varphi_q=(q, q+2)\varphi_{q+2}+(q, q-2)\varphi_{q-2} \quad \ldots (24)$$

where

$$(q, q+2)=1, (q, q-2)=\frac{1}{2}(q-1) \quad \ldots (25)$$

For higher powers one has

$$\omega^i\varphi_q=\sum_{j=2i}^{-2i}S_i(q, j)\varphi_{q+j} \quad \ldots (26)$$

and a recursion relation can be written down for the coefficients S_i. The first approximation $\varphi=\varphi^{(0)}$ then leaves uncompensated terms amounting to

$$R_q^{(0)}=\left\{\frac{2\Delta}{h}-\sum_{i=3}^{\infty}\left(\frac{v^{(i)}(Z_0)}{v^{(2)}(Z_0)}\right)\frac{\omega^i}{i!h^{i-2}}\right\}\varphi_q(\omega)=\frac{2\Delta}{h}\varphi q-\sum_{i=3}^{x}\frac{1}{h^{i-2}}\sum_{j=2i}^{-2i}\tilde{S}_i(q,j)\varphi_{q+j}(\omega) \quad \ldots (27)$$

where

$$\tilde{S}_i(q,j)=\frac{v^{(i)}(Z_0)}{v^{(2)}(Z_0)}\frac{1}{i!}S_i(q,j) \quad \ldots (28)$$

Rewriting Eq. (27) in the form

$$R_q^{(0)}=\sum_{i=3}^{\infty}\frac{1}{h^{i-2}}\sum_{j=2i}^{-2i}[q, q+j]_i\varphi_{q+j}(\omega) \quad \ldots (29)$$

where

$$[q,q]_3 = 2\Delta - \tilde{S}_3(q,0)$$

and for $j \neq 0$

$$[q,q+j]_3 = -\tilde{S}_3(q,j) \qquad \ldots (30)$$

and for

$$i>3,\ -2i \leq j \leq 2i$$

$$[q,\ q+j]_i = -\tilde{S}_i(q,j)$$

Since $\mathscr{D}_{q+j} = \mathscr{D}_{q-j}$, $\mathscr{D}_q \varphi_{q+j} = j\varphi_{q+j}$, a term $\mu\varphi_{q+j}$ in $R_q^{(0)}$ can be removed by adding to $\varphi^{(0)}$ contribution $\mu\varphi_{q+j}/j$ except, of course, when $j=0$. Hence the next-order contribution of φ becomes

$$\varphi^{(1)} = \sum_{i=3}^{\infty} \frac{1}{h^{i-2}} \sum_{\substack{j=2i \\ j\neq 0}}^{-2i} \frac{[q,q+j]_i}{j} \varphi_{q+j}(\omega) \qquad \ldots (31)$$

This contribution, in turn, leaves uncompensated

$$R_q^{(1)} = \sum_{i=3}^{\infty} \frac{1}{h^{i-2}} \sum_{\substack{j=2i \\ j\neq 0}}^{-2i} \frac{[q,q+j]_i}{j} R_{q+j}^{(0)}$$

and gives the next order contribution of φ

$$\varphi^{(2)} = \sum_{i=3}^{\infty} \frac{1}{h^{i-2}} \sum_{\substack{j=2i \\ j\neq 0}}^{-2i} \frac{[q,q+j]_i}{j} \sum_{i'=3}^{\infty} \frac{1}{h^{i'-2}} \times \sum_{\substack{j'=2i' \\ j+j'\neq 0}}^{-2i'} \frac{[q+j,q+j+j']_{i'}}{j+j'} \varphi_{q+j+j'} \qquad \ldots (32)$$

Proceeding this way one gets the solution

$$\varphi = \varphi^{(0)} + \varphi^{(1)} + \varphi^{(2)} + \ldots$$

which is an asymptotic expansion in descending powers of h valid for

$$Z - Z_0 = O(1/h) \qquad \ldots (33)$$

i.e. around $Z = Z_0$. In addition to this solution, we obtain an eigenvalue equation from which Δ in Eq. (20) can be determined. The latter is obtained by setting equal to zero the sum of the terms φ_q in $R_q^{(0)}$, $R_q^{(1)}$, ... which have been unaccounted for so far. Thus

$$0 = \sum_{i=3}^{\infty} \frac{1}{h^{i-2}} [q,q]_i + \sum_{i=3}^{\infty} \frac{1}{h^{i-2}} \sum_{\substack{j=2i \\ j\neq 0}}^{-2i} \frac{[q,q+j]_i}{j} \times \sum_{i'=3}^{\infty} \frac{1}{h^{i'-2}} [q+j,\ q]_{i'} + \ldots \qquad \ldots (34)$$

or

$$0 = \frac{1}{h}[q,q]_3 + \frac{1}{h^2}\{[q,q]_4 + \sum_{\substack{j=6 \\ j\neq 0}}^{-6} \frac{[q,q+j]_3}{j} [q+j,q]_3\} + O(1/h^3) \qquad \ldots (35)$$

From this equation Δ and hence the eigenvalues are determined.

Thus

$$\begin{aligned} 2h\Delta = {} & [\tilde{S}_4(q,0) - \tfrac{1}{6}\tilde{S}_3(q,6)\tilde{S}_3(q+6,-6) + \tfrac{1}{6}\tilde{S}_3(q,-6) \\ & \times \tilde{S}_3(q-6,6) - \tfrac{1}{2}\tilde{S}_3(q,2)\tilde{S}_3(q+2,-2) \\ & + \tfrac{1}{2}\tilde{S}_3(q,-2)\tilde{S}_3(q-2,2)] + O(1/h^2) \\ = {} & \frac{q^2+1}{4}\left\{19 + \frac{7\eta}{\alpha} - \frac{45\beta\delta(k-1)}{2\alpha^2k^2} + \frac{57\beta\delta[a]}{4\alpha^2} - \frac{3\beta\delta[C']}{4\alpha^2}\right\} \\ & - \frac{(15q^2+7)}{2^4.3^2}\left\{25 + \frac{10\eta}{\alpha} - \frac{45\beta\delta(k-1)}{\alpha^2k^2} + \frac{75\beta\delta[a]}{2\alpha^2} - \frac{15\beta\delta[b]}{2\alpha^2}\right\} + O(1/h^2) \end{aligned}$$

Using Eqs (3), (16), (17) and (20), we obtain

$$\begin{aligned} \left(l+\frac{1}{2}\right)^2 = {} & \frac{4\alpha^3}{27\beta^2} + \frac{2\alpha\delta}{3\beta k} + \frac{4\alpha^2\eta k}{9\beta^2} + \frac{\delta^2(k-1)}{2\alpha k^3} \\ & - \frac{2\alpha^{3/2}q}{3\beta}\left[1 + \frac{\eta(6k+1)}{4\alpha} + \frac{15\beta\delta(k-1)}{8\alpha^2k^2} - \frac{3\beta\delta[a]}{8\alpha^2}\right] + + \frac{(51q^2+1)}{72} + \frac{(87q^2+7)\eta}{288\ \alpha} \\ & - \frac{(105q^2+25)}{64}\frac{\beta\delta(k-1)}{\alpha^2k^2} + \frac{(579q^2+17q)}{384}\frac{\beta\delta[a]}{\alpha^2} \\ & + \frac{3(q^2+1)}{128}\frac{\beta\delta[C']}{\alpha^2} - \frac{5(15q^2+7)}{192}\frac{\beta\delta[b]}{\alpha^2} \\ & + \frac{3\beta q}{1024\alpha^{3/2}}\left[1 + \frac{\eta(6k+1)}{4\alpha} + \frac{15\beta\delta}{8\alpha^2}\frac{(k-1)}{k^2} - \frac{3\beta\delta[a]}{8\alpha^2}\right]^{-1}\Big[(19.8518q^2 + 0.2963) \\ & + (65.481q^2 + 114.37)\frac{\eta}{\alpha} \\ & - (896.666q^2 + 556.666)\frac{\beta\delta(k-1)}{\alpha^2k^2} \\ & + (1211.222q^2 + 979.888)\frac{\beta\delta[a]}{\alpha^2} \\ & - (596.111q^2 + 662.777)\frac{\beta\delta[b]}{\alpha^2} \\ & + (129.333q^2 + 212.666)\frac{\beta\delta[C']}{\alpha^2} \\ & - (11.666q^2 + 31.666)\frac{\beta\delta[d]}{\alpha^2} \\ & + (0.333q^2 + 1.666)\frac{\beta\delta[e]}{\alpha^2}\Big] + O\left(\frac{1}{h^3}\right) \qquad \ldots (36) \end{aligned}$$

where

$$[d]=[(Z_0-C)^{-1}-5(Z_0-C)^{-2}+20(Z_0-C)^{-3}$$
$$-60[Z_0-C)^{-4}+120(Z_0-C)^{-5}-120(Z_0-C)^{-6}]$$

and

$$[e]=[(Z_0-C)^{-1}-6(Z_0-C)^{-2}+30(Z_0-C)^{-3}$$
$$-120(Z_0-C)^{-4}+360(Z_0-C)^{-5}$$
$$-720(Z_0-C)^{-6}+720(Z_0-C)^{-7}]$$

It may be of interest to note that for $\eta=0$ the expression (36) reduces to the eigenenergy expansion for combination of a quark-confining linear potential and a short-range gluon exchange modified Coulomb potential. This expression is found to be in exact agreement up to $O(1/h^2)$ with that obtained by Sharma *et al.*[20]

3 Applications

3.1 Regge Trajectories

We have utilized the square roots of the expansion (36) for plotting Regge trajectories. The Regge trajectories for potential (1) have been shown in Fig. 1. The values of quark mass (m), β, η and δ chosen for plotting these trajectories have been given in Table 1. We find that these trajectories are almost linear over the range of immediate interest. Hence it is concluded that the Regge trajectories for our superposed potential do not lose their linearity and their behaviour is similar to the ones obtained for pure logarithmic and linear potentials.

3.2 Calculation of Bound Quark-Antiquark Mass

Since the quark mass is twice the reduced mass μ, the mass M_q of the bound quark-antiquark pair in state q is given by

$$M_q=4\mu+E \qquad \ldots (37)$$

In Table 1, the calculated values of lowest S, and P states along with their corresponding experimental values are given. The values of corresponding parameters used in the calculation (i.e. β, η, δ, r_0 and m) are also given. The values obtained for the higher S states agree with those predicted by other authors[25,26]. The P states are corrected for tensor forces and spin-orbit and spin-spin coupling; this is done in the following sub-section 3.3.

3.3 Spin-dependent Corrections

Spin-dependent corrections have been considered in many previous investigations[27-31] and are generally taken over from the corresponding work on positronium. To leading order in $(v/c)^2$, where v is the relative velocity of the quark and antiquark (each of mass m), the correction to be applied to the potential (1) is

$$V_c(r)=\frac{3}{2m^2}\frac{1}{r}\frac{dV(r)}{dr}\mathbf{L}\cdot\mathbf{S}+\frac{1}{6m^2}\nabla^2V(r)\sigma_1\cdot\sigma_2$$
$$-\frac{1}{12m^2}\left(\frac{d^2V(r)}{dr^2}-\frac{1}{r}\frac{dV(r)}{dr}\right)S_{12} \qquad \ldots (38)$$

where $\mathbf{L}$ is the orbital angular momentum operator, $\mathbf{S}=\frac{1}{2}(\sigma_1+\sigma_2)$ and S_{12} is the standard tensor operator, given by

$$S_{12}=3(\sigma_1\cdot\hat{r})(\sigma_2\cdot\hat{r})-\sigma_1\cdot\sigma_2$$

In the usual way, we have for $S=1$ and respectively $J=L-1,\ L,\ L+1$:

$$\mathbf{L}\cdot\mathbf{S}=-(L+1),\ -1,\ L \qquad \ldots (39)$$

Similarly, we have for $S=1$ and respectively[32] $L=J-1,\ J,\ J+1$:

$$S_{12}=-\frac{2(J-1)}{2J+1},\ 2,\ -\frac{2(J+2)}{2J+1} \qquad \ldots (40)$$

Substituting V into V_c, we obtain terms which are singular at $r=0$ (i.e. more divergent than $1/r^2$). Since there are no acceptable bound states for such singular potentials, we have to regularize the singularities by the introduction of cut-off parameters a, b and c' into the potential. We choose these parameters by using the following replacement in the singular terms[18]

$$\frac{1}{r^3\log(r/r_0)}\rightarrow\frac{1}{r\log(r/r_0)}\frac{1}{(r^2+a^2)}$$

$$\frac{1}{r^3[\log(r/r_0)]^2}\rightarrow\frac{1}{r\log(r/r_0)}\frac{1}{[r^2\log(r/r_0)+b^2]} \qquad \ldots (41)$$

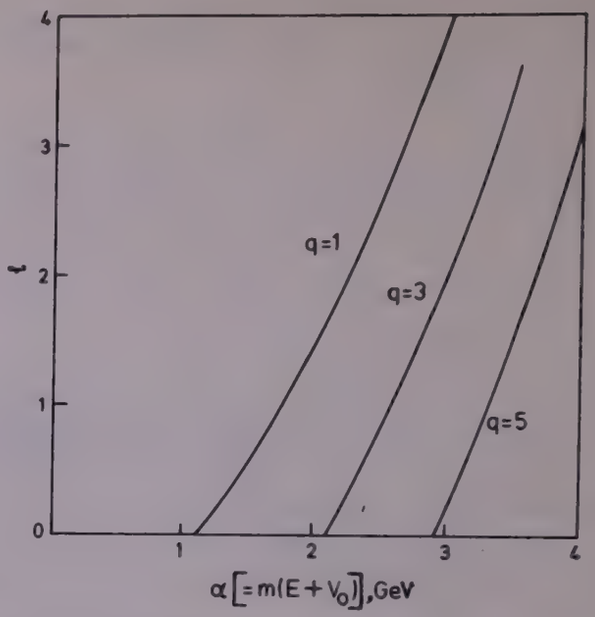

Fig. 1—The first three Regge trajectories for potential (1)

$$\frac{1}{[r\log(r/r_0)]^3}\rightarrow\frac{1}{r\log(r/r_0)}\frac{1}{\{[r\log(r/r_0)]^2+c'^2\}}$$

Substituting V into V_c, we then have

$$V_c(r)=\frac{3}{2m^2}\left[\frac{g_1}{r}-\frac{g_2}{r^2}+\frac{g_3}{r\log(r/r_0)(r^2+a^2)}+\frac{g_3}{r\log(r/r_0)[r^2\log(r/r_0)+b^2\}}\right]\mathbf{L}\cdot\mathbf{S}$$
$$+\frac{1}{6m^2}\left[\frac{2g_1}{r}-\frac{g_2}{r^2}-\frac{g_3}{r\log(r/r_0)[r^2\log(r/r_0)+b^2\}}-\frac{2g_3}{r\log(r/r_0)\ [r\log(r/r_0)]^2+c'^2}\right]\boldsymbol{\sigma}_1\cdot\boldsymbol{\sigma}_2$$
$$+\frac{1}{12m^2}\left[\frac{g_1}{r}-\frac{2g_2}{r^2}+\frac{3g_3}{r\log(r/r_0)(r^2+a^2)}+\frac{4g_3}{r\log(r/r_0)[r^2\log(r/r_0)+b^2]}+\frac{2g_3}{r\log(r/r_0)\ [r\log(r/r_0)]^2+c'^2}\right]S_{12} \quad \ldots (42)$$

The Coulomb terms here can be treated as a further perturbation. We next assume that on the average the separation of quark and antiquark in the meson is such that

$$0\ll r/a;\ [r^2\log(r/r_0)]/b^2$$

$$[r\log(r/r_0)]/c'\ll 1$$

In such a case, we can expand the regularized denominators in rising powers of r and ignore all powers of r higher than the first, since these would have to be treated as further perturbations of the linear confinement potential. Under these conditions we have to add to $V(r)$ the contribution

$$V_c(r)=\frac{d_1}{r^2}+\frac{d_2}{r\log(r/r_0)} \quad \ldots (43)$$

where

$$d_1=\frac{3}{2m^2}(g_1-g_2)\mathbf{L}\cdot\mathbf{S}+\frac{1}{6m^2}(2g_1-g_2)\boldsymbol{\sigma}_1\cdot\boldsymbol{\sigma}_2+\frac{1}{12m^2}(g_1-2g_2)S_{12}$$

and

$$d_2=\frac{3g_3}{2m^2}\left(\frac{1}{a^2}+\frac{1}{b^2}\right)\mathbf{L}\cdot\mathbf{S}-\frac{g_3}{6m^2}\left(\frac{1}{b^2}+\frac{2}{c'^2}\right)\times\boldsymbol{\sigma}_1\boldsymbol{\sigma}_2+\frac{g_3}{12m^2}\left(\frac{3}{a^2}+\frac{4}{b^2}+\frac{2}{c'^2}\right)S_{12} \quad \ldots (44)$$

This means that, in this case, the coupling constant g_3 associated with the $[r\log(r/r_0)]^{-1}$ term in $V(r)$ has to be replaced by (g_3+d_2), and a term d_1 has to be added to the centrifugal term of the Schrödinger equation to obtain the well known p states.

Table 3—The charmonium states $1^{2s+1}P_J$ for potential (1) after corrections for spin interactions

(All parameters are as given in Table 1 along with $a=4.5$ GeV, $b=c'=2.25$ GeV)

State	Mass calculated for potential (1) GeV	Mass observed (Ref. 10) GeV
1^3P_2	3.496	$3.561\pm7\times10^{-3}$
1^3P_1	3.4778	$3.511\pm7\times10^{-3}$
1^3P_0	3.456	$3.413\pm9\times10^{-3}$

In Table 3 the charmonium states $1^{2s+1}P_J$ for the potential (1) along with the corresponding experimentally observed values[28] are given. It will be noted that agreement of our results with the experimentally-observed values is quite good.

3.4 Calculation for Leptonic Decay Widths

Decay widths play an important role in exploring the origin of a newly found hadronic state. The leptonic decay widths of a vector quark-antiquark bound state such as ψ can be expressed in terms of the s-wave bound-state wavefunction at the origin. Thus,

$$\Gamma(\psi\rightarrow l\bar{l})=\frac{16\pi\alpha^2e_Q^2}{M_\psi^2}|\psi(0)|^2 \quad \ldots (45)$$

where α is the fine structure constant [not to be confused with α of Eq. (3)] and e_Q is the charge of the constituent quark of ψ.

In the case of an s-wave bound state, the wavefunction is related to the potential V by the following expression:

$$|\psi(0)|^2=\frac{\mu}{2\pi}\left\langle\frac{dV}{dr}\right\rangle=\frac{\mu}{2\pi}\int\psi^*(r)\frac{dV}{dr}\psi(r)\,dr \quad \ldots (46)$$

In order to calculate $\langle dV/dr\rangle$ and hence $|\psi(0)|^2$, the WKB approximation method[33] is used.

Thus for our potential

$$|\psi(0)|^2=\frac{\mu}{2\pi}\frac{\mathrm{M}}{\mathrm{N}} \quad \ldots (47)$$

where

$$\mathrm{M}=\int_{r_0}^{r}dr\left[E-g_1r+g_2\log(r/r_0)+\frac{g_3}{r\log(r/r_0)}+V_0\right]^{-1/2}$$

$$\frac{dV}{dr}\quad\text{and}\quad \mathrm{N}=\int_0^r dr\left[E-g_1r+g_2\log(r/r_0)+\frac{g_3}{r\log(r/r_0)}+V_0\right]^{-1/2}$$

where $\bar{r}$ is the classical turning point, $r_0 = 1$ and

$$\frac{dV}{dr} = g_1 - \frac{g_2}{r} + g_3 r^{-2}\{(\log r)^{-1} + (\log r)^{-2}\}$$

Eq. (47) has been solved analytically to obtain $|\psi(0)|^2$. The results obtained for decay widths for potential (1) are shown in Table 2 and they are compared with the experimentally observed values.

4 Discussion

In the above treatment, we have shown that it is by no means essential to use numerical integration techniques to evaluate the meson spectrum and its decay widths from the nonrelativistic wave equation. Perturbation technique can also be utilized for solving any problem of this type.

The investigations of this paper were based on the assumption that the Coulomb potential is sufficiently weak to allow it to be treated as a perturbation of the confinement potential which we have taken as a combination of linear and logarithmic potentials. We have replaced the usual Coulomb potential by the improved form $-g_3/r\log(r/r_0)$ as suggested by asymptotic-freedom arguments[8-11]. In our study, we have used perturbation terms up to O $(1/h^2)$ only. It might appear at the first sight that accuracy of our results could have been further improved had we evaluated perturbation terms beyond second order. It has, however, been found from actual calculations that the contribution from the terms in the third order and beyond are negligibly small and are of no consequence.

It is observed that our results show definite improvement over those obtained for either linear or logarithmic potentials taken separately, thereby indicating that the combination of these two potentials along with short-range modified Coulomb potential is more appropriate for the quark confinement.

Acknowledgement

One of the authors (AB) is thankful to Dr H A Vachhani for encouragement, and to the University Grants Commission, New Delhi, for the award of a fellowship

References

1 Appelquist T & Politzer H D, *Phys Rev Lett (USA)*, **34** (1975) 43; *Phys Rev D (USA)*, **12** (1975) 1404.
2 Appelquist T, De Rujula A, Politzer H D & Glashow S L, *Phys Rev Lett (USA)*, **34** (1975) 365.
3 Eichten E, Gottfried K, Kinoshita T *et al.*, *Phys Rev Lett (USA)*, **34** (1975) 369.
4 De Rujula A & Glashow S L, *Phys Rev Lett (USA)*, **34** (1975) 46.
5 Callan C G, Kingsley R L, Treiman S B *et al.*, *Phys Rev Lett (USA)*, **34** (1975) 52.
6 Harrington B J, Park S Y & Yildiz A, *Phys Rev Lett (USA)*, **34** (1975) 168, 706.
7 Kang J S & Schnitzer H J, *Phys Rev D (USA)*, **12** (1975), 841, 2791.
8 Lichtenberg D B & Wills J G, *Nuovo Cimento A (Italy)*, **47** (1978) 483.
9 Aubert J J, Becker V, Biggs P J, *et al.*, *Phys Rev Lett (USA)*, **33** (1974) 1404.
10 Fischler W, *Nucl Phys B (Netherlands)*, **129** (1977) 157.
11 Antippa A F, Everett A E & Phares A J, *Nuovo Cimento A (Italy)*, **43** (1978) 347.
12 Poggio E C, *Phys Lett B (Netherlands)*, **71** (1977) 381.
13 Quigg C & Rosener J L, Fermilab-Pub-77/82-THY, unpublished.
14 Quigg C & Rosener J L, Fermilab-Pub-77/90-THY, unpublished.
15 Thacker H B, Quigg C & Rosener J L, Fermilab-Pub-77/108-THY and 77/100-THY, 1977, unpublished.
16 Krammer M & Krasemann H, *Nuovo Cimento A (Italy)*, **32** (1976) 394.
17 Müller-Kristen H J W & Bose S K, *J Math Phys (USA)*, **20** (1979, 2741.
18 Müller-Kristen H J W, Hite G E & Bose S K, *J Math Phys (USA)*, **20** (1979) 1878.
19 Eichten E, Gottfried K, Kinoshita T *et al.*, *Phys Rev D (USA)*, **17** (1978) 3090.
20 Sharma L K, Iyer V P, Mehta Sheilly, *et al.*, *J Math Phys (USA)*, **23** (1982) 780.
21 Sharma G S & Sharma L K, *Indian J Pure & Appl Phys*, **20** (1982) 706.
22 Kajwadkar A P & Sharma L K, *Acta Phys Acad Sci Hung (Hungary)*, **52**(2) (1982) 189.
23 Feinberg F L, *Phys Rev Lett (USA)*, **39** (1977) 316.
24 Appelquist T, Dine M & Muzinich I, *Phys Lett B (Netherlands)*, **69** (1977) 231.
25 Appelquist T, Barnett R M & Lane K, SLAC-PUB-2100 (Stanford, California) 1978.
26 Schopper H, DESY preprint 77/79 (1977), Lectures given at the Erice School, Erice, Italy, 1977.
27 Barbieri R, Kogerler R, Kunszt Z & Gatto R, *Nucl Phys B (Netherlands)*, **105** (1976) 125.
28 Pignon D & Piketty C A, University of Paris preprints LPTENS 77/21, 78/2, unpublished.
29 Jackson J D, *Lectures on the new particles*, LBL-5500, edited by M C Zipf (SLAC, Stanford, California), 1976.
30 Schnitzer H J, *Phys Rev D (USA)*, **13** (1975) 74.
31 Schnitzer H J, *Phys Rev Lett (USA)*, **35** (1975) 1540.
32 Dover C B, Kahana S H & Trueman T L, *Phys Rev D (USA)*, **16** (1977) 799.
33 Quigg C & Rosner J L, Fermilab-Pub-77/106-THY and Fermilab-Pub-78/19-THY, unpublished.

Indian Journal of Pure & Applied Physics
Vol. 21, November 1983, pp. 651-658

Superluminal Lorentz Transformations in Six-Dimensional Space-Time

H C CHANDOLA & B S RAJPUT
Department of Physics, Kumaun University, Naini Tal 263002

Received 22 *September* 1982; *revised received* 14 *March* 1983

Superluminal Lorentz transformations (SPLT) of two types in six-dimensional space-time have been derived in different special cases by using relative matrix velocities between the frames. The first type of transformations are shown to be complex while those of second type are real. A new idea of tachyon corridor in six-dimensional extended relativity has been introduced. Both types of transformations have been generalized into a convenient form and it has been shown that the second type of SPLT in six-dimensional space are more akin to the spirit of relativity.

1 Introduction

A large number of workers have spent considerable efforts in the attempts to include the faster than light particles (tachyons) and superluminal frames (moving with the relative velocity faster than light) with even more respectability than permitted on its own by the reinterpretation principle of the original work by Bilaniuk *et al.*[1] In the two-dimensional case the superluminal Lorentz transformations (SPLT) were first introduced by Parker[2], generalized by Mariwalla[3] and then independently rediscovered[4] and completed[5,6] by several other workers. In the generalization of SPLT from one to three spatial dimensions, one faces 'no-go' theorem of Gorini[7] that essentially stated no such extension to exist when these transformations are required to satisfy the reality condition and to preserve space isotropy and light speed invariance. Similar incompatibility of extended relativity with standard formalism has also been shown recently by Mariwalla[8]. Realising the requirement of reality, the generalized Lorentz transformations were derived by Recami and Mignani[9] in four-dimensional space. Though these transformations have some good properties such as being linear, leaving the light speed invariant and being close to the spirit of relativity in the light of Gorini's theorem, there are a large number of inconsistencies associated with these transformations due to the occurrence of imaginary quantity in them. Under these transformations, the interior of light cone cannot be transformed onto its exterior and vice-versa and the chronotopical mapping $(3,1)\rightarrow(1,3)$ associated with these transformations leads[10] to unphysical mapping of a body of finite shape and size into an indefinite unbounded region[11]. Furthermore, these transformations do not form the group along with subluminal Lorentz transformations (SBLT) without introducing space-time inverters[12] and they cannot be used[13] to derive the reduction of fields of tachyons of various spins in terms of standard helicity representation of Poincare group. All these difficulties are removed by using real SPLT[14,15], though these transformations appear to violate rotational invariance, the invariance of topological rigidity and the principle of constancy of light speed. Under these transformations the roles of time and space coordinate along the direction of relative motion between the frames S and S′ (tachyon-corridor) get interchanged such that the velocities zero and infinite correspond to each other in frames S and S′ respectively (reciprocity principle) and the tachyon corridor remains invariant. The set of all special SBLT and SPLT along tachyon corridor forms a group. Choosing the tachyon corridor along the x_3-axis, it has been shown in our recent paper[16] that the reciprocity principle, which maps the usual bradyonic four-space $\{x_\mu\}\equiv(it,\ x_1,\ x_2,\ x_3)$ in frame S to tachyonic four-space $\{X_\mu\}\equiv(iT,X_1,X_2,X_3)$ $\equiv(ix_3,x_1,x_2,t)$ in frame S′ under real SPLT, removes some of the difficulties raised by Gorini's theorem about these transformations and retains the norm of four-vector, constancy of light speed, topological rigidity and the isotropy of space. Due to the violation of Lorentz covariance by introducing tachyon corridor, these transformations make the Lorentz invariant theory of second quantization[17,18] two-dimensional one.

In order to remove these difficulties encountered in extending the SPLT to four-dimensional space-time, recently the proposal of a symmetric six-dimensional space-time with three temporal and three spatial dimensions has been put forward by many workers[19-23] and it became clear that the extension of the principle of relativity to superluminal phenomena is possible only in the pseudo-Euclidean space-time having the same number of space and time axes.

In the present paper, the extension of SPLT of both the types (complex and real) in six-dimensional space-

time has been examined and it has been shown that the complex SPLT suffer from many inconsistencies and drawbacks even in six-dimensional space and attempts made so far are insufficient to interpret the occurrence of imaginary quantity in these transformations. It has also been shown that with real SPLT in six-dimensional space, many drawbacks of four-dimensional transformations are removed and these SPLT become more akin to the spirit of relativity.

2 Superluminal Lorentz Transformations of First Type in Six-Dimensional Space-Time

In order to solve various difficulties encountered with the four-dimensional complex SPLT of Recami and Mignani[9], an attempt has been made by various workers[21-23] to write these transformations in six-dimensional space-time. Let us re-examine in the general case whether this formalism is suitable for solving those difficulties in a consistent way. Maintaining the complete symmetry between space and time, in six-dimensional space-time, let us represent a point in an inertial frame S by the spatial vector $\mathbf{r}$ and the temporal vector $\mathbf{t}$ such that an event P may be described by the six real coordinates;

$$P \equiv (x_1, x_2, x_3; t_1, t_2, t_3) \qquad \ldots (2.1)$$

and an interval may be written as

$$ds^2 = -|d\mathbf{r}|^2 + |d\mathbf{t}|^2 = d_{\sigma\rho}\, dx_\sigma dx_\rho \qquad \ldots (2.2)$$

where $x_{j+3} = t_j (j = 1, 2, 3)$ and $\sigma, \rho = 1 \ldots 6$. The reference metric may then be defined as follows:

$$d_{\sigma\rho} = (-1, -1, -1, 1, 1, 1) \qquad \ldots (2.3)$$

Relative velocity between the inertial frames S and S′ then becomes a 3×3 matrix given by;

$$\hat{v} = \begin{pmatrix} v_{11} & v_{12} & v_{13} \\ v_{21} & v_{22} & v_{23} \\ v_{31} & v_{32} & v_{33} \end{pmatrix} \qquad \ldots (2.4)$$

where $v_{ij} = \partial x_i / \partial t_j$ with $x_{p \neq i}$ and $t_{m \neq j}$ constants and all indices i, j, p and m run from 1 to 3 (it may be noticed here that the first and second subscripts (i and j) of velocity v_{ij} correspond to spatial and temporal components respectively so that velocity is always defined as rate of change of space).

Let us now consider the following special cases of this relative velocity.

2.1 Column Generalization of Velocity

If we take the relative velocity matrix, corresponding to the superluminal relative motion of frame S′ with respect to S, as follows;

$$\hat{v} = \begin{pmatrix} v_{11} & 0 & 0 \\ v_{21} & 0 & 0 \\ v_{31} & 0 & 0 \end{pmatrix} \qquad \ldots (2.5)$$

surviving only first column, where $v_{j1} = \partial x_j / \partial t_1$ with $x_{p \neq j}$ = constant, then the SPLT of four-dimensional case may be generalized into the following form in six-space;

$$x'_\mu = \Lambda(v) x_\mu \qquad \ldots (2.6)$$

where x_μ is a six-vector and the transformation matrix may be written as;

$$\Lambda(v) = \begin{pmatrix} (e + Kv_{11}^2) & Kv_{11}v_{21} & Kv_{11}v_{31} & -\gamma_1 v_{11} & 0 & 0 \\ Kv_{11}v_{21} & (e + Kv_{21}^2) & Kv_{21}v_{31} & -\gamma_1 v_{21} & 0 & 0 \\ Kv_{11}v_{31} & Kv_{21}v_{31} & (e + Kv_{31}^2) & -\gamma_1 v_{31} & 0 & 0 \\ -\gamma_1 v_{11} & -\gamma_1 v_{21} & -\gamma_1 v_{31} & \gamma_1 & 0 & 0 \\ 0 & 0 & 0 & 0 & e & 0 \\ 0 & 0 & 0 & 0 & 0 & e \end{pmatrix} \qquad \ldots (2.7)$$

where $K = (\gamma_1 - e)/v^2$, $v^2 = \text{trace}\ (\hat{v}\hat{v}^T)$, $\gamma_1 = [\text{tr}(\hat{v}\hat{v}^T) - 1]^{-1/2}$, $e = \sqrt{-1}$ and T denotes the transpose. Let us now consider another frame S″ moving with the superluminal relative velocity $\hat{u}(u_{ij} = \partial x_i / \partial t_j)$ with respect to S′ such that all the three frames are parallel. Then the product of the transformation matrices corresponding to these two superluminal motions gives the direct transformation between frames S and S″ which is obviously a subluminal transformation with all real elements of transformation matrix satisfying the relation

$$\Lambda(v)\Lambda(u) = \Lambda(u)\Lambda(v) = \Lambda(V) \qquad \ldots (2.8)$$

where the correct usual velocity addition law is obtained in the following form only when one of these transformations is combined with space and time reflections:

$$v_{ji} = \frac{u_{j1} + v_{j1}}{1 + \text{tr}(\hat{v}^T \hat{u})} \qquad \ldots (2.9)$$

Furthermore, the commutation equation (2.8) holds good only in the case of parallel motion of frames, i.e. when

$$\frac{v_{11}}{u_{11}} = \frac{v_{21}}{u_{21}} = \frac{v_{31}}{u_{31}} = \frac{1}{A} \qquad \ldots (2.9a)$$

where A is a constant. Then we have

$$\gamma = -[1 - \text{tr}(\hat{V}\hat{V}^T)]^{-1/2} = -\gamma_1\gamma_2(1 + Av^2) \qquad \ldots (2.9b)$$

where γ_2 is associated with velocity $\hat{u}$. Another condition for Eq. (2.8) to hold good is given by

$$\gamma_1\gamma_2\left[1 + \frac{v^2u^2}{\text{tr}(\hat{v}^T\hat{u})}\right] - e(\gamma_1 + \gamma_2) - 1 = 0 \qquad \ldots (2.9c)$$

which obviously is not a physical condition. In the general case, the matrices of Eq. (2.8) do not commute, allowing the Thomas precession. Keeping in mind the fact that the quadratic form given by Eq. (2.2) changes its sign under the transformation (2.6), we get the following relation:

$$t'^2 = \gamma_1^2[(vx)^2 - 2t_1(vx) + v^2t_1^2] - t^2 \qquad \ldots (2.10)$$

where $(vx)=\sum_{n=1}^{3} v_{n1}x_n$. It leads to the correct form of proper time only for the special case of four-dimensional relativity (i.e. for $t=t_1$, $t_2=t_3=0$) and to the correct form of length contraction only when the relative velocity is taken along x_j and t_j(i.e. $v_{jj}=v$).

2.2 Row Generalization of Velocity

If we take the relative velocity matrix as

$$\hat{v}=\begin{pmatrix} v_{11} & v_{12} & v_{13} \\ 0 & 0 & 0 \\ 0 & 0 & 0 \end{pmatrix} \qquad \ldots (2.11)$$

then the transformation matrix of SPLT may be written in the following form:

$$\Lambda(v)=\begin{pmatrix} \gamma_1 & 0\ 0 & -\gamma_1 v_{11} & -\gamma_1 v_{12} & -\gamma_1 v_{13} \\ 0 & e\ 0 & 0 & 0 & 0 \\ 0 & 0\ e & 0 & 0 & 0 \\ -\gamma_1 v_{11} & 0\ 0 & (e+Kv_{11}^2) & Kv_{11}v_{12} & Kv_{11}v_{13} \\ -\gamma_1 v_{12} & 0\ 0 & Kv_{11}v_{12} & (e+Kv_{12}^2) & Kv_{12}v_{13} \\ -\gamma_1 v_{13} & 0\ 0 & Kv_{11}v_{13} & Kv_{12}v_{13} & (e+Kv_{13}^2) \end{pmatrix} \qquad \ldots (2.12)$$

which gives the following relationship

$$r'^2=\gamma_1^2[(vt)^2-2x_1(vt)+v^2x_1^2]-r^2 \qquad \ldots (2.13)$$

where $(vt)=\sum_{n=1}^{3} v_{1n}t_n$. It leads to the length contraction of four-dimensional relativity but the correct relation of proper time may be obtained from this transformation only when the relative velocity is taken along x_j and t_j (i.e. $v_{jj}=v$). The requirements of commutation of two successive transformations and velocity addition here are the same as discussed in the previous case. Transformations (2.7) and (2.12) may be generalized in the following form:

$$\mathbf{r}'=e\mathbf{r}+\frac{(\gamma_1-e)}{\mathrm{tr}(\hat{v}\hat{v}^{\mathrm{T}})}(\hat{v}\hat{v}^{\mathrm{T}})\mathbf{r}-\gamma_1[\mathbf{t}\hat{v}_c]$$

$$\mathbf{t}'=e\mathbf{t}+\frac{(\gamma_1-e)}{\mathrm{tr}(\hat{v}\hat{v}^{\mathrm{T}})}(\hat{v}^{\mathrm{T}}\hat{v})\mathbf{t}-\gamma_1[\mathbf{r}\hat{v}_{\mathrm{R}}^{\mathrm{T}}] \qquad \ldots (2.14)$$

where we have introduced the vectors $[\mathbf{t}\hat{v}_c]$ and $[\mathbf{r}\hat{v}_{\mathrm{R}}^{\mathrm{T}}]$ in the following form:

$$[\mathbf{t}\hat{v}_c]=t_1\begin{pmatrix} v_{11} \\ v_{21} \\ v_{31} \end{pmatrix}+t_2\begin{pmatrix} v_{12} \\ v_{22} \\ v_{32} \end{pmatrix}+t_3\begin{pmatrix} v_{13} \\ v_{23} \\ v_{33} \end{pmatrix}$$

and

$$[\mathbf{r}\hat{v}_{\mathrm{R}}^{\mathrm{T}}]=x_1\begin{pmatrix} v_{11} \\ v_{12} \\ v_{13} \end{pmatrix}+x_2\begin{pmatrix} v_{21} \\ v_{22} \\ v_{23} \end{pmatrix}+x_3\begin{pmatrix} v_{31} \\ v_{32} \\ v_{33} \end{pmatrix} \qquad \ldots (2.15)$$

In writing the transformation equations (2.14), we have not imposed any restriction like $\mathbf{r}\perp\mathbf{t}$, in contrast to Maccarone and Recami[24], who, considering the pseudo-rotations in six-space, wrote the transformations by generalizing the transcendent boosts along preferred direction without taking into account all the components of velocity.

2.3 Diagonal Generalization of Velocity

Let us consider the case of relative velocity matrix which has non-zero elements only along the principal diagonal, i.e.

$$\hat{v}=\begin{pmatrix} v_{11} & 0 & 0 \\ 0 & v_{22} & 0 \\ 0 & 0 & v_{33} \end{pmatrix} \qquad \ldots (2.16)$$

from which it appears as if the space-time is made of three equivalent two-dimensional spaces (x_1-t_1), (x_2-t_2) and (x_3-t_3) in each of which SPLT of extended relativity may be written in the following way:

$$x'_j=(v_{jj}^2-1)^{-1/2}[x_j-v_{jj}t_j]$$
$$t'_j=(v_{jj}^2-1)^{-1/2}[t_j-v_{jj}x_j] \qquad \ldots (2.17)$$

where $j=1, 2, 3$. These transformations are the superluminal analogue of those derived by Pappas[20] for subluminal case. Metric (2.3) and the quadratic form changes by a negative sign in this case also as in the previous cases. In the transcendental case, i.e. $v_{jj}\to\infty$, these transformations are reduced to the following form:

$$x'_j\to -t_j \text{ and } t'_j\to -x_j$$
$$\text{or } \mathbf{x}\rightleftharpoons -\mathbf{t} \qquad \ldots (2.17a)$$

from which it appears that the axes called t_x, t_y, t_z by subluminal observer S are considered as spatial axes x, y, z by the transcendent superluminal observer S′. In the recent work of Maccarrone and Recami[24], only this restricted special case has been interpreted in terms of pseudo-rotations in six-space by generalizing transcendent boosts along preferred directions. From transformations (2.17) we get

$$t'^2=\sum_{j=1}^{3}\gamma_{jj}^2(x_j-v_{jj}t_j)^2+\sum_{j=1}^{3}x_j^2-t^2 \qquad \ldots (2.18)$$

where $\gamma_{jj}=(v_{jj}-1)^{-1/2}$. It leads to the correct form of proper time only for $x_1=x_2=x_3=0$ with $t_1=t$, $t_2=0=t_3$ (i.e. four-dimensional case). For the choice of $t_1=t_2=t_3=t$, Eq. (2.18) leads to

$$t'^2=t^2[(\gamma_{11}^2+1)+(\gamma_{22}^2+1)+(\gamma_{33}^2+1)-t^2 \qquad \ldots (2.19)$$

which gives the correct expression of proper time only when $v_{11}=v$ and $v_{22}=0=v_{33}$. Therefore, the transformations (2.17) give the correct relativistic time dilation only in the special case of four-dimensional space-time. Furthermore, for a particle at origin of the frame S, the transformations (2.17) give the following form of magnitude of time vector in S′:

$$t_m'^2=\mathbf{t}'^{\mathrm{T}}\mathbf{t}'=\sum_{j=1}^{3}\gamma_{jj}^J\mathbf{t}_j^2 \qquad \ldots (2.20)$$

which reproduces the correct form of proper time only when either

$$t_1 = t,\ t_2 = 0 = t_3 \text{ (four-dimensional case)} \quad \ldots (2.21a)$$

or

$$t'^2 = \sum_{j=1}^{3} K_j^2 t_j'^2 \quad \ldots (2.21b)$$

where $K_j = (v_{jj}^2 - 1)^{1/2} / \sum_i v_{ii}^2 - 1)$.

In other words, this scheme gives the correct time dilation only for the four-dimensional case or for an artificial condition given by Eq. (2.21b).

Transformation matrix $\Lambda(v)$ may be written from the transformation equations (2.17) in the form similar to that obtained earlier[25] in subluminal case with changed definition of γ_{jj}. Unlike in previous cases, the commutation of two successive transformations and the velocity addition law does not require any extra condition and consequently these transformations suffer from the defect that there is no room for Thomas precession with them.

All these cases discussed above may be generalized into the following most general form of the interval inverting and light speed preserving transformations in six-dimensional space-time:

$$\left.\begin{aligned} \mathbf{r}' &= \hat{A}\mathbf{r} + \hat{v}'\hat{R}\mathbf{t} \\ \mathbf{t}' &= \hat{R}\mathbf{t} - \hat{R}\hat{v}^{\mathrm{T}}\mathbf{r} \end{aligned}\right\} \quad \ldots (2.22)$$

where velocity matrix $\hat{v}$ given by Eq. (2.4) is the velocity of spatial origin of S′ in S, $\hat{v}'$ is that of spatial origin of S in S′ and the matrices $\hat{A}$ and $\hat{R}$ are given by:

$$\hat{R}\hat{v}^{\mathrm{T}} = -(\hat{v}')^{\mathrm{T}}\hat{A} \quad \ldots (2.23)$$

satisfying the following conditions in the present case:

$$\left.\begin{aligned} \hat{A}^{\mathrm{T}}\hat{A} &= -(\hat{I} - \hat{v}\hat{v}^{\mathrm{T}})^{-1} \\ \hat{R}^{\mathrm{T}}\hat{R} &= (\hat{I} - \hat{v}^{\mathrm{T}}\hat{v})^{-1} \end{aligned}\right\} \quad \ldots (2.24)$$

These relations show that the matrices $\hat{A}$ and $\hat{R}$ are no more real and that is why the corresponding transformation equations in all these cases (except the third one) are complex, in contrast to the conclusion of Cole[22]. The transformations (2.22) are similar to those derived by Cole[22] in a very sophisticated way.

The foregoing analysis shows that the generalization of complex SPLT of Recami and Mignani[9] to six-dimensional space-time, also contains imaginary quantities and thus suffers from the same defects as those for four-dimensional space-time, in contrast to the conclusion of Mignani and Recami[21]. The correct law of velocity addition given by Eq. (2.9) can be obtained with these transformations in six-dimensional space only when one of these successive transformations is combined with space and time inversions. In other words, these transformations cannot form the group along with their subluminal counterparts without including the operators corresponding to these inversions. It is an unphysical result and has no analogy in subluminal frames in six-dimensional space-time[25]. In view of these difficulties, in the following section the real SPLT in six-dimensional formulation are considered.

3. Superluminal Lorentz Transformations of Second Type in Six-Dimensional Space-Time

Keeping in view the various merits[26,17,18] of real SPLT over those of first type of transformations in four-space, let us make an attempt to examine these transformations in six-dimensional space-time. In order to derive these SPLT in six-dimensional space-time, first of all we consider the tachyon corridor in this space.

The idea of a preferred axis in space was proposed by Antippa *et al.*[14], in order to generalize the one-dimensional causal theory of tachyon to three spatial dimensions and specially to make three-dimensional theory internally consistent[16] when dealing with real SPLT. This preferred spatial direction is the tachyon corridor along which the motion of tachyon is unidirectional. In real superluminal six-dimensional formalism, the definition of tachyon corridor will not remain so simple. Here it will be specified by six-dimensional velocity given by Eq. (2.4) which is a dyadic. It clearly shows that the tachyon corridor no more remains a line vector here like that in the four-dimensional space-time but it has the form of a curved sheet made up of three spatial and three temporal dimensions. Its position may be prescribed by fixing all the nine components of velocity defined by three space coordinates each of which corresponds to three time coordinates. If the preferred relative velocity has only one non-zero element v_{ij} then the projection of this curved sheet onto $x_i - t_j$ plane will define the tachyon corridor. Postulating such a tachyon corridor is necessary to explain the tachyon-bradyon reciprocity which is the result of interchange of coordinates x_i and t_j under the six-dimensional real SP between the frames moving with relative velocity defined in $x_i - t_j$ plane. All the six-dimensional inertial frames having relative velocity lying in this plane of tachyon corridor may be defined as preferred frames. It will be shown in the following analysis that the principle of four-dimensional extended relativity is consistently valid for the set of all these preferred frames.

In order to write the real SPLT in six-dimensional space-time, let us consider two inertial frames S and S′ whose axes are parallel and whose origins coincide at $t = t' = 0$. Relative velocity between these two frames in the general case (with tachyon corridor as a curved sheet) is expressed as a 3×3 matrix given by Eq. (2.4). The generalized space-time six-vector here is x_μ and the

reference metric is given by Eq. (2.3). The space-time interval in frame S in this case also is given by Eq. (2.2) with

$$d\mathbf{r} = (d\mathbf{r}_{\parallel} + d\mathbf{r}_{\perp}) \text{ and } dt = (dt_{\parallel} + dt_{\perp})$$

where $d\mathbf{r}$ and dt are the spatial and temporal parts of six-space vector along the sheet of tachyon corridor while $d\mathbf{r}_{\perp}$ and $dt_{\perp}$ are those perpendicular to it. Eq. (2.2) then becomes:

$$ds^2 = -|d\mathbf{r}_{\parallel}|^2 - |d\mathbf{r}_{\perp}|^2 + |dt_{\parallel}|^2 + |dt_{\perp}|^2 \quad \ldots (3.1)$$

The components of spatial and temporal vectors parallel and perpendicular to the sheet of tachyon corridor may be written as follows in the reference frame S:

$$\mathbf{r}_{\parallel} = \frac{(\hat{v}\hat{v}^{\mathrm{T}})}{v^2}\mathbf{r};\ \mathbf{r}_{\perp} = \mathbf{r} - \frac{(\hat{v}\hat{v}^{\mathrm{T}})}{v^2}\mathbf{r}$$

$$t_{\parallel} = \frac{(\hat{v}^{\mathrm{T}}\hat{v})}{v^2}t;\ t_{\perp} = t - \frac{\hat{v}^{\mathrm{T}}\hat{v})}{v^2}t \quad \ldots (3.2)$$

For the cases of column and row generalizations of relative velocity given by Eq. (2.5) and Eq. (2.11) respectively, the real SPLT may be written in the following manner as a generalization of those for four-dimensional space[14]:

$$\begin{aligned}
\mathbf{r}' &= \mu\gamma\left\{\frac{(\hat{v}\hat{v}^{\mathrm{T}})}{v^2}\mathbf{r} - [\mathbf{t}\hat{v}_c]\right\} \\
t' &= \mu\gamma\left\{\frac{(\hat{v}^{\mathrm{T}}\hat{v})}{v^2}t - [\mathbf{r}\hat{v}_{\mathbf{R}}^{\mathrm{T}}]\right\} \\
\mathbf{r}'_{\perp} &= \mathbf{r}_{\perp} = \mathbf{r} - \frac{(\hat{v}\hat{v}^{\mathrm{T}})}{v^2}\mathbf{r} \\
t'_{\perp} &= t = t - \frac{(\hat{v}^{\mathrm{T}}\hat{v})}{v^2}t
\end{aligned} \quad (3.3)$$

where $v^2 = \mathrm{tr}(\hat{v}\hat{v}^{\mathrm{T}})$, $\gamma = [\mathrm{tr}(\hat{v}\hat{v}^{\mathrm{T}}) - 1]^{-1/2}$, $\mu = \pm 1$ and $[\mathbf{t}\hat{v}_c]$ and $[\mathbf{r}\hat{v}_{\mathbf{R}}^{\mathrm{T}}]$ are column matrices defined by Eqs (2.15). These transformations are real in contrast to corresponding transformations for the case of first type of SPLT in six-dimensional space. Furthermore, the vectors $\mathbf{r}$ and $\mathbf{t}$ come in exactly symmetric form in these transformations.

In transformation relations (3.3), $\mathbf{r}'$, $\mathbf{r}'_{\perp}$, t' and $t'_{\perp}$ have same operational meaning in frame S′ as those of unprimed vectors in frame S, but when the events of frame S′ are observed by frame S, the component $\mathbf{r}'_{\parallel}$ appears as playing the role of the component t' and vice-versa. That is why it can be shown easily that with these real SPLT the quadratic form of ds^2 given by Eq. (3.1) does not remain invariant as such but becomes so when the space and time components parallel to the tachyon corridor are interchanged in frame S′ (reciprocity principle) so that ds'^2 may be defined as:

$$ds'^2 = -|dt'_{\parallel}|^2 - |d\mathbf{r}'_{\perp}|^2 + |d\mathbf{r}'_{\parallel}|^2 + |dt'_{\perp}|^2 \quad \ldots (3.4)$$

This interchange and the corresponding interchange in the components of momentum and energy is necessary for the validity of special theory of relativity while passing from a subluminal to a superluminal frame in six-dimensional space-time. Such an interchange is also needed for the tachyon-bradyon reciprocity in six-dimensional space. With these transformations all the dynamical variables remain real and the corresponding Hamiltonian remains Hermitian while passing from subluminal to superluminal world. These transformations (3.3) may also be written in the form of Eq. (2.6) in terms of transformation matrix which has the forms given in the following, for the cases of column and row generalizations of velocity. For the column generalization:

$$\Lambda(v) = \begin{pmatrix}
(1+Kv_{11}^2) & Kv_{11}v_{21} & Kv_{11}v_{31} & -\mu\gamma v_{11} & 0 & 0 \\
Kv_{11}v_{21} & (1+Kv_{21}^2) & Kv_{21}v_{31} & -\mu\gamma v_{21} & 0 & 0 \\
Kv_{11}v_{31} & Kv_{21}v_{31} & (1+Kv_{31}^2) & -\mu\gamma v_{31} & 0 & 0 \\
-\mu\gamma v_{11} & -\mu\gamma v_{21} & -\mu\gamma v_{31} & \mu\gamma & 0 & 0 \\
0 & 0 & 0 & 0 & 1 & 0 \\
0 & 0 & 0 & 0 & 0 & 1
\end{pmatrix} \quad \ldots (3.5)$$

and for row generalization:

$$\Lambda(v) = \begin{pmatrix}
\mu\gamma & 0 & 0 & -\mu\gamma v_{11} & -\mu v_{12} & -\mu\gamma v_{13} \\
0 & 1 & 0 & 0 & 0 & 0 \\
0 & 0 & 1 & 0 & 0 & 0 \\
-\mu\gamma v_{11} & 0 & 0 & (1+Kv_{11}^2) & Kv_{11}v_{12} & Kv_{11}v_{13} \\
-\mu\gamma v_{12} & 0 & 0 & Kv_{11}v_{12} & (1+Kv_{12}^2) & Kv_{12}v_{13} \\
-\mu\gamma v_{13} & 0 & 0 & Kv_{11}v_{13} & Kv_{12}v_{13} & (1+Kv_{13}^2)
\end{pmatrix} \quad \ldots (3.6)$$

where $K = (\mu\gamma - 1)/v^2$ The transformation matrix given by Eq. (3.5), gives the following relations for time interval in S′:

$$\Delta t' = \begin{pmatrix} -\mu\gamma v_{11} & -\mu\gamma v_{21} & -\mu\gamma v_{31} \\ 0 & 0 & 0 \\ 0 & 0 & 0 \end{pmatrix}\Delta\mathbf{r} + \begin{pmatrix} \mu\gamma & 0 & 0 \\ 0 & 1 & 0 \\ 0 & 0 & 1 \end{pmatrix}\Delta t \quad \ldots (3.7)$$

An instantaneous temporal displacement in frame S measured along t_1-direction is then given by the following equation in the frame S′:

$$\Delta t' = \mu\gamma\Delta t$$

which is identical to the four-dimensional time dilation for $\mu = 1$, but the same is not true for spatial interval. The transformation matrix (3.5) gives the correct length contraction in S′ only when the relative velocity is taken along x_j and t_1, when the measurements of length are made along x_j in the frame S. Similarly, the

transformation matrix (3.6) gives the correct space contraction in four-dimensional limit but the correct time dilation is obtained only in the case of relative velocity taken in x_1-t_j plane when temporal measurements in the frame S are made along t_j. In other words, for both the transformation matrices, the usual four-dimensional relativity is reproduced if the temporal and spatial measurements are made in the plane of tachyon corridor.

Any two successive transformations for both these transformation matrices commute only when all the three frames have collinear motion as shown by condition (2.9a). In contrast with the previous case of SPLT (first type), in the present case there is no restriction of space-time inversion to be coupled with any of two successive transformations to give the correct law of velocity addition. In other words, in place of condition (2.9b), here we have

$$\gamma=\gamma_1\gamma_2(1+Av^2) \qquad \ldots (3.8)$$

and in place of the unphysical condition (2.9c) containing imaginary number, here we have

$$\gamma_1\gamma_2\left[1+\frac{v^2u^2}{\mathrm{tr}(\hat{v}^{\mathrm{T}}\hat{u})}\right]-\mu(\gamma_1+\gamma_2)+1=0 \qquad \ldots (3.9)$$

for the commutation of two successive transformations. This condition is similar to that derived earlier[25] for SBLT in six-dimensional space-time. For the general case of motion, the successive transformations do not commute for either of the transformation matrices given by Eqs (3.5) and (3.6), and hence in both these generalizations of relative velocity the Thomas precession will be observed in general.

In case of the diagonal generalization of velocity given by Eq. (2.16), the real SPLT in six-dimensional space are similar to those given by Eq. (2.17) except that a factor $\mu=\pm 1$ will come in each equation. In order to write these transformations in the consistent form of Eqs (3.3), we may define the tachyon corridor in this case by the following equations:

$$(\mathbf{r}_{\parallel})_j=\frac{(\hat{v}\hat{v}^{\mathrm{T}}\mathbf{r})_j}{v_{jj}^2} \text{ or } \mathbf{r}_{\parallel}=\mathbf{r}$$

$$(\mathbf{t}_{\parallel})_j=\frac{(\hat{v}^{\mathrm{T}}\hat{v}\mathbf{t})_j}{v_{jj}^2} \text{ or } \mathbf{t}_{\parallel}=\mathbf{t} \qquad \ldots (3.10)$$

such that $\mathbf{r}_{\perp}=\mathbf{t}_{\perp}=0$. In other words, in this case the tachyon corridor is specified by the plane in which the vectors $\mathbf{r}$ and $\mathbf{t}$ lie. Transformations (2.17) reveal that the six-dimensional space-time here is made of three two-dimensional spaces for each of which the tachyon corridor is the projection of the general tachyon corridor $\mathbf{r}$-$\mathbf{t}$ onto it. In other words, each of these subspaces is $(1+1)$ dimensional with its own tachyon corridor, i.e. subspace corresponding to the velocity v_{11} has the tachyon corridor along x_1-axis and so on. Transformation equations (2.17) may now be written in the following form:

$$\mathbf{r}'_{\parallel}=\mu(\hat{v}\hat{v}^{\mathrm{T}})\begin{pmatrix}(\gamma_{11}/v_{11}^2) & x_1\\ (\gamma_{22}/v_{22}^2) & x_2\\ (\gamma_{33}/v_{33}^2) & x_3\end{pmatrix}-\mu\begin{pmatrix}\gamma_{11}v_{11} & t_1\\ \gamma_{22}v_{22} & t_2\\ \gamma_{33}v_{33} & t_3\end{pmatrix} \ldots (3.11a)$$

$$\mathbf{t}'_{\parallel}=\mu(\hat{v}^{\mathrm{T}}\hat{v})\begin{pmatrix}(\gamma_{11}/v_{11}^2) & t_1\\ (\gamma_{22}/v_{22}^2) & t_2\\ (\gamma_{33}/v_{33}^2) & t_3\end{pmatrix}-\mu\begin{pmatrix}\gamma_{11}v_{11} & x_1\\ \gamma_{22}v_{22} & x_2\\ \gamma_{33}v_{33} & x_3\end{pmatrix} \ldots (3.11b)$$

Under these transformations also, the space-time interval given by Eq. (2.2) remains invariant only when the components of space and time parallel to the tachyon corridor are interchanged in S′ frame of reference. The effects of space contraction and time dilation under these transformations have already been discussed in the previous Section 2 from which we may conclude that the usual four-dimensional special relativity can be reproduced from these transformations also, provided that the spatial and temporal measurements are performed in the planes of tachyon corridors, or in other words, when the space is splitted into three two-dimensional spaces. Transformation matrix $\Lambda(v)$ in this case may be written as:

$$\Lambda(v)=\begin{pmatrix}\mu\gamma_{11} & 0 & 0 & -\mu\gamma_{11}v_{11} & 0 & 0\\ 0 & \mu\gamma_{22} & 0 & 0 & -\mu\gamma_{22}v_{22} & 0\\ 0 & 0 & \mu\gamma_{33} & 0 & 0 & -\mu\gamma_{33}v_{33}\\ -\mu\gamma_{11}v_{11} & 0 & 0 & \mu\gamma_{11} & 0 & 0\\ 0 & -\mu\gamma_{22}v_{22} & 0 & 0 & \mu\gamma_{22} & 0\\ 0 & 0 & -\mu\gamma_{33}v_{33} & 0 & 0 & \mu\gamma_{33}\end{pmatrix} \qquad \ldots (3.12)$$

from which it follows that the successive transformations of this type always commute leaving no room for Thomas precession.

All the real SPLT in six-dimensional space-time discussed above may be generalized in the form given by Eqs (2.22) where the matrices $\hat{A}$ and $\hat{R}$ satisfy the conditions (2.23) but not those given by Eq. (2.24) and, consequently, their reality is maintained in this case in contrast to the previous case of SPLT of the first type.

4 Discussion

The first type of SPLT in six-dimensional space-time have been derived in the form of Eqs (2.14) and (2.17) for the special cases of velocity generalizations and all of them have been generalized in the form of Eqs (2.22) where the matrices $\hat{A}$ and $\hat{R}$ satisfy the conditions (2.23) and (2.24). This generalized form is identical to the Cole's scheme[22] of SPLT and it may therefore be concluded that Cole's scheme is the generalization of the first type of SPLT which,

in general, gives the transformations in terms of imaginary quantities in contrast to the claim of Cole[22]. These transformations suffer from all those drawbacks which the first type of SPLT do in the four-dimensional space[26] and attempts made so far are insufficient to interpret the occurrence of imaginary quantity in these transformations. Even in the generalized form given recently by Recami and Maccarrone[12], the complex transformations do not form the group without introducing the space and time inversions which have automatically been included in the group of dilations in writing the generalized transformations. Even the transcendent SPLT which follow from these generalized Lorentz transformations, are not real and cannot act as identity elements and hence the inversion operators associated with these transformations cannot be assigned to describe the anti-tachyons in as simple manner as has been recently[27] for subluminal case. The whole interpretation procedure[11,28] of the entire set of complex SPLT does not explain satisfactorily the imaginary quantities occurring in these transformations. Actually, by this approach[11,28] the complex SPLT are only partially interpreted and then these transformations lose their group theoretical properties. As such, any scheme introducing three temporal components do not help in the explanation of the occurrence of imaginary quantity in the first type of SPLT in four-dimensional space. Furthermore, the invariance of ds^2 given by Eq. (2.2) under complex SPLT in six-dimensional space, requires the interchange of each spatial component with the corresponding temporal component. It is therefore needed with these transformations to retain the three-dimensionality of space in addition to three-dimensional time in superluminal frames, in contrast to the results obtained by Mignani and Recami[21] and recently by Pavsic[29] about the coupling of spatial components in these frames. With these transformations, the correct law of velocity addition given by Eq. (2.9) in six-dimensional space can be obtained only when one of the two successive transformations is coupled with space-time inversions. It is an unusual result and has no analogy in the subluminal frames in six-dimensional space[25]. Furthermore, the conditions (2.9b) and (2.9c) for the commutation of two successive transformations are unphysical and contradict similar results for subluminal frames. In the light of all these points, we may conclude that no attempt made in six-dimensional space-time to interpret the imaginary unit occurring in four-dimensional SPLT can improve the situation and such SPLT do not make much sense in six-dimensional space-time.

On the other hand, SPLT of the second type given by Eqs (3.3), (3.11a) and (3.11b) in the six-dimensional space are always real under which the space-time interval given by Eq. (2.2) does not remain invariant as such, but its invariance is achieved at once when the spatial and temporal projections onto the plane of tachyon corridor are interchanged in the superluminal frame. With these transformations, all the results of usual four-dimensional extended relativity are reproduced when the spatial and temporal measurements are made in the plane of tachyon corridor. With them, any two successive transformations give the correct law of velocity addition. The conditions (3.8) and (3.9) for the commutation of two such successive transformations are similar to those derived earlier[25] for SBLT in six-dimensional space. As such these SPLT in six-dimensional space are more akin to the theory of relativity than the first type of SPLT. Using these transformations the second-quantized theory of tachyons[17,18] in energy-time representation can be made four-dimensional one, while with the first type of SPLT even in four-space no reduction and second quantization of tachyon fields have been possible[13].

Acknowledgement

The authors are grateful to Prof. E A B Cole (Univ. of Leeds) and Prof P T Pappas (Univ. of Athens) for sending the reprints and preprints of their recent work. One of the authors (HCC) is also grateful to the CSIR, New Delhi for financial assistance.

Reference

1 Bilaniuk O M, Deshpande V K & Sudarshan E C G, *Am J Phys (USA)*, **30** (1962) 718.
2 Parker L, *Phys Rev (USA)*, **188** (1969) 2287.
3 Mariwalla K H, *Am J Phys (USA)*, **37** (1969) 1281.
4 Olkhovsky V S & Recami E, *Visn Kiiv Univ Ser Fiz (USSR)*, **11** (1970) 58.
5 Mignani R & Recami E, *Nuovo Cimento A (Italy)*, **14** (1973) 169.
6 Antippa A F, *Nuovo Cimento A (Italy)*, **10** (1972) 389.
7 Gorini V, *Commun Math Phys (Germany)*, **21** (1971) 150.
8 Mariwalla K H, *Phys Lett A (Netherlands)*, **79** (1980) 43.
9 Recami E & Mignani R, *Rev Nuovo Cimento (Italy)*, **4** (1974) 209.
10 Rajput B S, Joshi Prabhakar & Negi O P S, *Lett Nuovo Cimento (Italy)*, **35** (1982) 147.
11a Caldirola P, Maccarrone G D & Recami E, *Lett Nuovo Cimento (Italy)*, **28** (1980) 251.
11b Recami E & Maccarrone G D, *Lett Nuovo Cimento (Italy)*, **29** (1980) 241.
12 Maccarrone G D & Recami E, *Lett Nuovo Cimento (Italy)*, **34** (1982) 251.
13 Rajput B S, Purohit K D & Negi O P S, *Indian J Pure & Appl Phys*, **19** (1981) 1081.
14 Antippa A F, *Phys Rev D (USA)*, **11** (1975) 724.
15 Lemke H, *Lett Nuovo Cimento (Italy)*, **17** (1976) 209.
16 Negi O P S & Rajput B S, *Phys Lett B (Netherlands)*, **113** (1982) 183.
17 Rajput B S, Negi O P S & Purohit K D, *Indian J Pure & Appl Phys*, **20** (1982) 22.
18 Negi O P & Rajput B S, *J Math Phys (USA)*, **23** (1982) 1964.
19 Demers P, *Can J Phys (Canada)*, **53** (1975) 1687.

20 Pappas P T, *Lett Nuovo Cimento* (*Italy*), **25** (1979) 429.
21 Mignani R & Recami E, *Lett Nuovo Cimento* (*Italy*), **16** (1976) 449.
22 Cole E A B, *Nuovo Cimento B* (*Italy*), **44** (1978) 157; *Phys Lett A* (*Netherlands*), **76** (1980) 371.
23 Ziino G, *Phys Lett A* (*Netherlands*), **70** (1979) 88.
24 Maccarrone G D & Recami E, Preprint PP/693 (Catania University, Italy), 1982.
25 Chandola H C & Rajput B S, *Nuovo Cimento B* (*Italy*), **72** (1982) 21.
26 Rajput B S, *Proc Einstein Cent Symp*, edited by K Kondo and T M Karade (Duhita Publishers, Nagpur, India), **1** (1980) 181.
27 Recami E & Rodrigues W A, *Found Phys* (*USA*), **12** (1982) 709.
28 Maccarrone G D & Recami E, *Nuovo Cimento A* (*Italy*), **57** (1980) 85.
29 Pavsic M, *Lett Nuovo Cimento* (*Italy*), **30** (1981) 111.

NOTES

Indian Journal of Pure & Applied Physics
Vol. 21, November 1983, pp. 659-660

Thermoluminescence of Quartz: Part X—Pre-dose Sensitization Used to Evaluate the Crystallization Temperature

M DAVID & C M SUNTA
Health Physics Division, Bhabha Atomic Research Centre, Bombay 400 085

Received 21 *September* 1981

The sensitization of a TL peak in a fired and irradiated quartz is studied. It is observed that the sensitization is dependent on the pre-dose and activating heat treatments. The optimum temperature of the activating heat treatment is, in turn, found to be dependent on the growth conditions of the mineral crystal. This temperature is thus correlated with the formation temperature of the natural quartz.

Sensitization of first glow peak of a pottery inclusion quartz due to irradiation and subsequent annealing is reported by Fleming and Thompson[1]. Later, a model was given by Zimmerman[2] to explain this phenomenon. It is observed that the sensitivity increases with the amount of pre-dose. This behaviour of the peak was used for evaluation of archaeological dose[3,4] of ancient pottery samples. The sensitization is also used to evaluate the kiln firing temperature[5] of ancient pottery samples.

The sensitization of first peak is found to depend on the activating temperature after the pre-dose. This note deals with a method to evaluate the crystallization temperature of natural quartz by finding out the optimum activation temperature, i.e. the temperature of heat treatment to produce maximum sensitization.

Natural quartz samples were crushed and particles of 100 'Tyler' mesh size were used for the experiments. The description of the TL reader is given in detail, elsewhere[6]. Five mg of the sample was used in each reading and the heating rate used was 60°C/min. Oxygen-free nitrogen atmosphere was maintained during the TL measurements over the sample to avoid tribo-luminescence.

Pre-dose TL sensitization of quartz as discovered by Fleming[1] is produced by a three-step sequential treatment. In Fig. 1, the representative glow peaks are shown to describe the experiment to calculate the sensitization. The readings are explained as follows:

Reading 1: A fired (800°C) pink quartz sample is first given a test dose of 16 rad (beta) (designed as S_0').

Reading 2: A pre-dose (700 rad-beta) was given to the sample and subsequently heated at 150°C on the setup to remove the TL peak induced by pre-dose. This sample was given a test dose of 16 rad-beta (designated as (S_0).

Reading 3: The above sample was heated again at 500°C (*activating temperature*) and given the test dose [designated as (S)].

It is seen that the TL peak is sensitized to twofold by the predose followed by a heat treatment. This sensitization is observed to be proportional to the pre-dose[3,4] and depends on the activating temperature, as shown in the following.

Small aliquots of fired and pre-dosed pink quartz sample were heated at different activating temperatures up to 600°C. The sensitivity was checked for each of the aliquots by giving a standard test dose (16 rad-beta). It is observed that maximum sensitivity was obtained when the sample was heated at an activating temperature of 375°C (Fig 2, curve A). Similarly, three more samples of natural quartz from different localities were tested for their optimum activation temperatures (Fig. 2, curves B-D).

The presence of Al is an indicator of the growth condition, especially the temperature of formation of

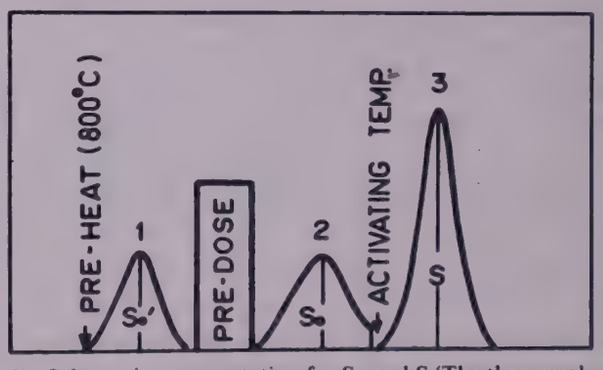

Fig. 1—Schematic representation for S_0 and S (The three peaks are the first glow peaks of natural pink quartz after different sequential treatments as explained in the text)

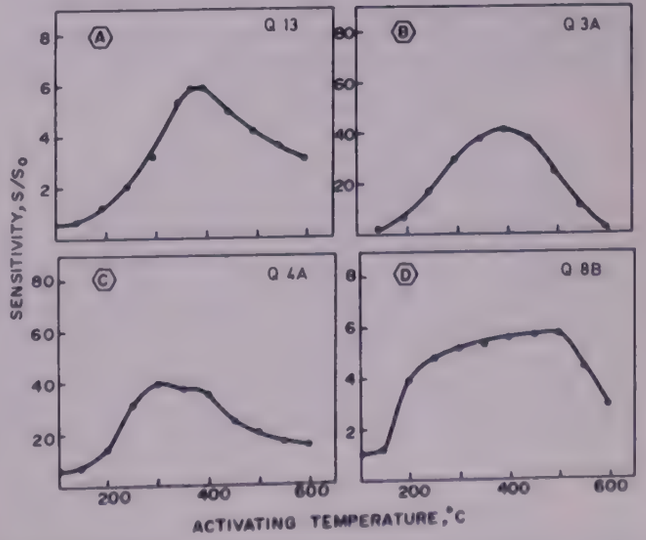

Fig. 2—Sensitization curves for four natural samples (Details of crystals given in Table 1)

Table 1—Analysis of Natural Quartz and Comparison of Crystallization Temperatures

Sample Code	Description of sample	Place of origin	Al impurity (ppm)	Temperature of crystallization (°C)		Remarks
				Impurity method	Sensitization method	
Q3A	Milky, massive	Lucknow, Uttar Pradesh	90	354	430	Sharp sensitization peak
Q4A	Transparent, single	Pune, Maharashtra	75	300	330	Wide sensitization peak
Q8B	Smoky, single	Jaduguda, Bihar	160	606	530	Wide sensitization peak
Q13	Pink, massive	—	105	408	405	Sharp sensitization peak

the crystal. Dennen *et al.*[7,8] have correlated the temperature of crystallization with aluminium impurity content by the following relation:

$$y = 3.6(\pm 0.07)x + \mathrm{RT}$$

where y is the crystallization temperature (°C); x, the Al impurity concentration (ppm); and RT, the room temperature.

The temperature of formation was evaluated for the four natural quartz samples used in this study using Dennen's method. It is observed that the activation temperature for maximum sensitization changes in conformity with the formation temperature evaluated by Dennen's method. The results are given in Table 1.

Formation of any natural crystal is generally not at a fixed temperature. They get their perfect crystal shape due to the slow cooling process during crystallization. Therefore, each growth layer of the crystal will have different amounts of Al impurity corresponding to the formation temperatures of these layers. In the present case, two samples (Q4A and Q8B) are natural single crystals which are powdered and homogenized for the experiment. Therefore, the sensitization curve is reflecting the formation temperatures of the different growth layers, indicated by a broad sensitization peak. The temperature at which the maximum sensitization was obtained is considered to be the formation temperature of the crystal and this value is given in Table 1.

In the case of massive crystals (Q13 and Q3A), they lost their individual crystal shape because of the fast cooling during crystallization. Therefore, there occur no growth layers in these crystals and the impurity concentration is the same everywhere in the crystal. Hence, we get a comparatively sharp sensitization peak as shown in Fig. 2.

Thus, these sensitization curves are also useful to get an idea about the mode of cooling during the crystal formation.

References

1 Fleming S J & Thompson J, *Health Phys (GB)*, **18** (1970) 567.

2 Zimmerman J, *J Phys C (GB)*, **4** (1971) 3265.

3 Fleming S J, Proc Specialists' seminar on TL, *Journal PACT (GB)*, 3 (1979) 314.

4 Aitken M J, Proc Specialists' Seminar on TL, *Journal PACT (GB)*, 3 (1979) 319.

5 David M & Sunta C M, *Indian J Pure & Appl Phys*, **19** (1981) 1054.

6 David M, *Studies on TL of quartz and its applications*, Ph D thesis, Gujarat University, Ahmedabad, 1980.

7 Dennen W H, *Geol Soc Am Bull (USA)*, **75** (1964) 75.

8 Dennen W H & Blackburn W H, *Centr Min Petrol (USA)*, **27** (1970) 332.

Indian Journal of Pure & Applied Physics
Vol. 21, November 1983, pp. 661-664

A Study of Indium Phosphide Single Drift and Double Drift Avalanche Diodes from Computer Analysis of Field and Current Profiles

J P BANERJEE, S P PATI & S K ROY
Centre of Advanced Study in Radiophysics and Electronics, University of Calcutta, Calcutta 700009

Received 25 *October* 1982; *accepted* 22 *August* 1983

A computer study of the electric field and carrier current profiles in the space charge region of single drift and double drift structures of indium phosphide diodes has been carried out, incorporating the effect of mobile space charge and diffusion. Recently reported ionization rates and drift velocities of charge carriers in InP have been used in the calculation. The profiles have been used to calculate the breakdown voltage, avalanche layer width and dc-to-microwave conversion efficiency of flat-profile SDR and DDR devices. The diode structures have been optimized for operation at frequencies of 10 GHz and 50 GHz and the resultant device properties have been presented. An efficiency of 12.9% for SDR and 17.0% for DDR has been obtained for 10 GHz from computer calculation while for 50 GHz the same is found to be 9.86% for SDR and 15.1% for DDR. For high-current operation, the effect of mobile space charge on the widths of avalanche regions and the conversion efficiency has been investigated. The results show that the expansion of avalanche zone at high current level and consequent efficiency degradation are less pronounced for SDR than for DDR InP devices.

In recent years, indium phosphide is emerging as an attractive semiconductor material for fabrication of high power and high efficiency avalanche diodes. In 1978, Berenz *et al.*[1] first reported fabrication of X-band InP SDR diodes which provided CW output power of 1.6 W with 11.1% conversion efficiency at 9.78 GHz. Earlier in 1977 Bauhahn and Haddad[2] presented theoretical calculations for the breakdown voltage and efficiency of Lo-Hi-Lo single drift InP diodes using the extrapolated low field ionization rate data of Molodyan *et al.*[3] from which it was predicted that InP should be a very good Impatt material as regards output power and conversion efficiency. The ionization rates of charge carriers in InP presented by Molodyan *et al.*[3] were, however, extracted from photomultiplication data using the assumption $\alpha=\beta$. Recently, carrier ionization rates in InP have been measured by Kao and Crowell[4] over the electric field range 2.4 to 4.5×10^7 V m^{-1} and by Armiento *et al.*[5] over the field range 4.85 to 6.37×10^7 V m^{-1}. The results indicate that ionization rates of holes in InP exceed those of electrons by a factor of 4 to 3 approximately. In the present note, these ionization rate data have been used for a computer study of the field and current profiles of SDR flat-profile InP Impatt devices over a wide range of doping concentration incorporating the effect of mobile space charge and carrier diffusion. The profiles obtained through computer solution have been used to investigate the extensions of avalanche and drift zones as well as the breakdown voltages of InP Impatts and their dc-to-microwave conversion efficiencies (η) for various doping levels. The effect of mobile space charge at high current level on the performance of SDR and DDR flat-profile Impatts has also been studied for X-band ($f\simeq10$ GHz) and millimetre wave band ($f\simeq50$ GHz) operation of the device and this indicates that SDR is less sensitive to mobile space charge than DDR.

Method—The structures and the realistic doping profiles of SDR n^+pp^+ and DDR n^+npp^+ Impatt devices are shown in Fig. 1. Exponential and error functions have been used for the doping profiles at the metallurgical junction and the interface of epitaxy and substrate respectively. The profiles of the electric field $E(x)$ in the depletion layer and those of the carrier current density $J_n(x)$ and $J_p(x)$ for various levels of the dc current have been obtained from simultaneous numerical solution of Poisson's equation and the continuity equations, using a double iterative computer method which involves prior determination of the location and the magnitude of the electric field

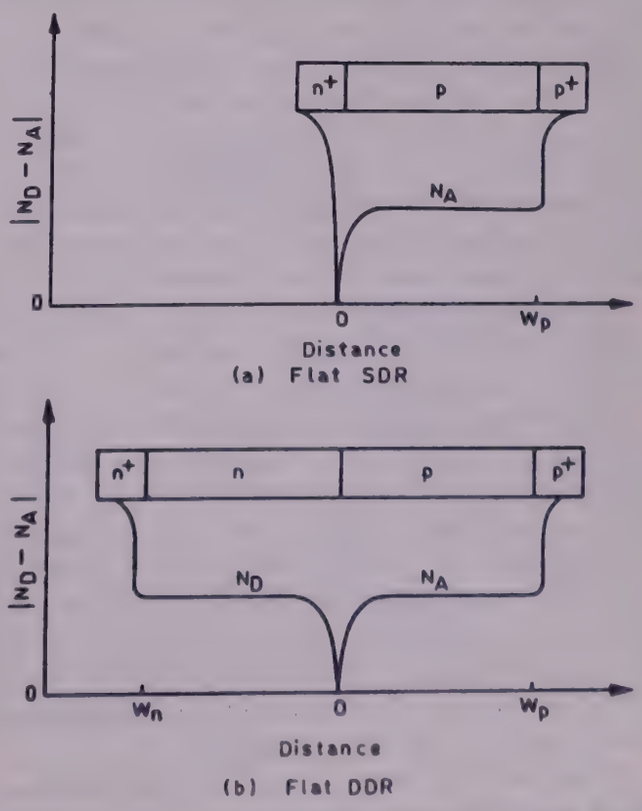

Fig. 1—The realistic doping profiles of SDR and DDR Impatt structures (used in the calculation)

Table 1—Material Parameters of InP

Parameters Carrier	Constants of ionization rates[4,5]			V_s ($10^5 m s^{-1}$)	μ^+ ($m^2 V^{-1} S^{-1}$) (Ref. 14)	Relative dielectric constants (Ref. 15)
	Field range ($10^7 V m^{-1}$)	A (m^{-1})	B ($V m^{-1}$)			
Electron	2.40-4.50	4.03×10^8	2.95×10^8	0.75[8]	0.460	9.55
	4.85-6.37	1.07×10^9	4.31×10^8			
Hole	2.40-4.50	1.39×10^9	2.93×10^8	0.80[2]	0.015	
	4.85-6.37	9.63×10^8	3.61×10^8			

maximum in the space charge layer[6,7]. The computation incorporates the effect of the mobile space charge and both the drift and diffusion components of carrier currents have been taken into account.

The material parameters for indium phosphide used in the calculation are as follows:

The ionization rates α, β as functions of the electric field are given by $\alpha, \beta = A \exp -[(B/E)]$ where the values of the constants A and B for electrons and holes in InP are given in Table 1. The electron drift velocity in InP passes through a peak value ($\simeq 2.5 \times 10^5 m s^{-1}$) at an electric field around $E_c = 11 \times 10^5$ V m^{-1} before attaining a saturated value ($v_{sn} = 0.75 \times 10^5 m s^{-1}$) at high electric field[8]. The velocity for electrons in InP for various electric fields has been computed using the expression given by Bauhahn and Haddad[2]. The field dependence of hole velocity in InP is assumed to have the usual exponential form[2] given by $v_p(E) = v_{sp}[1 - \exp(-\mu_p E(x)/v_{sp})$. The values of saturated drift velocities (v_s) and mobilities (μ) for electrons and holes are also listed in Table 1. The slight modification of the carrier currents due to the incorporation of diffusion has been obtained by using a perturbation approach[7] and the values of diffusion constants for electrons and holes in InP have been obtained from Bauhahn *et al.*[2]

The electric field and carrier current profiles thus obtained can be used to compute the width (x_A) of the avalanche multiplication region, breakdown voltage (v_B) and the voltage drops across the drift zone (v_D) and the avalanche zone (v_A)[6,7]. The value of η has been calculated by using Scharfetter-Gummel semi-quantitative formula[9]. The theoretical results based on the computer method have initially been compared with the available experimental results on X-band InP Impatt diode[1]. Using the same doping profile, v_B and η have been computed and are found to be 57.7 V and 11.7% as against the corresponding experimental values of 60.0 V and 11.1% respectively.

Results and discussion—Using the method outlined above, the field $E(x)$ and carrier current $P(x)$ profiles of single drift (n^+pp^+) and double drift (n^+npp^+) flat-profile Impatt structures in the presence of mobile space charge and diffusion are first obtained for different values of background doping concentration in the range of 7×10^{21}-$10^{23} m^{-3}$ at a fixed dc current density of $10^7 A m^{-2}$. The characteristic parameters of both SDR and DDR devices, i.e. depletion layer width (W), x_A, maximum field at breakdown (E_m), v_B, v_A, v_D and η are then computed from $E(x)$ and $P(x)$ profiles. For the above range of doping concentration, the depletion layer widths of non-punch-through SDR devices range from 4.0 to 0.4 μm. This covers an operating frequency range 7-75 GHz as may be seen from the approximate relation[10] $f = (0.37 v_{sn,p})/W_{n,p}$, where $v_{sn,p}$ and $W_{n,p}$ are respectively the saturated velocities and depletion widths of charge carriers.

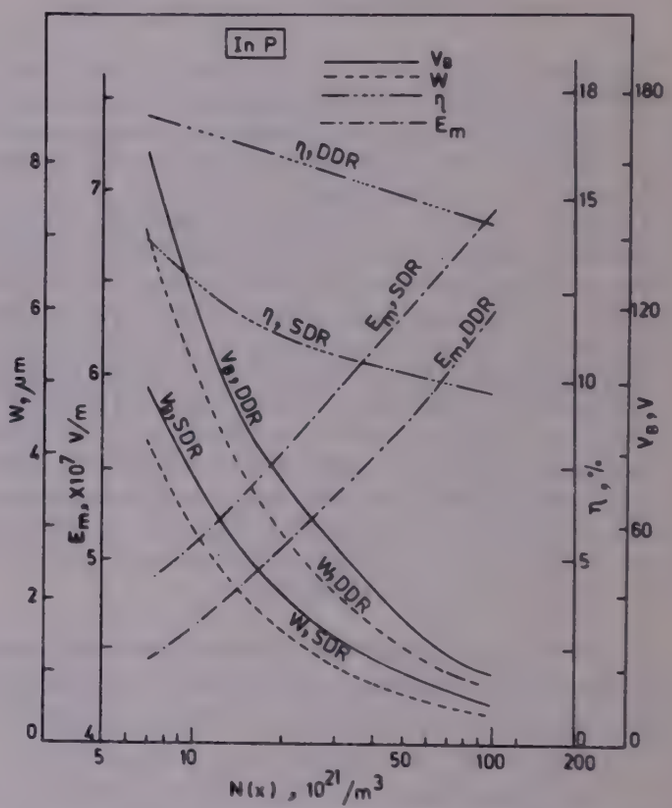

Fig. 2—Plots of W, V_B, E_m and η against background doping concentration for flat-profile InP SDRs and DDRs

Fig. 2 shows the variations of W, v_B, E_m and η with doping concentration for both SDR and DDR

Table 2—Structural Parameters and Properties of SDR and DDR Devices
[$J_0 = 10^7$ A m^{-2} at 10 GHz and $J_0 = 5 \times 10^7$ A m^{-2} at 50 GHz]

Device parameters and properties	SDR structure		DDR structure	
	10 GHz	50 GHz	10 GHz	50 GHz
N_D(m^{-3})	—	—	1.13×10^{22}	6.22×10^{22}
N_A(m^{-3})	1.10×10^{22}	6.80×10^{23}	1.12×10^{22}	6.20×10^{22}
W_n(μm)	—	—	2.60	0.565
W_p(μm)	2.81	0.579	2.80	0.569
E_m(V m^{-1})	5.16×10^7	6.62×10^7	4.70×10^7	5.91×10^7
V_B(V)	71.6	18.4	121.4	35.2
V_A(V)	42.6	12.7	56.7	18.50
x_A(μm)	1.010	0.243	1.410	0.380
η(%)	12.9	9.86	17.0	15.1

structures. For SDR and DDR InP devices, v_B and E_m are higher than those of corresponding silicon and GaAs Impatt structures[11,12] as shown in Fig. 2. The physical basis of higher values of v_B for InP Impatts is mainly due to lower values of ionization rates of charge carriers in InP. For an increase of doping level of the lightly doped region from 7×10^{21} m^{-3} to to 10^{23} m^{-3}, η for SDR devices decreases from 13.8% to 9.5% while the same for DDR decreases from 17.5% to 14.0%.

Suitable structural parameters (given in Table 2) of SDR and DDR Impatt devices are determined from the computer analysis in order to realize the operating frequencies of the devices around 10 GHz in X-band and 50 GHz in millimetre wave region. The properties of these optimized structures are then investigated and the results are given in Table 2. From Table 2 it is seen that DDR devices would provide efficiencies of 17.0% and 15.1% and breakdown voltages of 121.4 V and 35.2 V at 10 GHz and 50 GHz respectively. It may be noted that the computed values of η and v_B of InP DDRs at 10 GHz and 50 GHz are higher than the corresponding values for optimized silicon DDRs at about the same frequencies[13].

The effect of diffusion in InP Impatt diodes has also been investigated. It has been observed that the field profile and v_B for 10 GHz SDR and DDR diodes are very little affected due to diffusion while the same undergo slight changes for the corresponding 50 GHz device. For 50 GHz SDR and DDR diodes, v_B decreases from 19.2 V and 35.6 V to 18.9 V and 35.2 V respectively when diffusion is taken into account.

The effect of mobile space charge on the performance of these optimized structures at 10 GHz and 50 GHz has been investigated. Figs 3 and 4 show the $E(x)$ and $P(x)$ profiles of X-band ($f \simeq 10$ GHz) SDR and DDR devices for various current densities. The almost triangular shape of field profiles at lower current density is very much distorted at higher current level. The $P(x)$ profiles of SDR and DDR devices show that the avalanche centre is located on the p-side of the

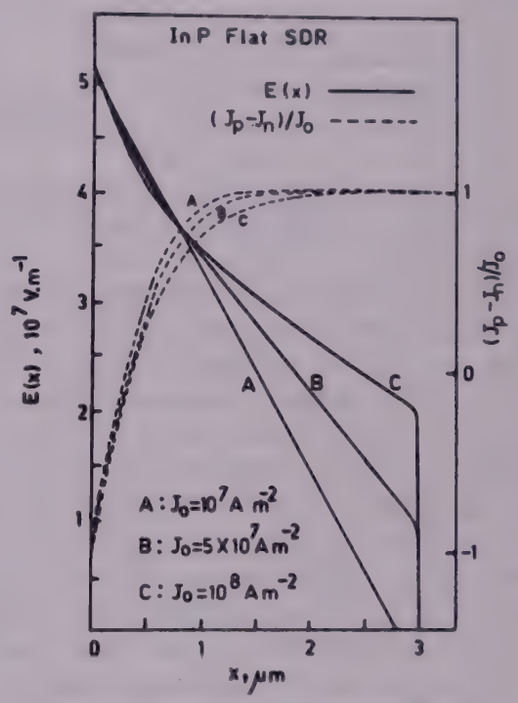

Fig. 3—Field and carrier current profiles of SDR devices (X-band) for different current densities

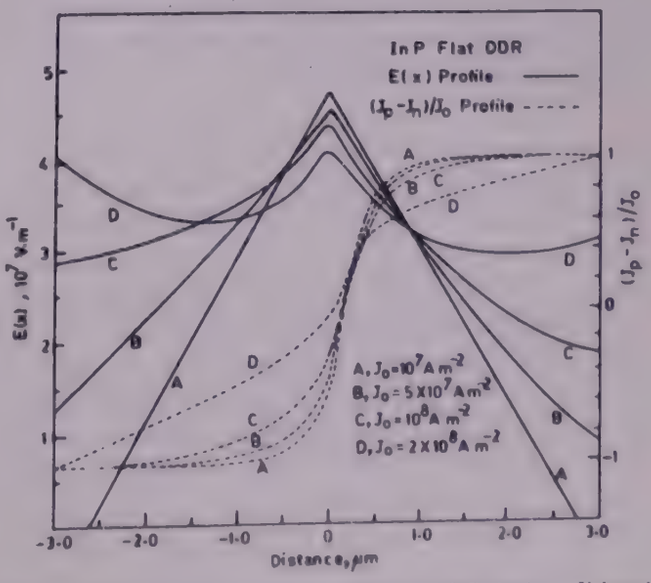

Fig. 4—Field and carrier current profiles of DDR devices (X-band) for different current densities

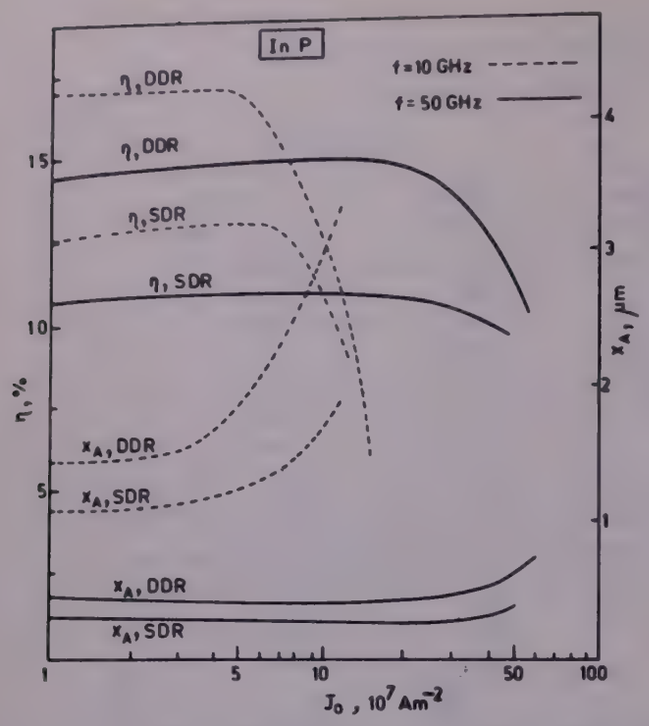

Fig. 5—Plots of x_A and η against current density for SDRs and DDRs at 10 GHz and 50 GHz

metallurgical junction and shifts towards the junction at high current density. The location of the avalanche centre on the *p*-side of the junction can be understood from the fact that the space variation of both types of carrier current will be higher in the *p*-region of the space charge layer owing to higher ionisation rates of holes. The expansion of avalanche zone and consequent fall in efficiency at high current level are sharper in case of DDR than for SDR which can be seen from Fig. 5. Thus x_A expands from 0.26 W to 0.54 W in case of DDR when J_0 increases from 10^7 to 10^8 A/m^2 whereas the corresponding variation of x_A in case of SDR is from 0.36 W to 0.53 W for the same increase of current. It may be noted that the expansion of avalanche zone for DDR takes place on both sides of the junction whereas for SDR avalanche zone expands only on the lightly doped side.

The variation of x_A and η with current density for millimetre wave operation ($f \simeq 50$ GHz) of the device is also shown in Fig. 5. It is observed from the figure that at high current density the decrease of conversion efficiency owing to expansion of x_A is less pronounced for 50 GHz operation than for *X*-band operation. The performance of mm wave devices as regards the value of x_A and η remains almost unaffected up to as high a current density as 3×10^8A/m^2.

The authors wish to thank Prof. M S Basu, Head of the Centre of Advanced Study in Radio Physics and Electronics for his interest and encouragement. Two (JPB and SPP) of the authors gratefully acknowledge the awards of teacher fellowships by the University Grants Commission, New Delhi.

References

1 Berenx J J, Fank F B & Hiert T L, *Electron Lett (GB)*, **14** (1978) 683.
2 Bauhahn P & Haddad G I, *IEEE Trans on Electron Devices (USA)*, *ED*-24 (1977) 634.
3 Molodyan I P, Radantsan S I, Russu E V & Slobodchikov S V, *Soviet Phys Semicond (USA)*, **8** (1975) 879.
4 Kao C W & Crowell C R, *Solid-State Electron (GB)*, **23** (1980) 881.
5 Armiento C A, Groves S R & Harwitz C E, *Appl Phys Lett (USA)*, **35** (1979) 333.
6 Roy S K, Sridharan M, Ghosh R & Pal B B, *Proc NASECODE-I Conf on Numerical Analysis of Semiconductor Devices* (Dublin, Ireland) 1979 266.
7 Pati S P, Banerjee J P & Roy S K, *Indian J Pure & Appl Phys*, **21** (1983), 558.
8 Levinshtein M E, *Soviet Phys Semicond (USA)*, **13** (1979) 735.
9 Scharfetter D L & Gummel H L, *IEEE Trans on Electron Devices (USA)*, *ED*-16 (1969) 64.
10 Sze S M & Ryder R M, *Proc IEEE (USA)*, **5** (1971) 1140.
11 Sze S M & Gibbons G, *Appl Phys Lett (USA)*, **8** (1966) 111.
12 Gibbons G, *Avalanche diode microwave oscillators* (Clarendon Press, Oxford), 1973, 33.
13 Chang L C, Hu D H & Wang C C, *IEEE Trans Electron Devices (USA)*, *ED*-24 (1977) 655.
14 Wolf H F, *Semiconductors* (Wiley Interscience, New York) 1971, 33.
15 Nag B R, *Electron transport in compound semiconductors* (Pergamon Press, London) 1980, 372.

Indian Journal of Pure & Applied Physics
Vol. 21, November 1983, pp. 665-667

Growth of Sb_2S_3 Films by Solution-Gas Interface Technique

S H PAWAR, (Miss) SHOBHA TAMHANKAR,
P N BHOSALE & M D UPLANE
Energy Conversion Laboratory, Department of Physics,
Shivaji University, Kolhapur 416004

Received 3 *May* 1983

Uniform, large-area films of Sb_2S_3 have been prepared by employing solution-gas interface technique. The solution of antimony chloride was exposed to hydrogen sulphide gas to form a thin solid film at the interface. The optical and electrical properties of these films are studied. The band-gap energy of Sb_2S_3 film is estimated by the optical absorption measurement and found to be in good agreement with the reported results.

In recent years, efforts have been made to construct low-cost and relatively-high efficiency solar cells, adopting various techniques. Among the low-cost devices, thin-film structures have the advantages of consuming the least raw materials and simple fabrication. Thin chalcogenide films have received more attention to serve as a photoanode in the solar cells. In this connection, thin films of Sb_2S_3 are of particular interest because of their semiconducting property and low band-gap to match with the maximum portion of the solar spectrum. There are various methods for fabrication of thin films of Sb_2S_3 such as vacuum evaporation[1-4], sintering[5], dip and dry technique[6] etc. However, to grow uniform, large-area semiconducting films by a simpler way, a relatively new method namely liquid-gas interface technique has been proposed. In this, an anion from gas and a cation from solution react to form a thin film at the interface of solution and gas. Growth of thin films of CdS, ZnO and Bi_2S_3 has been reported by this method[7-9]; but no data are available for the Sb_2S_3 films. In this note, thin-film formation of Sb_2S_3 by using $SbCl_3$ and H_2S gas is described. Some of the optical and electrical properties of these films are also discussed.

Experimental set-up—The experimental set-up designed and fabricated by us for the formation of thin films at the solution-gas interface is described elsewhere[9]. In brief, it consists of a gas chamber, uniform gas-exposing unit and the solution. Purified and dry H_2S gas is filled in the gas chamber for desired gas pressure. The quality and uniformity of the films mostly depend upon the gas-exposure unit and it is the key part of the technique. The solution is taken in a specially designed glass container having an arrangement to remove the solution from its bottom. A vibration-free mechanical arrangement is provided to move the solution up and down without disturbing the surface of the solution.

Preparation of films—Antimony trioxide is taken and dissolved in concentrated hydrochloric acid and then diluted with doubly distilled water to get clear solution of $SbCl_3$. As $SbCl_3$ is easily oxidized when exposed to air, every time freshly prepared solution of antimony chloride is taken. The pH of the solution is maintained in between 1.5 and 2, to avoid precipitation of $SbCl_3$ with addition of excess water. The chemical reactions explaining the above phemomenon are:

$$Sb_2O_3(\text{Solid}) + \text{conc.}6HCl \rightarrow 2SbCl_3 + 3H_2O \quad \ldots (1)$$

$$2SbCl_3 + H_2O \rightarrow SbCl_3\downarrow + SbOCl + 2HCl \quad \ldots (2)$$

Ultrasonically-cleaned glass substrates are immeresed into the solution. The container of the solution is moved up to fit with the platform of gas-exposing unit. The solution surface is allowed to attain a steady state, then the shutter is opened and H_2S gas is allowed to flow through the uniform gas-exposing unit for a specific period to form a film at the solution-gas interface. The solution is removed slowly from the bottom and uniform large-area films are supported on the glass substrates. The films are washed several times with double distilled water and finally supported on the glass substrates for further study. The immediate washing of the films formed at the interface is quite essential as $SbCl_3$ and Sb_2S_3 react with each other to form antimony according to the reaction:

$$2Sb_2S_3 + 2SbCl_3 \rightarrow 6Sb + 3S_2Cl_2\uparrow \quad \ldots (3)$$

The films are preserved in a dark desiccator. With the present experimental set-up and technique we could deposit uniform circular Sb_2S_3 films as large as 50 cm^2 area with a thickness of the order of 0.4 μm.

Optical and electrical measurements—The optical absorption study for the films is made with the help of the monochromator (Carl-Zeiss, Jena) in the photon energy range 1.4-3 eV. The dark conductivity measurenents for electrical characterisation are made in the temperature range between 300-600 K.

Results and discussion—The antimony sulphide films are grown at the interface between hydrogen sulphide gas and antimony chloride solution. By virtue of the surface tension effect, at the surface of the solution the ions are bound tightly and arranged in a two-dimensional regular fashion. When the molecule of H_2S comes in contact with the surface of the solution, the bonding between H^+ and SH^- ions of

H_2S is broken, as sulphur ions have strong affinity towards metallic ion (Sb^{3+}) rather than H^+ or Cl^- ions. In the solution, the solvated SbO^+ ions are weakly bound to unsolvated Cl^- ions. Thus S^{2-} and SbO^+ ions interact to form thin uniform films of Sb_2S_3 at the interface between solution and gas. The sequence of reactions taking place during the growth of Sb_2S_3 films can be represented as follows:

$$SbCl_3 + H_2O \rightarrow SbOCl + 2HCl \quad \ldots (4)$$

$$SbOCl + H_2O \rightarrow SbO^+ + HCl + OH^+ \quad \ldots (5)$$

$$H_2S \rightarrow H^+ + SH^-$$

$$SH^- + OH^- \rightarrow S^{2-} + H_2O \quad \ldots (6)$$

$$SbO^+Cl^- + H^+SH^- \rightarrow SbO^+SH^- + HCl \quad \ldots (7)$$

$$2SbO^+SH^- + H^+SH^- \rightarrow Sb_2S_3 + 2H_2O \quad \ldots (8)$$

The overall reaction can be written as

$$2SbCl_3 + 3H_2S \rightarrow Sb_2S_3 + 6HCl \quad \ldots (9)$$

The films formed at room temperature, show the orange red colour and amorphous structure. The films can be made crystalline by baking at higher temperature 200-250°C (Ref. 6). Nayak *et al.*[6] prepared Sb_2S_3 films by dip and dry technique and their results are in good agreement with our results. Beyond the particular thickness and after the specific period of gas exposure, the precipitation starts and the uniform large area film ruptures at places. The quality of the film is influenced by several parameters such as concentration, pH, surface tension of the solution and pressure of exposing gas. The work is in progress to optimize such parameters to get better results.

Optical and electrical characterization of Sb_2S_3 *films*—The optical absorption of the film as a function of photon energy is studied in the range 1.4-3 eV. The absorption coefficient α versus photon energy curve is shown in Fig. 1. The absorption coefficient for the optical gap is found to be of the order of $10^4\ cm^{-1}$ which is generally observed for amorphous material[10]. Fig. 2 shows a plot of photon energy E versus $(\alpha E)^{1/2}$ for the film which shows a linear relationship over a long range of photon energy. Such a power law dependence for Sb_2S_3 has been observed earlier[11]. In this case, absorption below 2 eV is mainly due to optical transitions between defect states and valence and conduction bands. The optical gap obtained by extrapolation is 1.65 eV less than direct gap which presumably is 1.88 eV. It can be compared to the apparently direct band gap of 1.88 eV observed in crystalline material. Although the extrapolated optical gap for amorphous material is 1.65 eV the change of the slope indicating interband transitions starts at around 1.9 eV. The disorder in amorphous materials is also

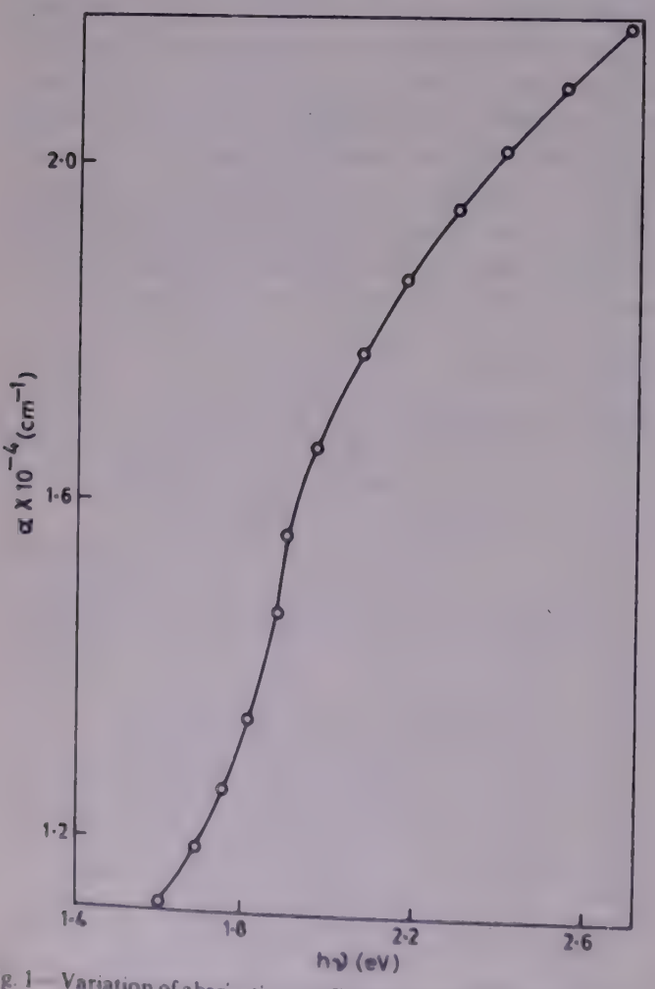

Fig. 1—Variation of absorption coefficient (α) with photon energy $h\nu$ for the Sb_2S_3 film

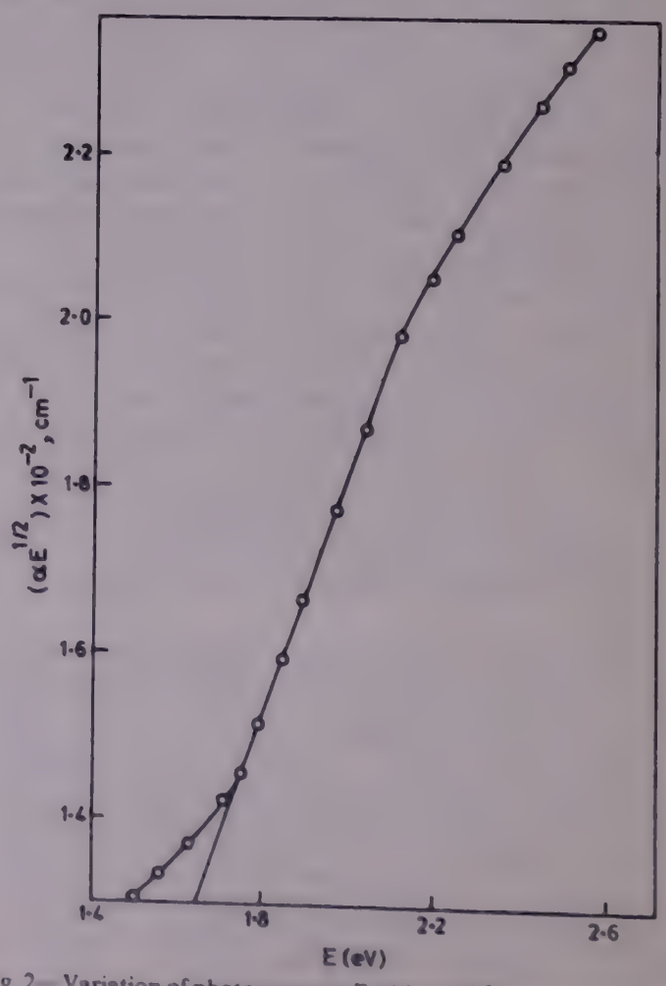

Fig. 2—Variation of photon energy E with $(\alpha E)^{1/2}$ for the Sb_2S_3 film

likely to broaden the band edge and the onset of indirect transitions in the amorphous materials appears to be at almost the same energy as the first structure due to direct transitions. Thus it appears likely that the band-gap of the material is of the direct type[4].

The electrical characterization study was carried out in the temperature range 300-600 K. The resistance is found to decrease with increasing temperature proving the semiconducting nature of the film. The plot of log R versus $1/T$ shows a linear nature. The band-gap energy estimated from this plot in the intrinsic region was found to be 1.58 eV. This is in fair agreement with the value calculated from optical study.

The authors are grateful to the Department of Science and Technology, New Delhi for financial support to carry out this work. They would like to thank Prof. R N Patil for encouragement and to Sarvshri C D Lokhande and S K Jamadar for technical assistance.

References

1 Badachhape S B & Goswami A, *Indian J Pure & Appl Phys*, **5** (1967) 477.

2 Mikalkevicius M & Rinkevicius, *Liet Fiz Rinkinys (USSR)*, **8** (1968) 625.

3 Ramanujam R & Vetury R, *Indian J Pure & Appl Phys*, **10** (1972) 356.

4 Ghosh C & Varma B P, *Thin Solid Films (Switzerland)*, **60** (1979) 61.

5 Chokalingam M J, Rao K N, Rangarajan N & Suryanarayana C V, *J Phys D (GB)*, **3** (1970) 1641.

6 Nayak B B, Acharya H N, Chaudhuri T K & Mirta G B, *Thin Solid Films (Switzerland)*, **92** (1982) 309.

7 Sathaye S D & Sinha A P B, *Thin Solid Films (Switzerland)*, **37** (1976) 15.

8 Sathaya S D & Sinha A P B, *Thin Solid Films (Switzerland)*, **44** (1977) 57.

9 Pawar S H, Bhosale P N, Uplane M D & (Miss) Tamhankar Shobha, *Thin Solid Films (Switzerland)*, **110** (1983) accepted.

10 Statue J, *J Non-Cryst Solids (Netherlands)*, **4** (1970) 1.

11 Hall J A, *Adv Electronics & Electron Phys (USA)*, **33** (1972) 229.

Indian Journal of Pure & Applied Physics
Vol. 21, November 1983, pp. 668-669

Photoionization of Deep Energy Levels in $Ga_{1-x}Al_xAs$ Alloys

ASHOK K SAXENA & A K SINHA

Department of Electronics & Communication Engineering, University of Roorkee, Roorkee 247667

Received 18 *March* 1983

The present work on $Ga_{1-x}Al_xAs$ alloys shows that the electrons are very tightly bound to the deep energy states in the alloys and the optical ionization energy is much larger than 1.1 eV. It is concluded that the phenomenon of persistent photoconductivity is not due to the lattice relaxation as reported earlier in the literature, but is due to the effect of the conduction band structure of the alloys.

Many investigators[1-3] have shown the presence of deep energy levels in the forbidden energy gap of both intentionally doped (*p*- and *n*-type) and undoped (*n*-type) $Ga_{1-x}Al_xAs$ alloys, from the temperature dependence ($T<300$K) of the Hall electron concentration. Nelson[4] first reported a long lifetime photoconductivity effect in Te, Se and Sn doped $Ga_{1-x}Al_xAs$ alloys from the photo-Hall measurements and concluded that a potential barrier exists to the electron capture by the deep level (shown to be donor-like) from time decay of photoexcited electrons at low temperatures. In these experiments, he used radiations corresponding to the peak ($h\nu=1.1$ eV) of the photo-ionization cross-section of the centres. It is important to note that for the experimental results presented for the Te-doped sample ($x=0.36$), the photoexcited electron concentration accounted nearly for all the conduction electrons present at 300 K, taking fully into account the Hall-to-drift mobility ratio for these alloys[5]. Saxena[6] has also reported similar effects for intentionally undoped *n*-type $Ga_{1-x}Al_xAs$ alloys using the radiations corresponding to the energy $h\nu=0.67$ eV. For direct gap alloy compositions, the phenomenon of persistent photoconductivity was explained on a new proposition of electron capture and emission by the deep level (shown to be acceptor-like) via the higher energy subsidiary L conduction band minima situated along the $<111>$ directions. It is the purpose of this note to show that we cannot photoionize all the centres in the deep levels not only with the radiation corresponding to the energy 1.1 eV but also with the white light, showing that the photoionization energy is much larger than 1.1 eV, a result in disagreement with the data reported by Nelson[4].

The high purity and intentionally undoped (*n*-type) $Ga_{1-x}Al_xAs$ ($0\leq x\leq 0.78$) layers used in these experiments were grown on Cr-doped semi-insulating GaAs substrates by a sliding boat technique. The layers had thicknesses of 5-15 μm and room temperature electron concentrations of $(5\text{-}10)\times 10^{15}$ cm^{-3}. The alloy compositions were determined by converting measured room-temperature cathodoluminescence band-gap energies into compositions by means of the energy-gap-composition curve given by Panish[7].

A low-temperature cryostat (Air product, model No. DE-202) was used which utilizes liquid He as the cooling agent. The Hall and photo-Hall measurements were made in a magnetic field of 5 kG. White light from an intense source was filtered through Ge and Si filters to obtain radiations with energies of 0.67 and 1.1 eV, respectively. The light intensity was increased till the photo-excited electron concentration almost saturated with intensity. The measured Hall and photo-Hall electron concentrations n_h are shown in Fig. 1 for a typical alloy composition $x=0.32$, where the Hall measurements are labelled 'in dark'. The initial decrease in n_h with lowering of temperature ($300\geq T\geq 80$K) is due to electron 'freeze out' to a deep level with a thermal energy of $(100+5)$meV[1], while the quasi-saturation below 80 K is due to electron capture by the deep level via the subsidiary L minima[6]. The photo-Hall measurements using radiations with energies of $h\nu=0.67$ and 1.1 eV are marked 'Ge filter' and 'Si filter', respectively. The data shown by full triangles are for optical excitation using white light. The corresponding Hall and photo-Hall mobilities are shown in Fig. 2. The arrows in both the figures show that no hysteresis effects were observed when the temperature cycle was reversed.

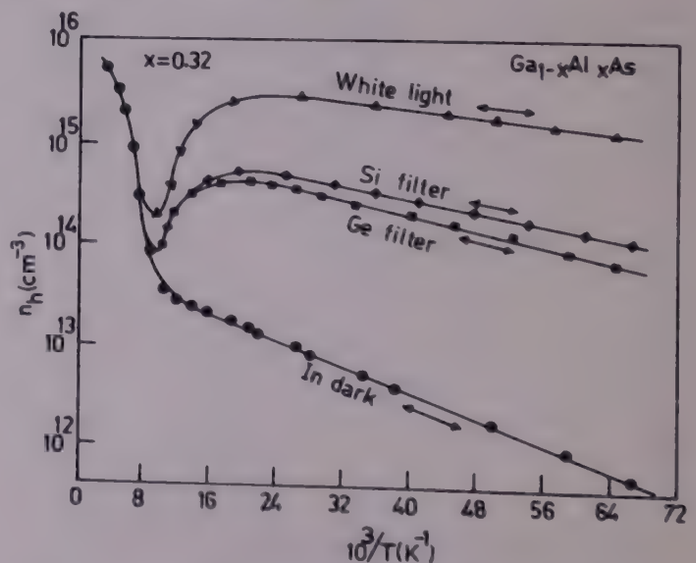

Fig. 1—Temperature dependence of the Hall and photo-Hall electron concentrations

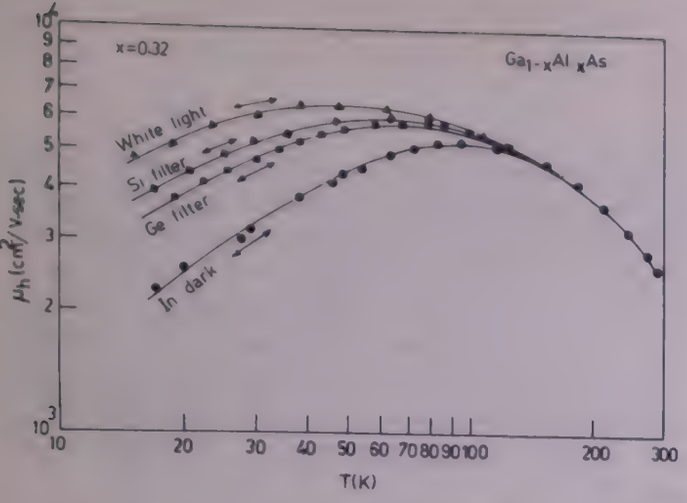

Fig. 2—Temperature dependence of the Hall and photo-Hall electron mobilities

For the alloy composition $x=0.32$, the Hall to drift mobility ratio is ~ 1.2 while the room-temperature electron concentration (Fig. 1) is $\sim 8\times10^{15}$ cm^{-3}. Thus the net donor concentration in this sample should be about 9.6×10^{15} cm^{-3}. On photoexcitation of samples at low temperatures using Ge filter ($h\nu = 0.67$ eV), persistent photoconductivity has been observed as reported earlier[6]. In the present work, we have repeated the similar measurements using Si filter ($h\nu = 1.1$ eV) and white light. With the Si filter, no appreciable increase in n_h or μ_h is obtained over the values obtained with Ge filter, showing that the photoionization energy of the deep level with a thermal energy of (100 ± 5) meV, is larger than 1.1 eV, in disagreement with the results of Nelson[4]. Then the white light was used, even then all the centres could not be ionized. For example at ~ 14 K ($10^3/T \approx 72$), the photo-Hall concentration is $\sim 10^{15}$ cm^{-3}, an order of magnitude less than the net donor concentration in the sample. It is, therefore, concluded that the electrons are very tightly bound to the deep states. Previously, 'tight bonding approximation' has been used to calculate theoretically the ionization energies of deep levels in $Ga_{1-x}Al_xAs$ alloys and the values were found to be in excellent agreement with the experimental values[1,8]. Since the deep level turns out to be donor-like for Te-doped samples[4] and acceptor-like for undoped samples (Fig. 2) and also because the photoionization energies in the two cases seem to be widely different, it suggests that the detailed electrical properties of the level depend strongly on the specific impurity incorporated during the growth.

Because of the large difference between the thermal and optical ionization energies of the deep level, as also observed in the present work, Nelson[4] argued that the phenomenon of persistent photoconductivity was consistent with the expected behaviour of an impurity centre with a significant amount of lattice relaxation. This does not seem to correlate with his observation that no such effects were observed in undoped (p-type) crystals. We, therefore, very strongly feel that the persistent photoconductivity is due to the electron capture and emission by the deep level via the L minima as explained earlier[6], and not due to lattice relaxation. The small capture cross-section of the centre may also contribute to the persistence of photoconductivity. In fact, Bhattacharya[9] has determined these cross-sections for $Ga_{1-x}Al_xAs$ alloys and typically they are of the order of 10^{-19} cm^2 for $x=0.32$ and 10^{-23} cm^2 for $x=0.78$. These values are much smaller than the capture cross-section ($\sim 10^{-15}$ cm^2) of deep levels in epitaxial GaAs[10].

In conclusion, the electrons are very tightly bound to the deep energy states in the alloys and the optical ionization energy is much larger than 1.1 eV. Further, it is concluded that the phenomenon of persistent photoconductivity is not due to the lattice relaxation as reported by Nelson[4], but is due to the effect of the conduction band structure of the alloys.

The authors are thankful to Dr I G A Davies of Standard Telecommunication Laboratory, England for providing the crystals. Various discussions with Profs A Majerfeld and P N Robson are gratefully acknowledged.

Financial assistances from the Department of Science and Technology, Indian National Science Academy, Kothari Scientific and Research Institute and University of Roorkee are very much appreciated. One of us (AKS) is thankful to the University Grants Commission, New Delhi, for granting a fellowship.

References

1 Saxena A K. *Phys Status Solidi (b) (West Germany)*, **105** (1981) 777.

2 Spring Thorpe A J, King F D & Becke A, *J Electron Mat (USA)*, **4** (1975) 101.

3 Kaneko K, Ayabe M & Watanabe W, *Proc Sixth international symposium on GaAs and related compounds, Edinburgh*, edited by C Hilsum (Institute of Physics, London), Ser. No. 33a, 1977, 216.

4 Nelson R J, *Appl Phys Lett (USA)*, **31** (1977) 351.

5 Saxena A K, *Solid State Commun (GB)*, **39** (1981) 839

6 Saxena A K, *Solid State Electron (GB)*, **25** (1982) 127.

7 Panish M B, *J Appl Phys (USA)*, **44** (1973) 2667.

8 Saxena A K, *Indian J Pure & Appl Phys*, **19** (1981) 537

9 Bhattacharya P K, *Deep levels and the conduction band structure of GaAs and $Ga_{1-x}Al_xAs$*, Ph D thesis, Sheffield University, UK, 1978.

10 Saxena A K, *J Inst Electron & Telecommun Eng (India)*, **26** (1980) 293.

Indian Journal of Pure & Applied Physics
Vol. 21, November 1983, pp. 670-671

HOMO & LUMO Energy Values for Bases of Nucleic Acids

K B LAL*, V K AGRAWAL, A K SRIVASTAVA & B KRISHNA

Department of Chemistry, University of Allahabad, Allahabad 211 002

Received 8 *March* 1983

The structures of bases of nucleic acids, adenine, guanine, thymine, cytosine and uracil have been explained in terms of their HOMO and LUMO energy values.

It is surprising that out of ninety two elements, nature has chosen only four elements namely carbon, hydrogen, nitrogen and oxygen for synthesis of bases of nucleic acids which play a vital role in genetics. It is further interesting to note that out of various possible combinations of these four elements, nature has accepted a typical set and that is also repeated in all the five bases. Adenine and guanine are the purines while thymine, cytosine and uracil are the pyrimidines. All the five are heterocyclic systems containing nitrogen and oxygen with more or less the same pattern, i.e. nitrogen at 1 and 3 position in the ring and $-NH_2$ and $-OH$ as functional groups. In the present communication, a possible explanation is given in terms of molecular parameters.

Calculation—Using simple Huckel molecular orbital method[1] various molecular parameters such as charge density[2], bond order[3], energy of highest occupied molecular orbital (HOMO) and lowest unoccupied molecular orbital (LUMO)[4] have been calculated for all the five bases. A relative matrix is formed with respect to α (Coulomb integral) and in terms of β (resonance integral), which is diagonalized using Jacobi method[5] to give eigenvalues, and corresponding eigenvectors. Eigenvectors are used to calculate charge density and bond order. The calculations have been done on a minicomputer with the precision of tenth place of decimal.

Results and discussion—It is observed that energies of HOMO and LUMO play an important role in acceptance of these bases by nature. As is clear from Tables 1-4, the energies of HOMO and LUMO for these bases fall near to $+0.5\beta$ and -0.5β respectively showing that they are moderate electron donors and acceptors, pyrimidines being poorer donor than the purines.

Calculations of energies of HOMO and LUMO have been performed on various possible modifications of these bases. It is observed that these are the systems for which the values of HOMO and LUMO energies lie close to $+0.5\beta$ and -0.5β respectively. It is further noted that, if one follows the synthesis of these bases in terms of HOMO and LUMO energy values, the system is acceptable as it reaches close to the one with HOMO and LUMO energy values to $+0.5\beta$ and -0.5β respectively.

Table 1—HOMO and LUMO Energy for Cytosine and Its Possible Modifications

Base*	HOMO(β)	LUMO(β)
1	1.0767	−0.7813
2	1.1021	−0.6583
3	1.1864	−0.7670
4	0.7139	−1.0119
5	0.7478	−0.7153
6	0.9527	−0.8872
7	0.7459	−0.8692

*The number below each of the following structures corresponds to that given in col. 1.

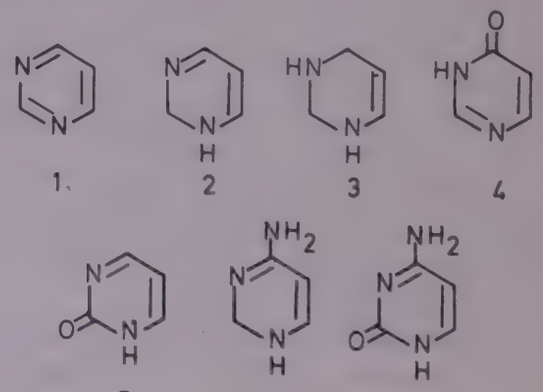

Table 2—HOMO and LUMO Energy for Thymine and Its Possible Modifications

Base*-	HOMO(β)	LUMO(β)
1	1.1864	−0.7670
2	0.9038	−0.7248
3	0.6542	−0.8889
4	1.0550	−0.7337

*Same as in Table 1

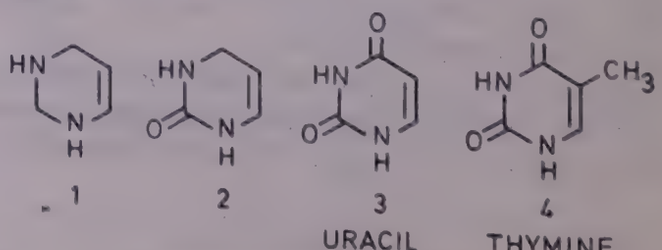

*Chemistry Department, St. John's College, Agra.

Table 3—HOMO and LUMO Energy for Adenine and Its Possible Modifications

Base*	HOMO(β)	LUMO(β)
1	0.2964	−1.1399
2	0.3244	−0.8999
3	0.3821	−1.0876
4	0.5380	−1.0607
5	0.6654	−0.9700
6	0.5876	−0.9163

*Same as in Table 1

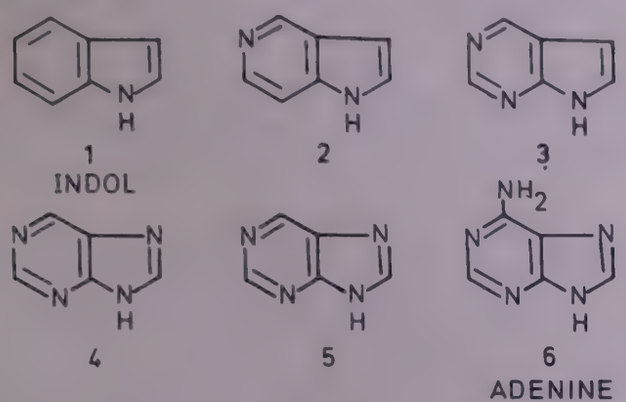

1 INDOL 2 3 4 5 6 ADENINE

Thus it seems that out of various possible combinations nature accepts only those which have moderate electron donor and acceptor properties (in terms of molecular parameters having HOMO and LUMO energies near to $+0.5\beta$ and -0.5β respectively). Adenine and uracil may be considered as

Table 4—HOMO and LUMO Energy for Guanine and Its Possible Modifications

Base*	HOMO(β)	LUMO(β)
1	0.7289	−0.8894
2	0.5046	−0.9201
3	0.4187	−0.9515

*Same as in Table 1

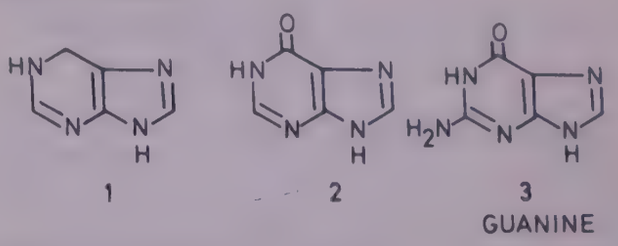

1 2 3 GUANINE

intermediate steps in the synthesis of guanine (Table 4) and thymine (Table 2) respectively. Their acceptance by nature may be attributed to their HOMO and LUMO energy values.

References

1 Huckel E, *Z Phys (Germany)*, **70** (1931) 204; **76** (1932) 628.

2 Roberts J D, *Notes on molecular orbital calculations* (W.A. Benjamin, New York), 1961.

3 Coulson C A, *Proc R Soc London Ser A*, **169** (1939) 413.

4 Pullman B & Pullman A, *Proc Natl Acad Sci (USA)*, **44** (1958) 1197.

5 Hameka H F, *Introduction to quantum theory* (Harper & Row, New York), 1967.

Indian Journal of Pure & Applied Physics
Vol. 21, November 1983, pp. 672-673

Effect of Environment in Hypersensitive Transitions of Nd^{3+} Ternary Complexes

ANUP K GUPTA & M P BHUTRA
Department of Physics, University of Jodhpur, Jodhpur

Received 22 January 1983

Absorption spectra of ternary complexes of Nd^{3+} in different environments, viz. methanol, formamide and dimethyl sulphoxide, have been recorded taking glycine, alanine, valine and methionine as primary ligands and propane-1,2-diol as secondary ligand. The transition $^4G_{5/2} \leftarrow {}^4I_{9/2}$ obeying the selection rule $\Delta J \leq 2$, known as hypersensitive transition has been studied for four Nd^{3+} complexes. The results indicate that the hypersensitivity may be explained by means of vibronic mechanism with inclusion of covalency. Effect of different environments on hypersensitive transition has been discussed.

The absorption spectra of rare earth complexes have been the subject of several investigations[1-5]. In this note, the absorption spectra of ternary complexes of Nd^{3+} in different environments, viz. methanol, formamide and dimethyl sulphoxide (DMSO) have been recorded taking glycine (G), alanine (A), valine (V) and methionine (M) as primary ligands and propane-1,2-diol (P) as secondary ligand. In Nd^{3+} complexes, the transition ($^4G_{5/2} \leftarrow {}^4I_{9/2}$) obeying the selection rule $\Delta J \leq 2$, is called as hypersensitive transition. Intensity of hypersensitive transition increases by changing both ligand and solvent[6]. The intensity of hypersensitive transition can be up to 200 times greater[7] than that of the corresponding aquo ion transition depending upon the particular complex. Also it has been observed that T_2-parameter is directly related to hypersensitivity and covalency[8] but in certain cases it does not hold good[9].

Theory—The oscillator strength P for intra-f^n transitions of rare earths is given by Judd[10] as

$$P = \sum_{\lambda=2,4,6} T_\lambda \nu (f^n \psi_J \| U(\lambda) \| f^n \psi'_{J'})^2 / (2J+1) \quad \ldots(1)$$

where ν is the energy (in cm^{-1}) of the transition $\psi_J \rightarrow \psi'_{J'}$, and $U(\lambda)$ the tensor operator of rank λ. The three quantities T_λ are treated as parameters. The experimental oscillator strength (P_{expt}) values have been due to contributions from induced electric-dipole (P_{ed}), magnetic-dipole (P_{md}) and electro-quadrupole (P_{eq}) modes.

Since P_{eq} ($\sim 10^{-11}$) and P_{md} ($\sim 10^{-8}$) are negligible in comparison with P_{expt} ($\sim 10^{-6}$), they are neglected. Hence in Eq. (1) the values of P_{expt} may be substituted.

Generally, the oscillator strengths for Nd^{3+} complexes are expressed in terms of T_4 and T_6 parameters only. But the effects of ligand and solvent on the intensity of hypersensitive transition can be explained by T_2 parameter only[11].

Karrakar[12,13] has studied the hypersensitive transitions in six-, seven- and eight-coordinated Pr^{3+}, Ho^{3+} and Nd^{3+} β-diketonates and has shown that the changes in oscillator strengths of these transitions may be correlated with the changes in the coordination and symmetry of the rare earth ion. It has also been observed that the intensity of hypersensitive transition depends upon the ability to donate the electron[14] of the ligand. Following are the proposals which have been advanced for the explanation of these transitions, discussed by Vaishnava and Tandon[15]: (a) Pseudo-quadrupole transitions; (b) Inclusion of spherical harmonics in the crystal field potential; (c) Polarization of surrounding ions; (d) Double photon transitions; and (e) Vibronic mechanism with the inclusion of covalency.

Henrie and Choppin[16] have proposed the phenomenon of hypersensitivity which can be explained with the inclusion of covalency within the framework of vibronic mechanism. According to the mechanism, the oscillator strength of hypersensitive transition should vary with νb^2, where b is the degree of covalency[16] and has been calculated by using the relation, $b^{1/2} = [\frac{1}{2}(1-\beta)]^{1/2}$, β is the nephelauxetic ratio[5].

Results—The values of oscillator strength (P_{expt}) and intensity parameter T_2 in different solvents, viz.

Table 1—Values of Oscillator Strength (P_{expt}) and T_2-parameter (in cm^{-1}) for Various Nd^{3+} Complexes in Different Solvents

Complex	Solvent					
	Methanol		Formamide		DMSO	
	$P_{expt} \times 10^6$	$T_2 \times 10^{10}$	$P_{expt} \times 10^6$	$T_2 \times 10^{10}$	$P_{expt} \times 10^6$	$T_2 \times 10^{10}$
$NdG(P)_2$	13.37	4.92	16.34	6.50	18.31	8.12
$NdA(P)_2$	13.41	5.72	18.69	8.44	19.71	8.51
$NdV(P)_2$	15.15	5.94	21.46	9.95	23.11	10.60
$NdM(P)_2$	19.47	8.58	24.00	11.33	24.30	11.93

Table 2—Values of Energy of Hypersensitive Transition ν (in cm^{-1}) and Degree of Covalency ($b^{1/2}$) for Various Nd^{3+} Complexes in Different Environments

Complex	Solvent					
	Methanol		Formamide		DMSO	
	ν	$b^{1/2}$	ν	$b^{1/2}$	ν	$b^{1/2}$
$NdG(P)_2$	17331	0.0508	17271	0.0504	17212	0.0224
$NdA(P)_2$	17301	0.0498	17271	0.0289	17241	0.0316
$NdV(P)_2$	17301	0.0433	17241	0.0267	17182	0.0500
$NdM(P)_2$	17301	0.0255	17271	0.0286	17241	0.0316

methanol, formamide and DMSO are given in Table 1. The values of energy of hypersensitive transition ν (in cm^{-1}) and degree of covalency ($b^{1/2}$) are given in Table 2.

We see from Table 1 that the values of parameter T_2 and oscillator strength (P_{expt}) increase with the solvents in the order: DMSO > formamide > methanol, in all the four Nd^{3+} complexes. It indicates that the solute-solvent interaction is maximum in the case of DMSO, and least in the case of methanol. It also indicates that the value of the parameter T_2 increases in the increasing order of molecular weight of the solvents. The value of T_2 also increases in all the solvents in the order: $NdM(P)_2 > NdV(P)_2 > NdA(P)_2 > NdG(P)_2$, which is also in the increasing order of molecular weight of the amino acids. These results indicate that the intensity of the hypersensitive transition increases as the molecular weight of the ligand or molecular weight of the solvent increases.

References

1 Misumi S, Kida S, Isobe T & Inazumi A, *Bull Chem Soc Jpn (Japan)*, **41** (1968) 25.
2 Tandon S P & Mehta P C, *J Chem Phys (USA)*, **52** (1970) 4896.
3 Peacock R D, *Struct of Bonding (Germany)*, **22** (1975) 83.
4 Joshi G K, Bhutra M P & Misra S N, *J Inorg & Nucl Chem (GB)*, **43** (1981) 525.
5 Bhutra M P & Gupta A K, *Indian J Pure & Appl Phys*, **20** (1982) 954.
6 Jørgensen C K & Judd B R, *J Mol Spectrosc (USA)*, **8** (1964) 281.
7 Gruen D M & Dekock C W, *J Chem Phys (USA)*, **45** (1966) 455.
8 Carnall W T, Fields P R & Wybourne B G, *J Chem Phys (USA)*, **42** (1965) 3797.
9 Peacock R D, *J Chem Soc A (GB)*, (1971) 2028.
10 Judd B R, *J Chem Phys (USA)*, **44** (1966) 839.
11 Bukietynska K & Choppin G R, *J Chem Phys (USA)*, **52** (1970) 2875.
12 Karrakar D G, *Inorg Chem (USA)*, **6** (1967) 1863.
13 Karrakar D G, *Inorg Chem (USA)*, **7** (1968) 473.
14 Blasse G, *Chem Phys Lett (Netherlands)*, **20** (1966) 189.
15 Vaishnava P P & Tandon S P, *Indian J Phys Part B*, **51** (1977) 404.
16 Henrie D E & Choppin G R, *J Chem Phys (USA)*, **49** (1968) 47.

Indian Journal of Pure & Applied Physics
Vol. 21, November 1983, pp. 674-676

Spectral Study of Ternary Complexes of Rare Earths with Different Amino Acids

M P BHUTRA & ANUP K GUPTA
Physics Department, University of Jodhpur, Jodhpur 342001

Received 29 January 1983

Absorption spectra of eight ternary complexes of neodymium and praseodymium with different amino acids (glycine, alanine, valine and methionine) as primary ligand and propane-1,2-diol as secondary ligand have been recorded in dimethyl sulphoxide (DMSO) in the visible region. The observed values of energy and intensity of various transitions have been compared with those calculated by using Judd-Ofelt relation. The observed and calculated values are in good agreement. Based on the calculated values of different energy and intensity parameters, the covalency and its dependence on atomic number of metal ion, metal-ligand interaction, nephelauxetic effect, etc. have been discussed.

Most of the $f \rightarrow f$ transitions in rare earths are found to be weak except one known as hypersensitive transition[1]. The intensity of hypersensitive transition changes with the change of environment of metal ion in different complexes[2,3]. Misumi *et al.*[4] showed that from the study of the different energy and intensity parameters, useful information regarding spin-orbit interaction, metal-ligand interaction, etc. can be obtained.

We have studied the bonding, nephelauxetic effect and covalency in binary complexes[5] of Pr^{3+} and Nd^{3+}. The present communication reports the dependence of energy parameters like Slater-Condon (F_2, F_4, F_6) and Lande parameter (ξ_{4f}) and intensity parameters, i.e. Judd-Ofelt parameters (T_2, T_4, T_6) on covalency of Nd^{3+} and Pr^{3+} ternary complexes. The metal-ligand interaction which is helpful in explaining the structure of complex has also been discussed in the light of these parameters.

The complexes of Pr^{3+} and Nd^{3+} were prepared by the method reported earlier[6]. The chemicals used were of AR grade and the metals 99.9% pure (Indian Rare Earths Ltd) were used. The complexes were prepared in the molar ratio 1:1:2.

The absorption spectra of the complexes were recorded on Carl Zeiss VSU-2 Spectrophotometer in the region 360-920 nm in DMSO.

Energy levels—The energy levels of various transitions were evaluated theoretically by using the relation[7].

$$E_j(F_k, \xi_{4f}) = E_{0j}(F_k^0, \xi_{4f}^0) + \sum_{k=2,4,6} \left(\frac{\partial E_j}{\partial F_k}\right) \Delta F_k + \left(\frac{\partial E_j}{\partial \xi_{4f}}\right) \Delta \xi_{4f} \quad \ldots (1)$$

Table 1—Observed and Calculated Values of Energy Levels for Various Pr^{3+} and Nd^{3+} Complexes in DMSO

Pr^{3+} complexes

Levels	$PrG(P)_2$		$PrA(P)_2$		$PrV(P)_2$		$PrM(P)_2$	
	Calc.	Obs.	Calc.	Obs.	Calc.	Obs.	Calc.	Obs.
$^3P_2$	22389	22472	22410	22472	22394	22447	22379	22472
$^3P_1$	21271	21322	21277	21322	21264	21322	21245	21299
$^3P_0$	20825	20790	20781	20747	20796	20747	20771	20725
$^1D_2$	17117	16935	17111	16935	17109	16935	17093	16892
rms dev. (σ)	104.69		97.47		98.55		116.28	

Nd^{3+} complexes

	$NdG(P)_2$		$NdA(P)_2$		$NdV(P)_2$		$NdM(P)_2$	
	Calc.	Obs.	Calc.	Obs.	Calc.	Obs.	Calc.	Obs.
$^2P_{1/2}$	23109	23095	23143	23148	23092	23095	23127	23095
$^4G_{11/2}$	21549	21598	21506	21645	21556	21692	21515	21598
$^4G_{9/2}$	21099	21142	21123	21142	21131	21142	21104	21097
$^2G_{9/2}$	19520	19531	19531	19531	19540	19531	19531	19569
$^4G_{7/2}$	19135	19157	19183	19157	19161	19157	19178	19194
$^4G_{5/2}$	17195	17212	17245	17241	17209	17182	17256	17241
$^4F_{9/2}$	14742	14684	14713	14663	14746	14706	14712	14684
$^4F_{7/2}$	13296	13333	13280	13333	13298	13333	13287	13351
$^4F_{5/2}$	12460	12346	12457	12346	12465	12361	12464	12361
$^4F_{3/2}$	11419	11468	11446	11494	11425	11481	11452	11494
rms dev. (σ)	50.47		63.51		60.19		52.09	

The observed energy (converting it from nm to wavenumbers) as well as calculated values of energy levels using Eq. (1) for both Nd^{3+} and Pr^{3+} complexes in solvent DMSO have been collected in Table 1. Low rms deviation between the observed and calculated values supports the validity of the relation used in case of Nd^{3+} complexes. High rms deviation in the case of Pr^{3+} complexes is due to the assumption of $4f$-wavefunctions to be hydrogenic[8].

The calculated values of Slater-Condon parameters F_2, F_4, F_6, Lande's parameter ξ_{4f}, nephelauxetic ratio β and bonding parameter $b^{1/2}$ are collected in Table 2. The decrease in the F_2 value from that of free ion supports the complexation. This decrease is more in case of Pr^{3+} complexes as compared with Nd^{3+} complexes, showing that on complexation the contraction of $4f$-orbital is reduced[9] with the increase of atomic number of the metal ion.

The relation between nephelauxetic ratio (β) and degree of covalency ($b^{1/2}$) is given by

$$b^{1/2}=\left(\frac{1-\beta}{2}\right)^{1/2} \quad \ldots (2)$$

Nephelauxetic effect[10] is obtained using the relation $\beta=F_2^c/F_2^f$ where subscripts c and f refer to complex and free ion respectively. The value of β for Nd^{3+} and Pr^{3+} complexes is less than 1.0, suggesting that they are covalent in nature. Change of ligand, i.e. change in outer sphere of complex will not affect the covalency of a metal complex, but with the change of metal, i.e. as the atomic number of the metal ion increases the covalency decreases.

The change in ξ_{4f} values on complexation is large compared with the change in $F_k(k=2, 4, 6)$ values, indicating that, on complexation, ξ_{4f} values are more affected as compared with F_k values.

Table 2—Computed Values of Slater-Condon and Lande Parameters, β and $b^{1/2}$ for Various Pr^{3+} and Nd^{3+} Complexes in DMSO

Complex	F_2	F_4	F_6	ξ_{4f}	β	$b^{1/2}$
$PrG(P)_2$	312.43	43.13	4.721	654.90	0.970	0.1225
$NdG(P)_2$	330.82	49.60	5.297	881.89	0.999	0.0224
$PrA(P)_2$	311.53	43.01	4.707	668.83	0.967	0.1284
$NdA(P)_2$	330.31	50.99	5.280	861.75	0.998	0.0316
$PrV(P)_2$	311.64	43.02	4.709	665.29	0.968	0.1265
$NdV(P)_2$	329.66	50.15	5.250	866.69	0.995	0.0500
$PrM(P)_2$	311.14	42.95	4.701	668.21	0.966	0.1304
$NdM(P)_2$	330.48	50.77	5.265	862.00	0.998	0.0316

Free ion
Pr^{3+}: $F_2=322.09$
Nd^{3+}: $F_2=331.159$

Table 3—Observed and Calculated Values of Oscillator Strength for Various Pr^{3+} and Nd^{3+} Complexes in DMSO

Pr^{3+} complexes

Levels	$PrG(P)_2$		$PrA(P)_2$		$PrV(P)_2$		$PrM(P)_2$	
	Calc.	Obs.	Calc.	Obs.	Calc.	Obs.	Calc.	Obs.
	$\times 10^6$		$\times 10^6$		$\times 10^6$		$\times 10^6$	
$^3P_2$	17.04	17.04	17.84	17.84	18.23	18.23	23.90	23.90
$^3P_1$	9.01	10.25	8.66	9.61	12.30	14.61	6.73	7.66
$^3P_0$	8.89	7.67	8.53	7.60	12.12	9.87	6.63	5.70
$^1D_2$	3.04	3.04	3.48	3.48	2.79	2.79	2.83	2.83
rms dev. (σ)	0.87×10^{-6}		0.67×10^{-6}		1.61×10^{-6}		0.66×10^{-6}	

Nd^{3+} complexes

	$NdG(P)_2$		$NdA(P)_2$		$NdV(P)_2$		$NdM(P)_2$	
	Calc.	Obs.	Calc.	Obs.	Calc.	Obs.	Calc.	Obs.
	$\times 10^6$		$\times 10^6$		$\times 10^6$		$\times 10^6$	
$^2P_{1/2}$	0.95	1.15	0.75	1.38	0.73	1.58	0.70	1.54
$^4G_{11/2}$	0.33	1.14	0.27	0.95	0.28	1.12	0.28	1.44
$^4G_{9/2}$	2.52	1.72	2.03	1.39	2.10	1.56	2.10	1.18
$^2G_{9/2}$	0.66	1.94	0.53	1.61	0.55	1.75	0.56	1.87
$^4G_{7/2}$	5.46	4.52	4.55	3.52	4.80	4.60	4.90	5.03
$^4G_{5/2}$	21.14	21.31	19.96	19.71	23.04	23.11	24.96	24.80
$^4F_{9/2}$	0.88	0.52	0.71	0.40	0.77	0.55	0.79	0.47
$^4F_{7/2}$	7.28	7.52	7.89	5.32	6.36	6.40	6.63	6.00
$^4F_{5/2}$	9.03	8.94	7.24	7.63	7.59	7.86	7.76	8.35
$^4F_{3/2}$	3.68	3.68	2.92	2.62	2.92	2.91	2.86	2.18
rms dev. (σ)	0.64×10^{-6}		0.65×10^{-6}		0.58×10^{-6}		0.77×10^{-6}	

Table 4—Computed Values of T_λ-Parameters and T_4/T_6 for Various Pr^{3+} and Nd^{3+} Complexes in DMSO

Complex	$T_2\times10^{10}$	$T_4\times10^{10}$	$T_6\times10^{10}$	T_4/T_6
$PrG(P)_2$	−458.4	24.8	49.4	0.50
$NdG(P)_2$	8.12	11.17	11.73	0.95
$PrA(P)_2$	−409.2	23.8	52.2	0.46
$NdA(P)_2$	8.51	8.79	9.50	0.92
$PrV(P)_2$	−605.5	33.8	50.9	0.66
$NdV(P)_2$	10.60	8.60	10.36	0.83
$PrM(P)_2$	−948.7	18.5	73.6	0.25
$NdM(P)_2$	12.76	8.59	9.87	0.76

Intensity parameters—Oscillator strength of each transition can be calculated by using the formula:

$$P_{exp}=4.6\times10^{-9}\times\varepsilon_m\times\Delta\nu_{1/2} \quad \ldots (3)$$

where ε_m and $\Delta\nu_{1/2}$ are the molecular extinction coefficient and half bandwidth respectively.

The experimentally observed values of oscillator strength for Nd^{3+} and Pr^{3+} complexes along with their calculated values using relation (3) are collected in Table 3. The value of T_2, T_4 and T_6 parameters have been computed using Judd-Ofelt relation[11,12] by partial multiple regression method[13] and have been collected in Table 4. The values of reduced matrix elements have been taken from Carnall *et al.*[14].

From Table 4 we see that the value of T_4 and T_6 remain nearly invariant while the values of T_2 which is sensitive to the environment of metal ion increases in Nd^{3+} complexes as the amino acids are changed in the order glycine (75)<alanine (89)<valine (117)<methionine (149). The value in parenthesis after each amino acid indicates the corresponding molecular weight. It has been found that T_2 increases linearly with the molecular weight of the amino acid. In the case of Pr^{3+} complexes where the wavefunction has been assumed to be hydrogenic, T_2 is negative, which has no physical significance.

It is observed from Table 4 that the ratio of $(T_4/T_6)<1.0$ in each metal and is fairly constant. The complexes containing oxygen-donor ligand have $(T_4/T_6)\sim0.3$ while complexes containing nitrogen-donor ligands[15] are found to have $(T_4/T_6)\sim0.9$. The complexes under study have the ratio of (T_4/T_6) for Nd^{3+} and Pr^{3+} to lie between 0.25 and 0.95 supporting that they have oxygen/nitrogen-donor ligands. This ratio also increases with the increase of atomic number of metal ion.

References

1 Jorgensen C K & Judd B R, *Mol Phys (GB)*, **8** (1964) 281.
2 Strek W, *Theor Chim Acta (Berlin)*, **52** (1979) 45.
3 Bhutra M P & Gupta Anup K, *Indian J Pure & Appl Phys*, **20** (1982) 954.
4 Misumi S, Kida S, Isobe T & Inazumi A, *Bull Chem Soc Jpn (Japan)*, **41** (1968) 25.
5 Joshi G K, Bhutra M P & Misra S N, *J Inorg & Nucl Chem (GB)*, **43** (1981) 525.
6 Vasireddi S P & Ramchandra Rao V, *J Inorg & Nucl Chem (GB)*, **39** (1977) 311.
7 Wong E Y, *J Chem Phys (USA)*, **38** (1963) 976.
8 Surana S S L, Mathur R C & Tandon S P, *Spectrosc Lett (USA)*, **11** (1978) 389.
9 Henrie D E & Choppin G R, *J Chem Phys (USA)*, **49** (1968) 477.
10 Tandon S P, Govil R C & Tandon K, *Spectrosc Lett (USA)*, **6** (1973) 125.
11 Judd B R, *Phys Rev (USA)*, **127** (1962) 750.
12 Ofelt G S, *J Chem Phys (USA)*, **37** (1962) 511.
13 Cyril H Goulden, *Method of statistical analysis* (Asia Publishing House, Bombay), 1964, Chap. 8, 134.
14 Carnall W T, Fields P R & Wybourne B G, *J Chem Phys (USA)*, **42** (1965) 3797.
15 Sinha S P, Mehta P C & Surana S S L, *Mol Phys (GB)*, **23** (1972) 807.

Indian Journal of Pure & Applied Physics
Vol. 21, November 1983, pp. 677-679

Spectra & Species of Fluorescein & 6-Hydroxy 9-Phenyl Fluoron in Frozen Solutions

J SHAH, N B JOSHI* & D D PANT
Th D S B Constituent College, Kumaun University
Naini Tal 263 002

Received 13 *September* 1982

The low temperature emission spectra of fluorescein and HPF are compared. The fluorescence and phosphorescence of dication, cation, neutral, mono and double anion species of fluorescein are assigned by taking the excitation spectra, lifetimes and by comparison with corresponding room temperature spectra. The dication is stabilized more in the excited state compared to the monocation.

Fluorescein is one of the earliest to be studied for fluorescence work and the pH dependence of emission spectra was elucidated in detail by various workers over a wide pH range in aqueous solutions[1-4]. The spectra of cations and dianions are, thus, well established both at 290 and 80 K. Obscurity, however, still exists in the location of fluorescence and phosphorescence bands of the neutral and monoanion species. Pant[3] reported a phosphorescence band at 595 nm at 80 K and tentatively suggested it to be due to monoanion. Even at room temperature the neutral and the monoanion species cannot be distinguished. Martin and Lindqvist[4] determined the fluorescence quantum efficiency and spectra of fluorescein over a wide pH range in aqueous solutions. They interpreted their results by comparison with a similar dye namely, 6-hydroxy 9-phenyl fluoron (HPF) and found that the neutral and monoanion have the identical spectra. But they did not report the low temperature data. A renewed interest in the investigations of the spectra and species of fluorescein arose in view of our red edge excitation (REE) effect which was interpreted as due to the excited state proton transfer[5-8]. In order to locate uniquely the position of the emission peaks of the individual species of fluorescein at 80 K and to ascertain that the change in the emission spectra on REE[7] of the first absorption band are not due to the presence of extraneous impurities, we undertook a thorough study of the spectra of fluorescein over a wider pH range at 290 and 80 K.

The complexity in the pH dependence of fluorescein is, to a large extent, due to the carboxyl group which makes possible the formation of the lactonic form. To specify, the emission spectra at 80 K, therefore, we have adopted the method of Martin *et al.*[4], viz. comparison with luminescence properties of HPF which lacks the carboxyl group. To make a more precise assignment, excitation spectra are taken for fluorescence and phosphorescence emissions.

Chromatographically pure fluorescein was obtained from M/s M E Merck, Germany and used as such. HPF donated by Prof. L Lindqvist (University Paris-Sud, France) was further purified by the method of reprecipitation. Solutions were prepared using triply distilled water, analytical grade sulphuric acid and sodium hydroxide. Glycerol (GR) was used in the less acidic solutions in order to make a clear glass at 80 K. The concentrations of the solutions were kept rather low ($5 \times 10^{-5} M$), so that the possibility of dimerization was negligible. The acidity was varied from $36N$ H_2SO_4 in pure aqueous solutions to pH 6 in glycerol solutions with the help of sulphuric acid and from pH 7 to pH 12 with the help of sodium hydroxide. The pH values were measured by a universal indicator (E Merck) and a comparator. The concentrated acid did not attack the aromatic ring and reversible spectra could be obtained by changing the pH of the same solution.

The emission spectra were recorded by a SPM-2 Carl Zeiss monochromator, a 1P21 photomultiplier and a galvanometer assembly and were corrected with

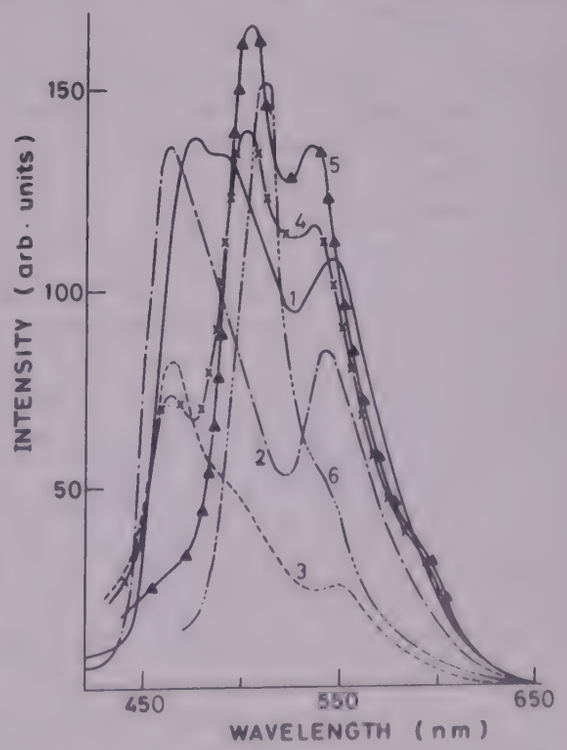

Fig. 1—Emission spectra of fluorescein for various pH values at 80 K [Curve: 1, $36N$ H_2SO_4; curve 2, $20N$ H_2SO_4; curve 3, pH 3.2; curve 4, pH 4; curve 5, pH 5.4 and curve 6, pH 12]

* Present address: National Research Centre, Maryland, Washington DC, USA

respect to the dispersion of the monochromator and spectral response of the photomultiplier. The absorption spectra were recorded by a Beckman DK-2A spectrophotometer. The excitation spectra were taken with Spex fluorolog model 1902. The lifetime of phosphorescence was measured by a mechanical phosphoroscope coupled with a Tektronix 502-A oscilloscope.

Fig. 1 shows emission spectra of fluoescein at 80K for different pH values. The band at 510 nm (pH > 10 is due to the fluorescence of the binegative ion and the shoulder at 540 nm (lifetime $\tau_P = 0.2$ sec) is due to overlap of phosphorescence and vibronic structure of fluorescence. In 20*N* H_2SO_4 solution, the band at 465 nm is the fluorescence band of the monocation and that at 540 nm ($\tau_P \sim 2.8$ sec) is the phosphorescence band. In the pH range 1 to 3, the spectra contain three bands at 465, 505 and 535 nm. The 465 nm peak is due to the presence of cation and its intensity decreases on increasing the pH. In the range pH 4-6, only two fluorescence bands at 505 and 535 nm are observed, with a phosphorescence band at 585 nm ($\tau_P \sim 0.65$ and 1.3 sec). As suggested by Martin *et al.*[4], the neutral and monoanion species have the same spectra and they show vibrational structure in absorption and emission; we assign these to the neutral and the monoanion species by comparison with the room temperature spectra. The 535 nm band being the resolved vibronic structure of the 505 nm band ($\Delta\nu_v = 1300\ cm^{-1}$). The excitation spectra obtained by monitoring at 535 nm or at 505 nm are the same and correspond to the absorption spectra of the neutral molecule (or monoanion) (Fig. 2). The vibronic structure obtained in the excitation spectrum is much superior to that obtained in absorption ($\Delta\nu_v = 1250\ cm^{-1}$). The 585 nm band is due to the phosphorescence of the neutral (or monoanion) molecule as shown by its large lifetime and the resemblance of the excitation spectra with those of the neutral (or monoanion) molecule. Although the spectra for neutral and monoanion species are the same, the extinction coefficients (ε) for the two species are different. At pH ~ 3.3, where monoanion is not expected, the neutral molecule has $\varepsilon = 1.2 \times 10^4 M^{-1} cm^{-1}$ whereas at pH ~ 5.5 where the monoanion is predominant, the value of $\varepsilon = 2.7 \times 10^4 M^{-1} cm^{-1}$. Similarly, the double lifetime of the phosphorescence band at 585 nm is 0.65 sec and 1.3 sec due to the presence of both the species. Thus, the double lifetimes of phosphorescence and value of ε in the absorption indicate that in spite of similar spectra, the neutral and monoanion species can be distinguished. The excitation spectra for 465 and 540 nm peak correspond to the absorption spectrum of the cation (Fig. 2). Similarly for the dianion $\lambda_P \sim 540$ nm and $\lambda_I \sim 510$ nm show identical excitation spectra.

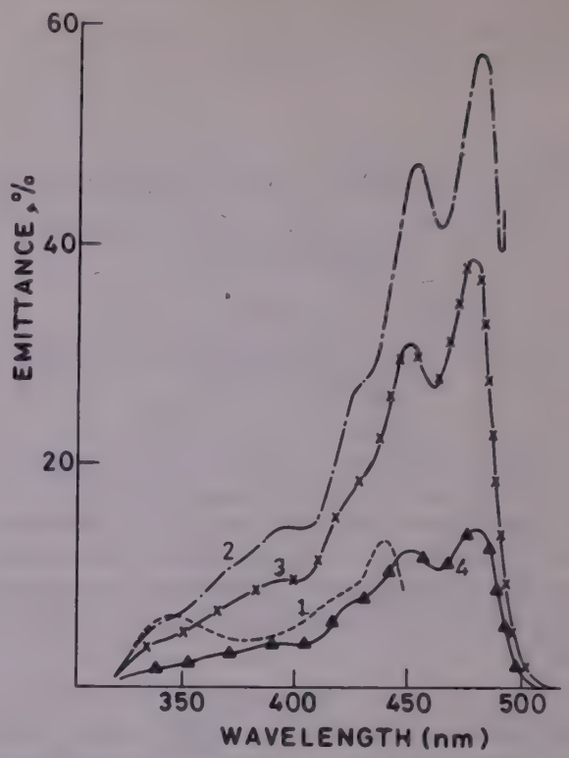

Fig. 2—Excitation spectra of fluorescein for pH 4 at 80 K monitored at different wavelengths [Curve 1, 465 nm; curve 2, 505 nm; curve 3, 535 nm and curve 4, 585 nm]

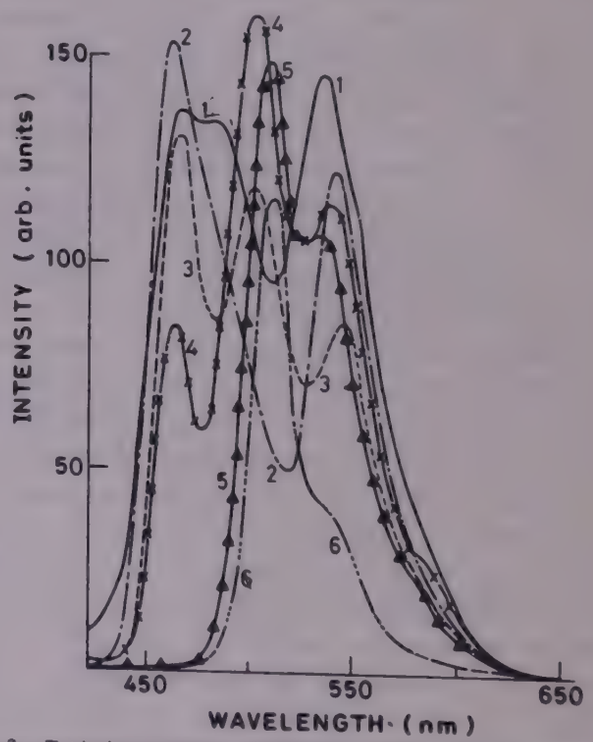

Fig. 3—Emission spectra of HPF for various pH values at 80 K [Curve: 1, 36 *N* H_2SO_4; 2, 10*N* H_2SO_4; 3, pH 4; 4, pH 5.5; 5, pH 6.5; and 6, pH 12]

In 36*N* H_2SO_4 solution one additional fluorescence band at 490 nm with the phosphorescence band at $\lambda_P \sim 540$ nm ($\tau_P \sim 2.4$ sec, 2.8 sec) is observed. We assign this band to double cation[9]. The 290 K emission band for double cation is at 495 nm and the corresponding absorption peak is at 432 nm, i.e. 50 Å blue shifted than the absorption peak of the monocation. This frozen solution contains monocation also; hence two lifetimes are observed for phosphorescence.

Table 1—The Positions of Emission and Absorption of Various Ionic Species of Fluorescein and the Corresponding Ground State pK values

Species	Ground state dissociation constants (Ref. 4)	Absorption maximum (nm)	Extinction coefficient ($M^{-1}cm^{-1}$)	Emission maximum R.T. (nm)	Emission maximum 80 K		Phosphorescence lifetime* (sec)
					Fluorescence maximum (nm)	Phosphorescence maximum (nm)	
Dication		432	3.4×10^4	495	490	540	2.4, 2.8
Cation	2.2	437	5.0×10^4	480	465	540	2.8
Neutral	4.4	445	1.2×10^4	520	505	585	0.65
		480		550	535		1.3
Monoanion	6.7	455	2.7×10^4	520	505	585	0.65
		480	2.6×10^4	550	535		1.3
Dianion		495	7.8×10^4	525	510	540	0.2

* It is generally observed that φ_p/φ_F and τ_p are higher for mono and dication than for neutral, mono and dianions. The two separate values of τ_p indicate presence of two species.

Table 2—The Positions of Emission and Absorption of Various Ionic Species of HPF and the Corresponding Ground State pK Values

Species	Ground state dissociation constants (Ref. 4)	Absorption maximum (nm)	Extinction coefficient ($M^{-1}cm^{-1}$)	Emission maximum R.T. (nm)	Emission maximum 80 K		Phosphorescence lifetime sec
					Fluorescence maximum (nm)	Phosphorescence maximum (nm)	
Dication		427	3.4×10^4	495	490	540	2.3,2.8
Cation	3.1	432	4.3×10^4	475	460	540	2.8
Neutral	6.3	455	3.1×10^4	520	505	585	0.6
		480	2.9×10^4	550	535		
Anion		490	8.6×10^4	525	510	540	0.2

Fig. 3 represents the luminescence spectra of the HPF at 80 K. The fluorescence of the anion is at 510 nm and the 540 nm band ($\tau_p \sim 0.2$ sec) is due to phosphorescence. At pH ~ 5.5, fluorescence peaks at 505 and 535 nm and phosphorescence peak at 585 nm ($\tau_P \sim 0.6$ sec) are observed which are due to the emission of neutral HPF molecule. On increasing the acidity, the fluorescence band of the monocation λ_F ~460 nm and the phosphorescence band at $\lambda_P \sim 540$ nm ($\tau_P \sim 2.8$ sec) are observed. In 36*N* H_2SO_4 solution the double cation emission is observed at $\lambda_F \sim 490$ nm and $\lambda_P \sim 540$ nm ($\tau_P \sim 2.3$ and 2.8 sec).

The curves show that the double cation emission is red shifted whereas the absorption is blue shifted as compared to the emission and absorption of the monocation. Thus, the Stokes shift is larger for dication while the temperature shift is more for the monocation. As shown above the same phenomenon is observed for fluorescence also. The stabilization of the excited state in the double cation after the absorption process cannot be due to an orientational relaxation process because the stabilization is observed in the frozen glass. It may be due to a phenomenon similar to the one discussed by Mulliken *et al.*[10] in charge transfer spectra where the idea of a constrained coordinate is used.

The excitation spectra for double cation of the fluorescein are broad and expand more towards blue compared to monocation. Obviously, the dication cannot be completely isolated. Tables 1 and 2 show the emission and absorption maxima of the different species of fluorescein and HPF respectively, in the pH range studied.

Authors are grateful to CSIR and UGC, New Delhi, for financial assistance.

References

1 Zanker V & Peter W, *Chem Ber (Germany)*, **1** (1959) 572.
2 Rozwadowski M, *Acta Phys Pol (Poland)*, **20** (1961) 1005.
3 Pant H C, *Indian J Pure & Appl Phys*, **6** (1968) 19.
4 Martin M & Lindqvist L, *J Lumin (Netherlands)*, **10** (1975) 381.
5 Shah J, Joshi N B & Pant D D, *Curr Sci (India)*, **49** (1980) 609.
6 Gangola P, Joshi NB & Pant D D, *Chem Phys Lett (Netherlands)*, **51** (1977) 44.
7 Gangola P, Joshi N B & Pant D D, *Chem Phys Lett (Netherlands)*, **60** (1979) 329.
8 Pande U, Joshi N B & Pant D D, *Chem Phys Lett (Netherlands)*, **72** (1980) 209.
9 Lindqvist L, Private communication, 1980.
10 Mulliken R S, *J Chim Phys (France)* **61** (1964) 20.

Indian Journal of Pure & Applied Physics
Vol. 21, November 1983, pp. 680-682

Vibrational Analysis of Some Axially Symmetric XYZ_3-type Molecules

S MOHAN & T J BHOOPATHY
Division of Applied Sciences, Anna University,
Madras Institute of Technology, Madras 600044

Received 28 *March* 1983

Calculations of molecular potential constants, compliance constants, vibrational mean amplitudes, Coriolis coupling constants, and centrifugal distortion constants are presented for four halo silanes and three halo-deutero silanes, belonging to the XYZ_3-type (C_{3v}), using the procedure involving kinetic constants. The nature, range and variation of these constants are discussed.

The kinetic constants of molecules appear to be of basic significance in the study of molecular vibrations[1-6]. They have been advantageously utilized not only in solving the secular equations but also to obtain other molecular constants such as compliance constants, mean amplitudes of vibration, vibrational coupling constants and rotational distortion constants. The present investigation has been undertaken to obtain a reasonable set of potential constants for four halo silanes and three halo-deutero silanes, by the kinetic constants method for the first time. The present set of kinetic constants and potential constants are utilized to evaluate compliance constants, vibrational mean amplitudes, Coriolis coupling constants and centrifugal distortion constants for these cases.

The symmetry co-ordinates and other details of the procedure are the same as those given in Ref. 6. In the kinetic constants method, the order of the secular equation has been reduced by providing an additional constraint, viz. $F_{ij}/F_{jj}=K_{ij}/K_{jj}$ $(i<j)$, where K's are the linear combinations of valence kinetic constants. The compliance constants are also determined for these cases by the Decius[7] method. The mean square amplitude matrix elements may be obtained using the normal co-ordinate transformation matrix L, from the relation[8] $\Sigma=L\Delta L'$ and hence mean amplitudes at 298.16 K are calculated. The zeta matrix elements have been evaluated from the relation[9]

$$\zeta^{\alpha}=L^{-1}C^{\alpha}(L')^{-1}$$

Table 1—Kinetic Constants (10^{-23} g) and Force Constants (10^5 dyn/cm)

Molecule	K_D	K_{dd}	$-K_{\alpha\alpha}$	$-K'_{d\alpha}$	f_D	f_{dd}	$f_{\alpha\alpha}$	$-f'_{d\alpha}$
	K_d	K_α	$-K'_{\alpha\theta}$	$K''_{d\alpha}$	f_d	f_α	$-f'_{\alpha\theta}$	$f''_{\alpha\alpha}$
	K_{Dd}	K_θ	$-K_{D\alpha}$	$-K'_{d\theta}$	f_{Dd}	f_θ	$-f_{D\alpha}$	$-f'_{d\theta}$
$SiFH_3$	1.9559	0.0018	0.0027	0.0017	5.4834	0.0171	0.0416	−0.0005
	0.1626	0.0145	0.0074	0.0012	0.5667	0.0758	0.0630	0.0064
	0.0212	0.0271	0.0144	0.0020	0.0594	0.4676	0.0404	0.0351
$SiClH_3$	2.7284	0.0020	0.0034	0.0018	3.1156	0.0030	0.0313	−0.0003
	0.1626	0.0139	0.0066	0.0011	0.5560	0.0597	0.0544	0.0045
	0.0296	0.0232	0.0175	0.0017	0.0338	0.3927	0.0200	0.0280
$SiBrH_3$	3.6957	0.0020	0.0026	0.0019	2.4246	0.0474	0.0421	0.0010
	0.1628	0.0146	0.0074	0.0011	0.4140	0.0665	0.0583	0.0033
	0.0401	0.0282	0.0271	0.0020	0.0263	0.4793	0.0178	0.0335
$SiIH_3$	4.1368	0.0022	0.0038	0.0019	1.9759	−0.0150	0.0243	0.0015
	0.1627	0.0135	0.0063	0.0010	0.5226	0.0471	0.0458	0.0023
	0.0448	0.0206	0.0240	0.0013	0.0214	0.3472	0.114	0.0227
$SiFD_3$	2.0241	0.0061	0.0050	0.0057	3.3857	0.1148	0.0401	−0.0012
	0.3179	0.0273	0.0114	0.0043	0.7205	0.0762	0.0602	0.0124
	0.0400	0.0475	0.0271	0.0067	0.0668	0.4254	0.0454	0.0598
$SiClD_3$	2.8632	0.0067	0.0064	0.0061	3.0664	−0.0134	0.0289	0.0004
	0.3177	0.0263	0.0110	0.0040	0.6297	0.0575	0.0503	0.0084
	0.0565	0.0426	0.0335	0.0057	0.0605	0.3887	0.0358	0.0517
$SiID_3$	4.4544	0.0075	0.0071	0.0065	1.9907	−0.0067	0.0226	0.0027
	0.3181	0.0257	0.0108	0.0036	0.5385	0.0455	0.0429	0.0043
	0.0879	0.0388	0.0470	0.0047	0.0393	0.3445	0.0210	0.0422

Table 2—Compliance Constants (Å/mdyn) and Bonded & Non-bonded Mean-square Amplitudes (10^{-3} Å) at 298.16 K

Molecule	C_D C_d $-C_{Dd}$	$-C_{dd}$ C_α C_θ	$-C_{\alpha\alpha}$ $-C'_{\alpha\theta}$ $C_{D\alpha}$	$C'_{d\alpha}$ $-C''_{d\alpha}$ $C'_{d\theta}$	σ_D σ_d σ_{Dd}	$-\sigma_{dd}$ σ_α σ_θ	$\sigma_{\alpha\alpha}$ $-\sigma'_{\alpha\theta}$ $\sigma_{D\alpha}$	$\sigma'_{d\alpha}$ $-\sigma''_{d\alpha}$ $\sigma'_{d\theta}$	σ_q σ_p
$SiFH_3$	0.1841	0.0647	2.3327	0.0642	1.6830	0.0106	−13.8612	0.3737	25.3841
	1.8026	5.0311	0.0380	0.0507	7.7372	46.2341	1.4092	0.1715	12.5205
	0.0193	0.4110	0.0116	0.0584	0.1636	21.2040	0.6339	0.1120	
$SiClH_3$	0.3227	0.0200	2.8392	0.0654	2.1490	0.0894	5.6459	0.3787	12.7021
	1.8255	6.0383	0.0348	0.0471	7.7065	8.6343	1.9918	0.1760	13.0780
	0.0202	0.5055	0.0113	0.0555	0.0893	26.6221	1.1184	0.0971	
$SiBrH_3$	0.4143	0.2901	3.3054	0.1094	2.3868	0.0229	6.4840	0.5552	13.6825
	2.5495	6.9924	0.0461	0.0644	7.9614	9.3322	2.5985	0.0067	20.4625
	0.0219	0.4117	0.0119	0.0762	0.2939	22.4235	1.6538	−0.0605	
$SiIH_3$	0.5079	−0.0464	3.5624	0.0719	2.7382	−0.1143	6.8980	0.7597	14.3945
	1.9404	7.4991	0.0430	0.0430	7.8642	10.1253	3.6663	−0.2024	13.7827
	0.0225	0.5907	0.0116	0.0512	0.5249	33.4570	2.1077	−0.4030	
$SiFD_3$	0.3004	0.2391	2.2030	0.1270	2.2957	0.1439	−11.2366	0.4262	17.9844
	1.5411	4.7815	0.0742	0.0872	5.5569	34.0679	1.1956	0.3142	9.2530
	0.0236	0.4595	0.0219	0.0969	0.0071	15.7335	0.8628	0.2545	
$SiClD_3$	0.3321	−0.0079	2.8064	0.1122	1.5469	−1.3540	4.1302	0.9123	13.2416
	1.6614	5.9992	0.0808	0.0847	6.9361	5.5666	2.1138	−0.1766	7.2121
	0.0363	0.5310	0.0227	0.0959	0.9991	7.6615	0.7719	−0.3379	
$SiID_3$	0.5085	0.0129	3.5325	0.1445	1.7615	−6.0270	−15.1505	−1.8562	34.4919
	1.9406	7.4624	0.0890	0.0866	11.6388	47.5764	3.2105	2.6101	11.5388
	0.0394	0.6191	0.0227	0.0987	−2.9410	25.2183	1.3910	3.1616	

Table 3—Mean Amplitudes of Vibration (10^{-2} Å) at 298.16 K

Molecule	Bonded		Non-bonded	
	l_D(X-Y)	l_d(X-Z)	l_p(Y...Z)	l_q(Z...Z)
$SiFH_3$	4.1024	8.7961	11.1895	15.9324
$SiClH_3$	4.6357	8.7787	11.4359	11.2704
$SiBrH_3$	4.8855	8.9227	14.3047	11.6972
$SiIH_3$	5.2328	8.8680	11.7400	11.9977
$SiFD_3$	4.7913	7.4545	9.6193	13.4106
$SiClD_3$	3.9331	8.3283	8.4924	11.5072
$SiID_3$	4.1970	10.7883	10.7419	18.5720

where L is the normal co-ordinate transformation matrix. Cyvin *et al.*[10] have reformulated the theory of rotational distortion by introducing certain new elements $T_{\alpha\beta,s}$ instead of partial derivatives of inertia tensor components, $J_{\alpha\beta,s}$ of Kivelson and Wilson[11,12]. The quantities $t_{\alpha\beta\gamma\delta}$ have been obtained using Cyvin's relation and hence $\tau_{\alpha\beta\gamma\delta}$ values have been evaluated.

The structural parameters and the vibrational frequencies used in the present investigation are taken from the Refs 13-16. The kinetic constants and the valence potential constants are given in Table 1. The magnitude of all the kinetic constants is found to increase with the increasing mass of the Z atom. With the increasing mass of the Y atom, the stretching constant K_D increases, and the stretching constants K_d remain more or less constant. On the other hand, the bending constants K_θ and K_α decrease, with $SiBrH_3$ as the exception. The angle-angle interaction constants $K_{\alpha\alpha}$, $K'_{\alpha\theta}$ and the bond-angle interaction constants $K_{D\alpha}$, $K'_{d\alpha}$, $K'_{d\theta}$ are uniquely negative in all the cases studied here. It is also interesting to note the same sign for the corresponding potential constants, except for $f_{\alpha\alpha}$. It may also be seen that the X-Y stretching potential constant f_D and the bending force constant f_θ as well as most of the interaction constants decrease with decreasing electronegativity of the substituent halogen atom, except for the $SiBrH_3$ molecule.

The compliance constants and bonded and non-bonded mean-square amplitudes at 298.16 K for the cases under study are given in Table 2. The compliance constants are invariant to the choice of co-ordinates defining the force field, and they may be used as a measure of the bond strengths and interactions instead of force constants as pointed out by Decius[7] and Jones[16]. It may also be noted that the compliance constants exhibit a trend opposite to that of the force constants. The mean amplitudes of vibration at 298.16 K for bonded and non-bonded distances are reported in Table 3. The mean amplitudes of the bonded X-Y, X-Z and the non-bonded Y.... Z and Z.... Z distances are in the expected range.

Table 4—Coriolis Coupling Constants and Rotational Distortion Constants (mHz)

Molecule	ζ_4	$-\zeta^z_{45}$	ζ_{14}	$-\zeta_{15}$	ζ_{16}	ζ_{45}	D_J
	ζ_5	ζ^z_{46}	$-\zeta_{24}$	ζ_{25}	$-\zeta_{26}$	ζ_{46}	D_{JK}
	$-\zeta_6$	$-\zeta^z_{56}$	ζ_{34}	ζ_{35}	ζ_{36}	ζ_{56}	D_K
$SiFH_3$	0.0470	0.0566	0.1332	0.2173	0.1697	0.4555	0.0184
	0.1257	0.9415	0.0477	0.7164	0.2123	0.1952	0.3356
	0.0901	0.3172	0.7096	0.0491	0.6173	0.4616	2.2241
$SiClH_3$	0.0464	0.0484	0.1590	0.1730	0.1852	0.4700	0.0041
	0.0702	0.9447	0.0390	0.7094	0.2175	0.1840	0.0211
	0.0786	0.3149	0.7048	0.0439	0.6165	0.4753	2.7092
$SiBrH_3$	0.0470	0.0571	0.1823	0.1725	0.2039	0.4663	0.0017
	0.0837	0.9435	0.0439	0.7139	0.2132	0.1899	0.0036
	0.0855	0.3151	0.6988	0.0490	0.6085	0.4731	0.4692
$SiIH_3$	0.0469	0.0436	0.1905	0.0757	0.1899	0.4766	0.0011
	0.0446	0.9462	0.0495	0.7176	0.2327	0.1783	0.0052
	0.0728	0.3133	0.6962	0.0404	0.6110	0.4813	3.0708
$SiFD_3$	0.0907	0.1002	0.1867	0.3503	0.2168	0.4202	0.0166
	0.2123	0.9458	0.0684	0.6897	0.1748	0.2129	0.0333
	0.1624	0.2904	0.7112	0.0879	0.5842	0.4559	0.3606
$SiClD_3$	0.0908	0.0877	0.1458	−0.1882	0.0870	0.4445	0.0029
	0.1221	0.9418	0.1771	0.7205	0.2903	0.1960	0.0147
	0.1447	0.2926	0.7020	0.0802	0.5795	0.4794	0.6198
$SiID_3$	0.0907	0.0796	0.2112	0.6693	0.3194	0.4562	0.0008
	0.0776	0.9446	−0.1749	0.2923	−0.0878	0.1870	0.0038
	0.1352	0.2926	0.6857	0.0735	0.5681	0.4903	0.7190

The vibrational coupling constants and the rotational distortion constants are given in Table 4. All the zeta constants obey the linear and quadratic sum rules derived by Boyd and Longuet Higgins[17] and Oka[18] respectively. The high values of the constants ζ_{34}, ζ_{36} and ζ^z_{46} in these molecules suggest that the coupling between the vibrations concerned is more significant than others. Also the constant ζ_5 decreases rapidly with the increasing mass of the substituent Y atom, except for $SiBrH_3$. The rotational distortion constants of these cases obtained in the present investigation are in the expected range.

References

1 Mohan S, *Bull Soc Chim Belg (Belgium)*, **86** (1977) 531.

2 Mohan S, *Proc Indian Acad Sci Ser A*, **88** (1979) 351.

3 Mohan S, *Acta Phys Pol A (Poland)*, **57** (1980) 433.

4 Mohan S & Ravikumar K G, *Indian J Pure & Appl Phys*, **18** (1980) 857.

5 Mohan S & Rajaraman S, *Indian J Pure & Appl Phys*, **19** (1981) 620.

6 Mohan S & Ravikumar K G, *Proc Indian Natl Acad Sci Sect A*, **48** (1982) 589.

7 Decius J C, *J Chem Phys (USA)*, **38** (1963) 241.

8 Cyvin S J, *Molecular vibrations: Mean-square amplitudes* (Elsevier, Amsterdam), 1968.

9 Meal J H & Polo S R, *J Chem Phys (USA)*, **24** (1956) 1119, 1126.

10 Cyvin S J, Cyvin B N & Hager G, *Z Naturforsch A (Germany)*, **23** (1968) 1649.

11 Kivelson D & Wilson E B (Jr), *J Chem Phys (USA)*, **20** (1953) 1575.

12 Kivelson D & Wilson E B (Jr), *J Chem Phys (USA)*, **21** (1953) 1229.

13 Nagarajan G, *Bull Soc Chim Belg (Belgium)*, **71** (1962) 226.

14 Newman C, Kenneth O'loane J, Polo S R & Kent Wilson M, *J Chem Phys (USA)*, **25** (1956) 855.

15 Sutton L E, *Tables of interatomic distance & configuration of molecules and ions*, Spl Publication No. 11 (Chemical Society, London) 1958.

16 Jones L H, *Inorganic vibrational spectroscopy*, Vol. 1 (Marcel Dekker, New York), 1971.

17 Boyd D R J & Longuet Higgins H C, *Proc R Soc London Ser A (GB)*, **213** (1952) 55.

18 Oka T, *J Mol Spectrosc (USA)*, **29** (1969) 84.

INSTRUCTIONS TO AUTHORS

SCOPE

The journal welcomes, for publication, full papers and short notes, reporting significant new results of research, in all areas of physics except space physics. The applied fields covered are electronics, electrical engineering, instrumentation and applied mathematics. However, papers in applied mathematics with emphasis on only derivation and proofs and having no direct physical significance, will not be considered. Review articles are not published normally.

SUBMISSION OF MANUSCRIPT

Manuscripts for consideration should be submitted, *in duplicate*, to Editor, Indian Journal of Pure & Applied Physics, Publications & Information Directorate, Hillside Road, New Delhi 110012. They should neither have been already published nor be under consideration elsewhere.

Manuscripts should be in English and typewritten on only one side of good quality paper, in double space, with adequate margin on all four sides. One original and one carbon or photo-copy, each complete in all respects including abstract, illustrations, appendixes, etc. are to be submitted.

PREPARATION OF MANUSCRIPT

Authors may consult recent issues of the Journal to familiarize themselves with the general style and practices adopted in regard to the various elements of a paper.

General

Manuscript should be presented in as concise a form as possible. Good attention should be given to spelling and grammar. In giving names of chemical compounds and structures, abbreviations of units of measurements, symbols and notations, the style and practices recommended by the IUPAP and IUPAC, should be followed.

Frequently repeating combinations of words, e.g. electric field gradient (EFG), junction field effect transistor (JFET), stimulated Raman emission (SRE), should be abbreviated subsequently, indicating the abbreviated form in parenthesis, as shown, at the place of their first occurrence.

Pages should be numbered consecutively and arranged in the following order: Title, authors' names with their institutional affiliations and abstract, along with relevant footnotes whenever necessary (on a separate sheet); introduction; experimental details/theory/method/analysis; results; discussion; conclusion(s); acknowledgement; references and appendixes. Tables, captions for figures (with legends) and appendixes should be typed *on separate sheets* and attached at the end of the manuscript.

Title

The title should be neither too brief/general nor unnecessarily long. It should reflect the content of the paper so as to derive the maximum advantage in indexing. If a paper forms part of a general series, a specific subtitle, indicating the particular aspect of the work covered in the paper, should be provided.

A short running title for the paper, the broad subject heading under which it should be classified in the contents page (authors may consult recent numbers of the journal for this purpose), and the author (indicated by an asterisk on the relevant author's name) and address for correspondence, should also be provided on the title page.

Abstract

The abstract, usually not exceeding 200 words, should indicate the scope and significant content of the paper, highlighting the principal findings and conclusions. It should be in such a form that abstracting periodicals can use it without modification.

Introduction

Long and elaborate introduction should be avoided. It should be brief and state the exact scope of the study in relation to the present status of knowledge in the field. Literature review should be limited strictly to what is necessary to indicate the essential background and the justification for undertaking the study.

Materials, methods, apparatus, etc.

The sources of materials and their purity, methods of preparation, procedure for measurements and their accuracies, etc. should be clearly stated to enable any other worker to repeat the work if necessary. New methods, techniques, theories, etc. should be described in adequate detail; but if they are well known, a mere literature reference to them will do; differences from standard ones, improvements or innovations should, however, be clearly mentioned.

Results

Only such primary data as are essential for understanding the discussion and main conclusions emerging from the study should be included. All secondary data as are of interest to a specific category of readership *should not be included* in the paper. Such data should be retained by the authors for supply, on request, to any interested research worker. A footnote to this effect may be inserted at the relevant place in the paper.

The results must be presented in a coherent sequence in a unified logical structure, avoiding repetition or confusion. Limitations of the results should be clearly stated.

The same data should not be presented in both tabular and graphic forms. Only such tables and figures as are essential should be included. Simple linear plots that can easily be discussed in the text, should not be included. Infrared, ultraviolet, NMR and other spectra, DTA curves, etc. should be included only if they pertain to new compounds and/or are essential to the discussion; otherwise only significant numerical data should be given in the text or in a table.

Discussion

Long rambling discussion should be avoided. The discussion should deal with the interpretation of results without repeating information already presented under results. It should relate new findings to the known and include logical deductions. A separate section on 'conclusions' can be given only when they are well established and of outstanding significance. Mere observation of qualitative trends of results should be distinguished from firm conclusions. Also, limitations, if any, to the conclusions should be clearly pointed out.

Mathematical portions

Special attention should be given to the mathematical portions of the paper. Equations must be well separated from the text and written clearly with good separation between the successive lines. The usual norms of breaking long mathematical expressions should be adhered to. Equations should be numbered consecutively in Arabic numerals with the number in parenthesis near the right hand margin. Superscripts and subscripts should be clearly indicated in pencil by V and Λ sign respectively. Capital and small letters,

particularly of the same letter when both occur, as well as letters or *symbols likely to be confused* one for the other, *should be* clearly *distinguished*. Special characters (e.g. Greek, script, vector, tensor, etc.) required must be indicated by marginal notes. Letters and symbols which should appear in bold face must be clearly indicated. To simplify typesetting: (i) long and complicated mathematical expressions which are frequently repeated should be replaced with single letter/symbol, *without clashing with the others used* in the paper; (ii) the "exp" form of complex exponential functions should be used; and (iii) to simplify fractions, the solidus (/) is to be used and fractional exponents are to be used instead of root signs, e.g.

write $\exp\{-i\omega_0(t_1-t_2)/2\}$ and *not* $e^{-i\omega_0(t_1-t_2)/2}$

write $(4\omega_{pl}\,K_{3\lambda}^2/\tilde{\omega}\,K_D^2)^{1/2}$ and *not* $\sqrt{\dfrac{4\,\omega_{pl}\,K_{3\lambda}^2}{\tilde{\omega}\,K_D^2}}$

Tables

Tables should be numbered consecutively in Arabic numerals and *should bear brief titles. Column headings should be brief.* Units of measurement should be abbreviated and placed below the headings. Nil results should be indicated and distinguished clearly from absence of data. Inclusion of structural formulae inside the tables should be avoided as far as possible. Tables should be referred to in the text by numbers and not by terms like 'above', 'below', 'preceding' or 'following'. Results should not be presented to a greater accuracy than that of the method employed.

Illustrations

The number of illustrations should be kept to the minimum. Wherever possible, e.g. a number of individual analogous figures referring to different variables, substances, molecules, etc. may be combined into one composite figure. All illustrations should be numbered consecutively in Arabic numerals. *Captions and legends* to the figures should be *self-explanatory*. Line drawings should be made with Indian ink on white drawing paper/cellophane sheet/tracing cloth, and drawn to approximately twice the printed size.

The lettering should be uniform, preferably in stencil, so as to be *not less than* 1.5 *mm after reduction* widthwise to full page size (165 mm) or column size (80 mm). The size of geometrical shapes (used to distinguish different graphs), dots, lines, etc. should be sufficiently *large to permit* the necessary *reduction without loss of detail*. In the case of photographs, *prints must be on glossy paper and contrasty*. If an illustration is taken from another publication, reference to the source should be given and prior permission secured. Illustrations should be referred to in the text by numbers and not by terms like 'above', 'following' etc.

Acknowledgement

Acknowledgements should not be exuberant and must be made only to real assistance rendered in connection with the work reported in the paper.

References

References cited should be limited to the absolute minimum (particularly in the case of short notes) based on their essential relevance. In the text, references to literature should be *numbered consecutively, in the order of their first occurrence*, and should be indicated by superscript Arabic numbers at the relevant places; as far as possible the placement of references on numerals or other symbols should be avoided; in such cases the reference may be given in parenthesis in running text, e.g. "this yielded for *n* a value of 2.3 (Ref. 5)". Full bibliographic details for all the references mentioned in the text should be listed in serial order at the end of the paper.

In citing references to research papers, names and initials of authors should be followed, in order, by the title of the periodical in the abbreviated form (underlined), the volume number (two lines underneath), the year within circular brackets and the page number [e.g. Chandra B P & Shrivastava K K, *J Phys & Chem Solids (GB)*, 39 (1978) 939]. For names of periodicals, the abbreviations followed by the *Physics Abstracts* should be used. For periodicals not covered by *Physics Abstracts*, the title abbreviations should be according to the *Bibliographic Guide for Editors and Authors*, 1974, published by the American Chemical Society, Washington DC, USA; additionally the country from which the journal is published should be given in parenthesis immediately after the title abbreviation. If a paper has been accepted for publication, the names of the authors and the journal (with volume number and year, if known) should be given followed by the words "in press" [e.g. Wahi P K & Patel N D, *Can J Spectrosc (Canada)*, in press.].

In references containing *up to four authors*, the *names of all* the *authors* with their respective initials should *be given*. The abbreviations *et al.*, idem and ibid should be avoided. When there are more than four authors, *only* the names of the *first three authors* with their respective initials should *be given*, followed by the words *'et al.'*

Reference to a book should include details in the following order: name and initials of authors, the title of the book (underlined), name of publisher and place of publication within circular brackets and year and page (s) [e.g. Clayton C B, *Operational amplifiers* (Newnes-Butterworths, London), 4th Edn, 1977, 26]. If the reference is to the work of an author published in a book by a different person, the fact that it is cited from the source book should be clearly indicated [e.g. Turnhout Van J, 'Thermally stimulated discharge of electrets' in *Topics in applied physics*: Vol. 33—*Electrets*, edited by C M Sessler (Springer Verlag, Berlin), 1980, 130].

Proceedings of conferences and symposia should be treated in the same manner as books. Reference to a paper presented at a conference, the proceedings of which are not published, should include, in the following order, names and initials of authors, title of the paper (underlined), name of the conference, and where and when it was held (e.g. Herczeg P, *Symmetry-violating kaon decays*, paper presented to the International Conference on High Energy Physics and Nuclear Structure, Vancouver, Canada, 13-17 August 1979).

Reference to a thesis should include the name of the author, title of the thesis (underlined), university or institution to which it was submitted and year of submission (e.g. Mehrotra S N, *Many-body techniques and their applications to interacting bosons*, Ph D thesis, Ranchi University, 1976).

Reference to a patent should include names of patentees, country of origin (underlined) and patent number, the organization to which the patent has been assigned (within circular brackets), date of acceptance of the patent and reference to an abstracting periodical where available [e.g. Labes M M, *US Pat.* 4,066,567 (to Temple University), 3 January 1978; *Chem. Abstr.*, **88** (No. 20) (1978), 138350 n].

PROOFS & REPRINTS

Authors will receive galley proofs and a reprint order form. The galley proofs, indicating the essential corrections, should be returned to the Editor without delay, enclosing the reprint order form. Authors are given 25 *free reprints* for each paper. *Extra* reprints can be had *at cost. If the reprint order is not received with the corrected proofs, it will be presumed that the author needs no extra reprints.* Later requests for *more* reprints cannot be complied with. Covers for reprints cannot be provided.

THE WEALTH OF INDIA

An Encyclopaedia of Indian Raw Materials and Industrial Products, published in two series:
(i) Raw Materials, and **(ii) Industrial Products**.

RAW MATERIALS

The articles deal with Animal Products, Dyes & Tans, Essential Oils, Fats & Oils, Fibres & Pulps, Foods & Fodders, Drugs, Minerals, Spices & Flavourings, and Timbers and other Forest products. Names in Indian languages, and trade names are provided.

For important crops, their origin, distribution, evolution of cultivated types, and methods of cultivation, harvesting and storage are mentioned in detail. Data regarding area and yield and import and export are provided. Regarding minerals, their occurrence and distribution in the country and modes of exploitation and utilization are given. The articles are well illustrated. Adequate literature references are provided.

Eleven volumes of the series covering letters A – Z have been published:

Vol. I(A-B) Rs. 80.00; Vol. II (C) Rs. 95.00; Vol. III (D-E) Rs. 105.00; Vol. IV (F-G) Rs. 65.00; Vol. IV: Suppl. Fish & Fisheries Rs. 40.00; Vol. V (H-K) Rs. 75.00; Vol. VI (L-M) Rs. 90.00; Vol. VI: Suppl. Livestock Rs. 60.00; Vol. VII (N-Pc) Rs. 30.00; Vol. VIII (Ph-Re) Rs. 86.00; Vol. IX (Rh-So) Rs. 104.00; Vol. X (Sp-W) Rs. 152.00; Vol. XI (X-Z) Rs. 102.00.

INDUSTRIAL PRODUCTS

Includes articles giving a comprehensive account of various large, medium and small scale industries. Some of the major industries included are: Acids, Carriages, Diesel Engines, Fertilizers, Insecticides & Pesticides, Iron & Steel, Paints & Varnishes, Petroleum Refining, Pharmaceuticals, Plastics, Ship & Boat-building, Rubber, Silk, etc.

The articles include an account of the raw materials and their availability, manufacturing processes, and uses of products, and industrial potentialities. Specifications of raw materials as well as finished products and statistical data regarding production, demand, exports, imports, prices, etc., are provided. The articles are suitably illustrated. References to the sources of information are provided.

Nine volumes of the series covering letters A – Z have been published.

Part I (A-B) Rs. 54.00; Part II (C) Rs. 64.00; Part III (D-E) Rs. 25.00; Part IV (F-H) Rs. 25.00; Part V (I-L) Rs. 30.00; Part VI (M-Pi) Rs. 28.00; Part VII (Pl-Sh) Rs. 60.00; Part VIII (Si-Ti) Rs. 66.00; Part IX (To-Z) Rs. 80.00.

HINDI EDITION: BHARAT KI SAMPADA—PRAKRITIK PADARTH

Vols. I to VI and two supplements of Wealth of India—Raw Materials series in Hindi already published.

Published Volumes:

Vol. I (अ-औ) Rs. 38; Vol. II (क) Rs. 36; Vol. III (ख-न) Rs. 36; Vol. IV (प) Rs. 83; Vol. V (फ-मेरे) Rs. 60; Vol. VI (मेल-रू) Rs. 80.

Supplements:

Fish & Fisheries (Matsya & Matsyaki) Rs. 49;
Liverstock (*Pashudhan aur Kukkut Palan*) Rs. 34.

Vols. VII to XI under publication.

Please contact:

Manager (Sales & Advertisement)
PUBLICATIONS & INFORMATION DIRECTORATE, CSIR
Hillside Road, New Delhi 110012

RN 7092/63

CSIR PUBLICATIONS

WEALTH OF INDIA

An encyclopaedia of the economic products and industrial resources of India issued in two series

RAW MATERIALS SERIES—contains articles on plant, animal and mineral resources

	Rs	$	£
Vol. I (A-B)	80.00	30.00	13.00
Vol. II (C)	95.00	33.00	17.00
Vol. III (D-E)	105.00	32.00	20.00
Vol. IV (F-G)	65.00	27.00	12.00
Supplement (Fish & Fisheries)	40.00	16.00	7.00
Vol. V (H-K)	75.00	28.00	12.50
Vol. VI (L-M)	90.00	34.00	15.00
Supplement (Livestock)	60.00	18.00	6.00
Vol. VII (N-Pe)	30.00	9.00	3.00
Vol. VIII (Ph-Re)	86.00	32.00	14.00
Vol. IX (Rh-So)	104.00	35.00	19.00
Vol. X (Sp-W)	152.00	65.00	23.00
Vol. XI (X-Z)	102.00	42.00	20.00

INDUSTRIAL PRODUCTS SERIES—deals with major, small-scale and cottage industries

Part I (A-B)	54.00	20.00	9.00
Part II (C)	64.00	24.00	11.00
Part III (D-E)	25.00	7.50	2.50
Part IV (F-H)	25.00	7.50	2.50
Part V(I-L)	30.00	9.00	3.00
Part VI (M-Pi)	28.00	8.00	2.80
Part VII (Pl-Sh)	60.00	18.00	6.00
Part VIII (Si-Ti)	66.00	27.00	10.00
Part IX (To-Z)	80.00	34.00	12.00

BHARAT KI SAMPADA (Hindi Edition of Wealth of India, Raw Materials)

Vol. I (अ-औ)	38.00	16.00	6.50
Vol. II (क)	36.00	15.00	6.00
Vol. III (ख-न)	36.00	15.00	6.00
Vol. IV (प)	83.00	34.00	16.00
Vol V (फ-मेरे)	60.00	22.00	10.00
Vol VI (मेल-ह)	80.00	27.00	13.00
Livestock (Kukkut Palan)	34.00	15.00	6.00
Fish & Fisheries (Matsya aur Matsyaki)	49.00	21.00	8.00
A Dictionary of Generic & Specific Names of Plants and Animals Useful to Man with their English and Latin pronunciation in Devanagari	30.00	11.00	5.00

OTHER PUBLICATIONS

	Rs	$	£
Proceedings seminar on primary communications in Science & Technology in India by Sh. R.N. Sharma & S. Seetharama	52.00	17.50	9.00
Flora of Delhi by J.K. Maheshwari	28.00	8.00	2.80
Indian Fossil Pteridophytes by K.R Surange	23.00	8.00	2.30
Indian Thysanoptera by T.N. Ananthakrishnan	26.00	8.00	2.60
The Millipede Thyropygus by G. Krishnan	12.00	3.50	1.20
Drug Addiction with special reference to India by R.N. Chopra & I.C. Chopra	12.00	3.50	1.20
Glossary of Indian Medicinal Plants by R.N. Chopra & I.C. Chopra	35.00	13.00	6.00
Fluidization & Related Processes	12.00	4.00	1.20
Evolution of Life by M.S. Randhawa, A.K. Dey, Jagjit Singh & Vishnu Mitre	22.50	7.00	2.25
Collected Scientific Papers of Meghnad Saha	30.00	9.00	3.00
Proteaceae by C. Venkata Rao	34.00	11.00	3.40
Pinus by P. Maheshwari & R.N. Konar	30.00	11.00	5.00
Cellulose Research I	3.00	0.90	0.30
Cellulose Research II	6.00	1.75	0.60
Chemical Process Design	9.00	2.50	0.90
Low Temperature Carbonization of Non-coking Coals & Lignites & Briquetting Coal Fines:			
Vol. I	17.50	5.50	1.75
Vol. II	17.50	5.50	1.75
Nucleic Acids	10.00	3.00	1.00
IGY Symposium: Vol. I	9.00	2.50	0.90
IGY Symposium: Vol. II	9.00	2.50	0.90
CNS Drugs	16.50	5.00	1.65
Kinetics of Electrode Processes & Null Points of Metals	2.50	0.75	0.25
Indian Sardines by R.V. Nair	22.00	7.00	2.20
Termite Problems in India	9.00	3.00	0.90
Loranthaceae by B.M. Johri & S.P. Bhatnagar	32.00	11.00	3.20
Abies and Picea by K.A. Chowdhury	14.00	6.00	2.10
Gnetum by P. Maheshwari and Vimla Vasil	20.00	6.00	2.00
Aquatic Angiosperms by K. Subramanyam	20.00	6.00	2.00
Supplement to Glossary of Indian Medicinal Plants by R.N. Chopra, I.C. Chopra & B.S. Varma	18.00	7.00	3.00
Herbaceous Flora of Dehra Dun by C.R. Babu	144.00	60.00	22.00
Diosgenin and Other Steroid Drug Precursors by Y.R. Chadha & Miss L.V. Asolkar	36.00	13.00	6.00
Research & Development Management by Inder Dev	25.00	10.00	—
Rural Development and Technology—A Status Report-cum-Bibliography by P.R. Bose & V.N. Vashist	100.00	38.00	17.00

Packing and Postage extra

Please contact:

Manager (Sales & Advertisement)

PUBLICATIONS & INFORMATION DIRECTORATE, CSIR

Hillside Road, New Delhi 110012

Printed & Published by D.S. Sastry, Editor, Publications & Information Directorate (PID) Hillside Road, New Delhi 110012, at PID Photocomposition Unit

D(C)540